Biodegradability and spectroscopic properties of DNOM affected by mercury transport and uptake

Eline Mosleth Færgestad

Thesis for a Master's
Degree in Chemistry

60 credits

Department of Chemistry
Faculty of Mathematics and Natural Sciences

UNIVERSITY OF OSLO

[06 / 2019]

Biodegradability and spectroscopic properties of DNOM affected by mercury transport and uptake

2019

Biodegradability and spectroscopic properties of DNOM affected by mercury transport and uptake.

Eline Mosleth Færgestad

http://www.duo.uio.no/

Trykk: Reprosentralen, Universitetet i Oslo

Abstract

Dissolved natural organic matter (DNOM) is a complex mixture of heterogeneous organic macromolecules that are formed in the environment, mainly by decay of plant and animal remains. All freshwaters contain a certain amount of DNOM, though in the boreal region the levels of DNOM are usually high. During the past decades, there has been a significant increase of DNOM in surface waters in the Nordic countries, Scotland and North-East America.

DNOM's ability to absorb light results in a characteristic yellow-brown colour of the water. DNOM has numerous functional groups giving the molecules specific properties, including serving as complexing agents for soft metals such as mercury. That way, DNOM increases the mercury mobility, thereby increasing the loading of the metals from soil to surface waters. On the other hand, the complexation of metals to especially high molecular weight (HMW) DNOM is expected to reduce the toxicity of the metals by making them less bioavailable. Long-term increase in DNOM may be associated with changes in the size fractions and thus biodegradability of the DNOM, which might affect bioavailability of mercury to the nutrient web.

In this thesis, it was hypothesised that mercury (totHg) is mainly bound to high molecular weight DNOM, and that this fraction is less bioavailable than the low molecular weight (LMW) DNOM. It was further hypothesised that because HMW DNOM is larger and more aromatic, it has higher sUVa (Abs254/DOC) and sVISa (Abs400/DOC) values, as well as lower SAR (Abs254/Abs400) values than LMW DNOM, which may result in lower bioavailability of mercury in the HMW fractions.

In order to study these hypotheses, samples from lake Langtjern were collected in the spring, late summer and fall at three different positions of the lake (outlet, inlet and hypolimnion (6 m depth)). The samples were fractionated using Tangential Flow Filtration (TFF) with a 100 kDa cut-off. Samples were fractionated into high molecular weight DNOM (>100 kDa) and low molecular weight DNOM (<100 kDa).

The results from this study showed that the main bulk of DOC was found in the high molecular fraction, and that the concentration of totHg was higher in the HMW fractions than in the LMW fraction as viewed across all seasons and collection sites. The mean value of totHg in the HMW fraction was 3.3 ngL^{-1}, and 0.93 ngL^{-1} in the LMW fraction. The mercury concentration in the LMW fraction decreased from the spring to the fall, whereas no change was observed in the HMW fractions. LMW fractions were smaller and less aromatic than the HMW fractions. Biodegradation experiments showed that the

HMW fractions were less easily biodegradable than the LMW fractions, which may be seen in relation to the larger size and more aromatic character.

There was a significant interaction between the fraction size and the season, and between the fraction size and the sample site in the mercury density of DNOM (measured as totHg/DOC). These interactions show that the extent to which mercury was bound to the different size fractions changed over the season and over the sampling sites. Differences in the mercury density of DNOM between the fractions were not observed in the spring, whereas in the late summer and fall samples the highest mercury density was found in the HMW DNOM. In the LMW fractions, the density of mercury in the DNOM decreased strongly from the spring to late summer and fall, whereas minor changes were observed for the HMW fractions. The interaction between the sampling sites and the fraction size showed that the differences in mercury density of DNOM was observed at the hypolimnion and in the outlet, but not in the inlet. These observations suggest that changes in the DNOM occur in the lake, which may lead to uptake of mercury in the nutrient chain. This would be in accordance with the observed higher biodegradation of the LMW fraction, measured as respiration rate.

Preface

Firstly, I would like to thank my supervisor, Rolf D. Vogt, for guidance, suggestions and for always providing plenty of feedback. Next, I would like to thank Heleen de Wit at NIVA for letting me take a small part in the CLIMER project.

Thank you, Alexander Håland, for your suggestions, help and for always keeping the door open for me to bother you with my questions.

I would like to thank all the people who helped me with my experimental design and analyses: Pawel Krzeminski for helping me with TFF and all the extra tests, Anne-Marie Skramstad for helping me with ICP-OES and Bo Emilsson for helping me with IC. Thank you, Alexander Håland and Cathrine Brecke Gundersen, for suggestions and clarifying discussions related to biodegradation. I would also like to thank Hans Fredrik Veiteberg Braaten for helping me with mercury analysis and Berit Kaasa for helping me with DOC analysis. Thank you to Uta Brandt for taking me to Langtjern and helping me with my samples. I would also like to thank my mother for helping me with data analysis and scientific writing.

I would like to thank everyone at the environmental chemistry group for making the past two years memorable.

Anne, thank you for keeping me company in our portable office. And to my other friends and colleagues, thank you for support and laughs. Last, but not least, I would like to thank my mother and father for teaching me the value of nature and my two sisters for everything we've shared.

List of abbreviations

NIVA	Norwegian Institute for Water Research
CLIMER	"Climatic, abiotic and biotic drivers of mercury in freshwater fish in northern ecosystems" (NIVA project)
DNOM	Dissolved Natural Organic Matter
HMW	High Molecular Weight (>100 kDa)
LMW	Low Molecular Weight (<100 kDa)
MeHg	Methyl Mercury ($HgCH_3^+$)
TotHg	Total Mercury
DOC	Dissolved Organic Carbon
RR	Respiration Rate
UV-VIS	Ultraviolet and visible light
TFF	Tangential Flow Filtration
RO	Reverse Osmosis
SDR	Sensor Dish Reader
DOC	Dissolved Organic Carbon
HPIC	High Pressure Ion Chromatography
ICP-OES	Inductively Coupled Plasma – Optical Emission Spectrometry
sUVa	Specific UV Absorbance

sVISa	Specific Visible Absorbance
SAR	Specific Absorbance Ratio
ANOVA	Analysis of variance
PCA	Principal Component Analysis
FDR	False Discovery Rate

Table of contents

1 Introduction

1.1 Background

During the past decades, there has been a significant increase in the yellow-brown colour of surface waters in the Nordic countries, Scotland and North-East America (Skjelkvåle 2003; Skjelkvåle et al. 2000). The colour is caused by a group of organic compounds collectively referred to as Dissolved Natural Organic Matter (DNOM). DNOM is formed by the incomplete decay of plants and animal remains and is thus naturally present in soil. DNOM is a diverse group of molecules with a wide range of functional groups (Leenheer and Croué 2003), giving the DNOM specific collective properties. The functional groups serve as complexing agents for soft metals such as iron, mercury and aluminium (Rahman et al. 2010; Al-Reasi, Wood, and Smith 2011). Mercury forms strong ionic bonds to reduced sulphur groups on DNOM (Ravichandran 2004). Thus, DNOM increases the mobility of these metals. However, the complexation of metals to DNOM reduces the toxicity of the metals by making them less bioavailable (Hollis, Muench, and Playle 1997; Al-Reasi, Wood, and Smith 2011).

There is a substantial pool or mercury in the Norwegian forest floor due to the accumulation of long-range transported pollutants. Mercury in soil is transported with DNOM to surface waters and enters the nutrient chain as methyl mercury, a neurotoxin (Poste et al. 2015). This neurotoxin bio-accumulates in the nutrient chain. Consequently, large fish may contain high concentrations of methyl mercury. Because of this, there are dietary guidelines involving certain freshwater fish in order to avoid the ingestion of harmful amounts of methyl mercury (Folkehelseinstituttet 2016). European Food Safety Authority (EFSA) evaluated whether the tolerable weekly intakes of methyl mercury and inorganic mercury set by Joint FAO/WHO Expert Committee on Food Additives in 2010 were still valid. They decided to reduce the weekly tolerable intake of methyl mercury from 1.6 μg per kg body weight to 1.3. The inorganic mercury limit of 4 μg per kg body weight was kept (EFSA 2018).

A number of policies and regulations have been established in order to reduce mercury emissions. The Minamata Convention on Mercury, which was signed by 93 countries in 2013, is a mercury emission control of high importance. The agreement aims to protect human health and environment from the effects of mercury at a global scale. Phase-out of mercury mining, reduction in the use of mercury in products, reduction in emission from industrial plants and proper storage and waste treatment of

mercury are important abatement actions (UN 2013). Emissions to the environment are thereby expected to be reduced. The agreement takes into account the mercury that has been accumulated in the environment over a longer period of time, and the impact climate change may have on the mobility of this mercury. For the Minimata convention to enter into force, 50 governments needed to ratify the agreement. In August, 2017, the convention enforced 90 days after reaching the 50-ratification milestone (UN 2017). As a result of the laws and regulations, there has been a decline in atmospheric mercury deposition over the recent decades. However, the mercury concentration in fish increases, which may be a result of in-lake processes or regional processes (Braaten, Fjeld, et al. 2014). Water chemistry, pH, temperature, trophic position and the fish's diet are parameters that can affect mercury concentrations in the fish.

Different size fractions of the continuum of organic compounds comprising DNOM have different properties, including metal-complexing abilities. It is hypothesised that methyl mercury bound to low molecular weight DNOM is more bioavailable than methyl mercury bound to high molecular weight DNOM. Although there are many factors that contribute to bioavailability, making it difficult to identify general tendencies, studies indicate that methyl mercury bound to low molecular weight (LMW) DNOM fractions tends to be more bioavailable (Chakraborty et al. 2014) because of the small size of the LMW DNOM. Their small size makes them easier to break down and thereby more bioavailable. The main portion of methyl mercury is usually found in the high molecular weight (HMW) DNOM fractions, and a strong link is observed between MeHg and DOC (Grigal 2002; Poste et al. 2015). This was further confirmed by previous master studies (Francés 2017; Ong 2018). The HMW DNOM fractions are known to be more refractory ("The case for Calcium Chloride" ; Marschner and Kalbitz 2003), and thus the methyl mercury present in the HMW DNOM fractions is likely to be less bioavailable. DNOM thus serves two roles related to mercury: both as a detoxifier and as a transport vector.

Better insight into the properties of DNOM and mercury's way of binding to DNOM is essential in order to understand the environmental factors governing the transport and bioavailability of mercury. Moreover, to better understand the impact that increased DNOM concentration has had on mercury levels in fish, it is necessary to gain a better understanding of how size fractions and biodegradability of DNOM are governed by seasonal variations.

1.2 CLIMER

The work presented in this thesis is an integral part of the research project "Climatic, abiotic and biotic drivers of mercury in freshwater fish in northern ecosystems" (CLIMER). CLIMER is led by the Norwegian Institute for Water Research (NIVA) and collaborates with the University of Oslo, the University of New Brunswick and Swedish University of Agricultural Sciences.

By studying spatial and temporal trends of mercury in freshwater systems, CLIMER aims to investigate how transport and uptake of mercury in boreal lakes is affected by climate change. Gaining a better understanding of how mercury and methyl mercury interact will be used to evaluate and prevent future mercury risk.

1.3 Aim of the study

The aim of this thesis was to study bio-physico-chemical properties of DNOM and its impact on environmental processes, as well as association of mercury to DNOM and its link to transport and bioavailability of mercury.

It was hypothesised that mercury (totHg) is mainly bound to HMW DNOM, whereas the LMW fraction is more bioavailable than the HMW DNOM. It was further hypothesised that characterisation of the DNOM by absorbance in the UV and visible region will give valuable insight into understanding how the structure of DNOM affects the complexation to mercury.

To investigate these hypotheses, samples from lake Langtjern were studied. Langtjern is a boreal lake located in southeast Norway, and is a part of a catchment that is continuously monitored and studied by NIVA. The samples were fractionated using tangential-flow filtration and analysed for cation, anions, carbon content (DOC), pH, conductivity and biodegradation in order to investigate spatial and temporal differences between the DNOM fractions.

2 Theory

2.1 DNOM

Natural organic matter (NOM), comprising soil organic matter (SOM) and organic matter in solution, is a complex mixture of organic compounds that is mainly formed by the decay of plant and animal remains. When plants and animals die, their organic residues are oxidised and partly mineralised. This process is mainly mediated by the presence of microorganisms. Dissolved natural organic matter (DNOM) is defined as the portion of the NOM in solution that is not retained by a 0.45 μm membrane filter (vanLoon and Duffy 2011).

All freshwaters contain DNOM (Gjessing, Egeberg, and Håkedal 1999). It plays a vital role in a number of biogeochemical processes governing the unique physical and chemical properties of the boreal freshwaters. DNOM may also have negative effects on the water quality due to the properties of the molecules. For example, the functional groups on the DNOM can work as complexing agents for type B metals, such as mercury, enhancing their solubility. Type B metals, also called soft metals, are metals that form covalent bonds to functional groups on DNOM. The DNOM thereby functions as a transport medium for these toxic elements increasing their flux from the soil to surface waters. DNOM may be divided into two different groups based on its origin: Allochthonous material is material that is made within the terrestrial environment and washed into the water, while autochthonous material is generated in the lake itself, primarily by microorganisms (McKnight et al. 2001; Al-Reasi, Wood, and Smith 2011).

Carbon, hydrogen, oxygen, nitrogen and sulphur are the main elements of DNOM. On average, carbon constitutes approximately 50% of the mass of DNOM. The compounds contain both aromatic and aliphatic structures, and functional groups such as hydroxyl groups, phenols, carboxylic acids, ketones, amides and sulfhydryl groups (Leenheer and Croué 2003; Gaffney, Marley, and Clark 1996). The latter is the most important functional group related to mercury mobility, transport and uptake. DNOM molecules are thus able to form strong metal complexes with mercury, among others (Al-Reasi, Wood, and Smith 2011). Complexation of mercury to DNOM reduces the toxicity of the metal (Hollis, Muench, and Playle 1997). Weak acid groups, specifically carboxylic groups, contribute to a lowered pH, and DNOM is thus involved in the regulation of pH in soft waters.

Increased colouration of surface waters in the Nordic countries, Scotland and North-Eastern America is related to an increased concentration of DNOM, as well as a change in the character of the DNOM. The presence of chromophores, specifically conjugated double bonds, gives DNOM the ability to absorb light in the UV and visible part of the spectrum (Leenheer and Croué 2003), and the absorption of blue light is the strongest (Evans 2005). This results in a brown colouring of the water. During the last 20-30 years, there has been an increased concentration of DNOM in boreal lakes in Northern Europe and North America (Evans 2005). This is measured as increased concentrations of Dissolved Organic Carbon (DOC) and increased colour, commonly referred to as "browning". There are several explanations for this. Firstly, the increasing global temperature over the latter years leads to longer growing seasons, which in turn leads to increased vegetation and biomass production, known as "greening". Increased greening leads to the production of more DNOM in the degradation process. Secondly, browning of freshwater is related to a decrease in sulphate deposition, which increases the solubility of organic matter and the transport of organic matter to surface waters (Finstad et al. 2016; Monteith et al. 2007). Thirdly, climate change, with increased precipitation amount and intensity, also contributes to the browning by causing increased flow through shallow sub-lateral flow-paths, rich in organic matter, directly into the stream. The DNOM thereby avoids the absorptive capacities of the deeper mineral soil horizons.

The molecular size distribution of the DNOM in the environment is an important explanatory factor for mercury exposure to aquatic organisms as it reflects DNOM properties such as its complexation capacity, as well as mobility and bioavailability. To be able to study these properties of DNOM, the molecules are categorised into fractions based on molecular weight, so that each fraction can be studied separately. Low-molecular weight (LMW) and high-molecular weight (HMW) DNOM are defined based on a chosen cut-off, which is set as 100 kDa in this thesis.

2.2 Mercury

Environmental research often involves monitoring changes over a long period of time. Mercury as an environmental contaminant is a relatively new field of environmental interest, and its levels in the environment have not been monitored for a long time. The accumulation and effects of mercury on freshwater fish has drawn increasing global interest the last years.

As mercury is a Type B metal, also called Soft metal, forming a strong ionic bond to reduced sulphur groups on DNOM (Ravichandran 2004), DNOM works as a complexing agent of mercury. Complexation of mercury to DNOM facilitates the transport of mercury from soil to streams and lakes. Both totHg and MeHg are significantly correlated to TOC (Braaten, de Wit, et al. 2014). As a result, lakes with high DOC content have higher totHg and MeHg concentrations than lakes with lower DOC content. The presence of DNOM stimulates microbial growth and thereby facilitates the methylation process (Ravichandran 2004).

Mercury can be methylated to form methyl mercury, $HgCH_3^+$, which is the mercury compound of highest concern due to its neurotoxicity and bioaccumulative properties (Poste et al. 2015). Methyl mercury has the ability to bio-concentrate in low trophic levels and biomagnify in the aquatic nutrient chains. Due to its small size and organometallic character it has the ability to be assimilated by organisms and accumulate in aquatic nutrient chains. Methyl mercury becomes available in the nutrient chain due to its high affinity for proteins containing sulfhydryl and thiol groups and binds to glutathione in the body (Hong, Kim, and Lee 2012; Ravichandran 2004). The compound biomagnifies up the trophic ladder, resulting in a significantly elevated concentration of mercury in predator fish. As a result, large freshwater fish, e.g. pike, contain mercury levels that are considered harmful to humans and other organisms. Methyl mercury is a neurotoxin and mainly attacks the nervous system. Once inside the organism, methyl mercury has the ability to damage the brain by crossing blood-brain barrier, as well as penetrating the placenta, causing harm to the foetus (Grigal 2002). Although the mercury concentration may not be high in the water, the compound accumulates in the aquatic food chains due to its high affinity for sulfhydryl groups in proteins (Braaten, de Wit, et al. 2014; Ravichandran 2004). Because of this accumulation, the Norwegian Food Safety Authority and the Norwegian Institute of Public Health have provided specific dietary guidelines regarding the amount and rate of intake of certain types of freshwater fish. The guidelines take into account the fish size, weight and mercury concentration in the different types of fish. World Health Organisation (WHO) and Food and Agricultural Organisation of the United Nations have set limits for mercury levels in fish. For the European community, the maximum recommended mercury level in most fish is 0.5 mg Hg per kg wet weight (UNEP 2002). Mercury levels in some freshwater fish from the Nordic region, among others, commonly exceed these limits. Pregnant and nursing women are advised to be extra careful with their intake of fish (Folkehelseinstituttet 2016). Foetuses who have been exposed to mercury concentrations higher than advised, can be born with an impaired nervous system, and concentration and speech disorders (Hong, Kim, and Lee 2012).

Methylation may occur by following biotic or abiotic pathways, but the biotic pathways involving microbes are the most important methylation pathways in aquatic systems (Ullrich, Tanton, and Abdrashitova 2001). Some bacteria are capable of methylating mercury, most importantly certain strains of sulphate-reducing bacteria (SRB)(Gilmour et al. 2011), in addition to certain iron-reducing bacteria (IRB) and methanogens. A gene cluster with two genes, *hgcA and hgcB*, is responsible for methylation, and the process readily occurs in slightly reducing conditions. The genes are required for mercury methylation by the sulphur-reducing bacteria *Desulfovibrio desulfuricans ND132* and *Geobacter sulfurreducens PCA,* among others. *hgcA* encodes HgcA, a methyl carrier protein, while *hgcB* encodes HgcB, a ferredoxin that serves as an electron donor in the reduction of the corrinoid protein (Parks et al. 2013). The mercury pathway, including the methylation mediated by microbes, is illustrated in Figure 2.1.

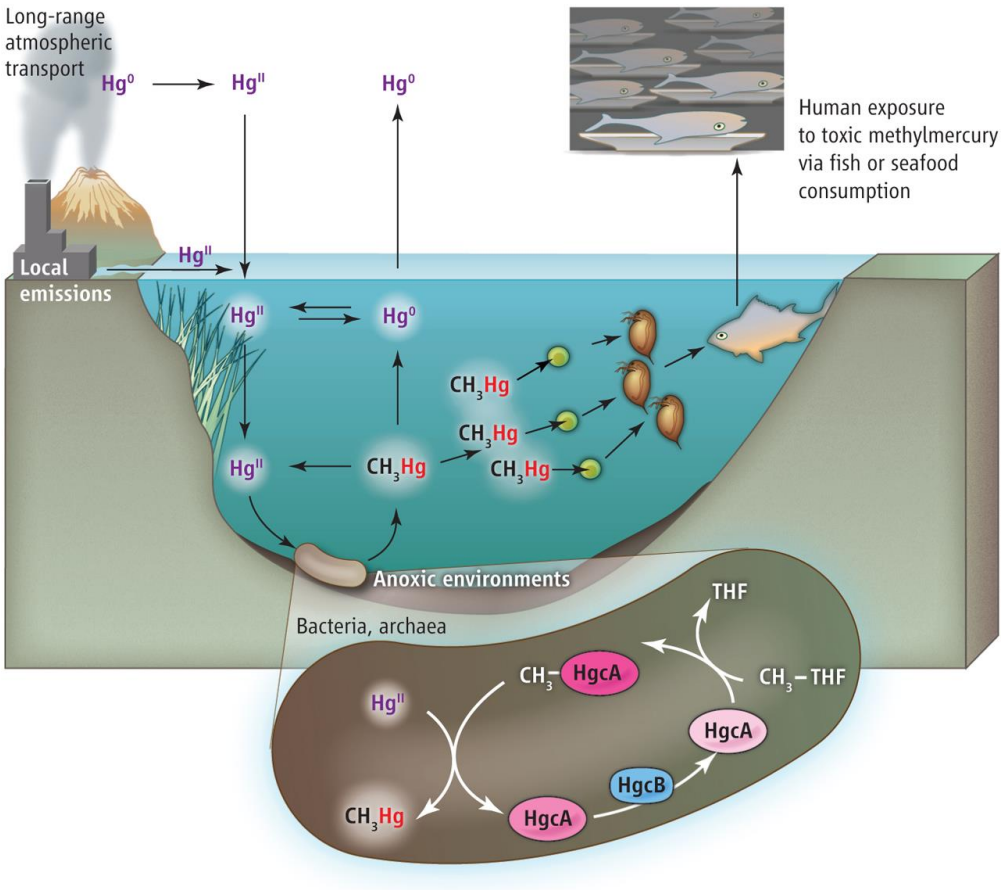

Figure 2.1: The mercury pathway (Poulain and Barkay 2013). Long-range transported mercury ends up in the water where it is methylated to form the neurotoxin methyl mercury, a bacteria-mediated process. Methyl mercury enters the food web and is biomagnified to higher trophic levels.

2.3 Sources of mercury and deposition of mercury in Norway.

There are two stable oxidation states of mercury: Hg^{2+} and Hg^{0}. The latter dominates in the atmosphere and is easily transported over long distances, while former dominates in in soil and sediments. Thus, Hg^{2+} is the form of mercury that is bound to organic matter.

Elevated mercury levels in the freshwater environment in Norway are mostly related to anthropogenic sources. Mercury may be subject to long-range transport in the atmosphere due to the low vapour pressure of Hg^{0}, allowing for a substantial gas phase. A global distillation of mercury has lead to accumulation of mercury in the soil in cooler regions. Southeast Norway contains boreal forest, which is rich in organic matter. Since the mercury binds strongly to organic matter the accumulation is especially large in the boreal region. Studies suggest significant inputs of anthropogenic mercury in the soil beyond the natural emissions (Fitzgerald et al. 1998), and anthropogenic sources play an important role in the elevated mercury levels (Pacyna et al. 2010).

Mercury is regarded as a global pollutant because it is more susceptible for long-range atmospheric transport around the world than cadmium, lead and other class B metals. Mercury originates from both natural and anthropogenic sources. Natural sources are volcanoes and diffusion from ore. Anthropogenic emission sources have increased since the beginning of the industrial period towards the end of the 18th century (Fitzgerald et al. 1998). The main anthropogenic mercury sources are coal burning, metal mining, chlor-alkali and cement production, as well as ferrous and non-ferrous metal industry (Grigal 2002; Harmens et al. 2008; Fukuda et al. 2011; Pirrone et al. 2010).

There are both primary and secondary sources of mercury, which contribute to the global pollution. The primary source is mercury of geological origin that is mobilised, naturally or by human activities, and transferred to the atmosphere, where it is transported, condensed and deposited in soil. Fossil fuel burning, where mercury might be present as a contaminant, and mining are examples of primary sources of mercury. The secondary source of mercury is mercury emissions from the use of mercury in products and industry (Pacyna et al. 2010). This process exchanges mercury among surface reservoirs by using the atmosphere (Zhang et al. 2016; Driscoll et al. 2013). In lakes with no local mercury contamination, the long-range atmospheric transported mercury dominates (Fitzgerald et al. 1998). This includes Langtjern.

In some regions of the world, including Norway, there has been a reduction in the mercury emissions the last decades due to the number of policies and emission limits that have been established and enforced. Figure 2.2 presents the reduction in mercury emissions to air, soil and water in Norway from 1995 to 2017.

Asia still has large emissions from anthropogenic activity, and emission controls are highly needed in this region (Braaten et al. 2017). However, the surface lake sediments and forest floor in the Nordic region still have high mercury levels caused by Hg^0 that has been transported over long distances and deposited in our soil the past century (Munthe et al. 2007). Fish in south-eastern Norway show increasing mercury concentrations in fish, which could be a result of local or regional processes, for instance water chemistry, TOC content, temperature and trophic position (Braaten, Fjeld, et al. 2014). Further studies in the following years will investigate the fate of the pool of long-range transported mercury that has accumulated in the soils.

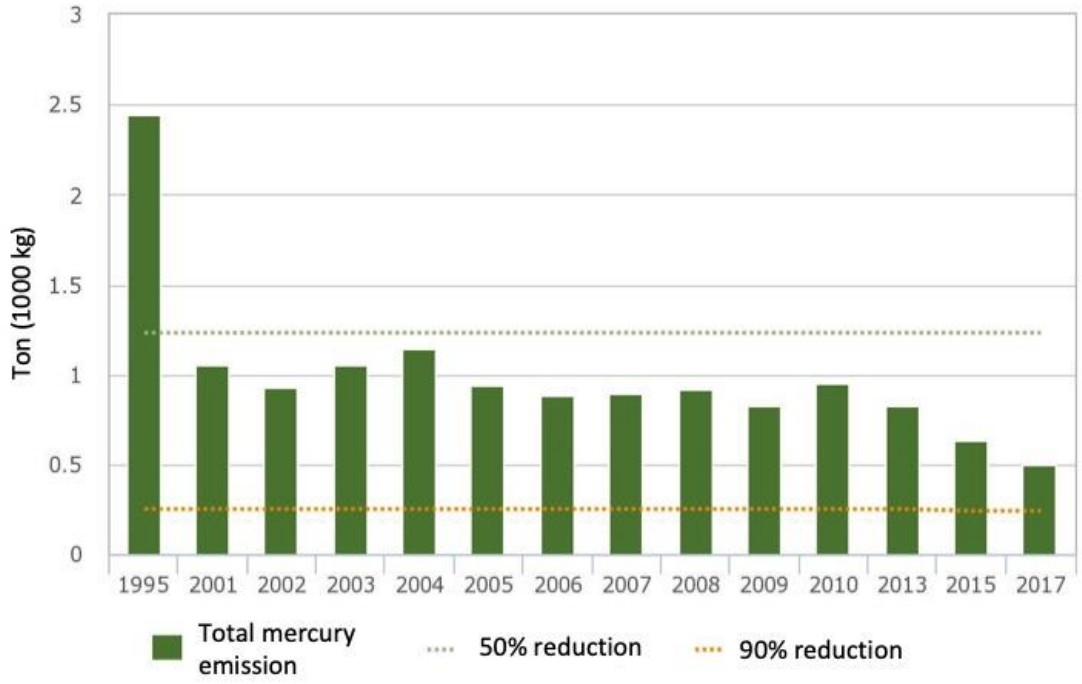

Figure 2.2: Mercury emissions in Norway to air, soil and water from all sources, including industrial emissions, municipal wastewater, products and production. It should be noted that there is a 6-year gap between bar 1 (1995) and bar 2 (2001). The graph is made by Miljødirektoratet (Norwegian Environment Agency)(https://www.miljostatus.no/kvikksolv).

2.4 Characterisation of DNOM using spectroscopic techniques

DNOM has a variety of functional groups that give the molecules specific properties that can be characterised using a variety of spectroscopic techniques. The optical properties that give the water a yellow-brown colour are related to conjugated double bonds. The absorbance of radiation by these chromophores can be measured to obtain information about the aromatic structure of DNOM. Ultraviolet radiation and visible light is the radiation at wavelengths between 100 and 700 nm. UV spectroscopy cannot be used to study the functional groups of DNOM directly, but it provides valuable information about the general structure of the organic matter in the sample.

Absorbance in the UV and visible region can be used to characterise the quality of the DNOM by means of spectroscopic proxies, such as the specific UV absorbance (sUVa), specific visible absorbance (sVISa) and specific absorbance ratio (SAR). sUVa is the UV absorbency at 254 nm relative to the amount of dissolved organic carbon (DOC), measured in mg L^{-1}. The proxy is a useful way to describe the relative amount of aromatic moieties in DNOM (Weishaar et al. 2003; Vogt and Gjessing 2008). A high sUVa corresponds to more aromatic character, and thereby generally a higher molecular weight and higher hydrophobicity (Leenheer and Croué 2003; Vogt and Gjessing 2008). The difference between sUVa and sVISa lies in the size. sVISa measures large aromatic systems that absorb light in the visible range.

Allochthonous material has generally a higher sUVa than the autochthonous DNOM. Specific visible absorbance (sVISa) is a similar proxy based on visible light instead of ultraviolet radiation, and it is defined as the absorbance at 400 nm relative to the concentration of DOC. Adsorption of radiation at higher wavelengths requires longer chains of conjugated double bonds. sVISa thus generally reflects the relative amount of larger molecular size aromatic moieties in the DNOM.

Specific absorption ratio (SAR) is defined as the UV absorbency at 254 nm relative to the visible absorbency at 400 nm. Reflecting the difference between the sUVa and sVISa addressed above, a higher SAR value corresponds smaller size, i.e. the absorbency is relatively greater at lower wavelengths than at higher wavelengths reflecting shorter chains of conjugated double bonds. SAR values are expected to be negatively correlated with molecular size (Hautala, Peuravuori, and Pihlaja 2000; Peuravuori and Pihlaja 1997).

2.5 Size fractionation of DNOM

The properties of DNOM compounds are greatly governed by their molecular sizes and structures. DNOM molecules can be divided into low molecular weight (LMW) and high molecular weight (HMW)

compounds. The LMW compounds include simple carbohydrates, amino acids and small organic acids. The HMW compounds include more complex carbohydrates and molecules with more aromatic character, and HMW compounds are generally known to be more refractory (Marschner and Kalbitz 2003).

Master studies conducted by Francés and Ong indicated that the majority of MeHg and totHg was complexed to the HMW DNOM fractions (Francés 2017; Ong 2018). This is also the fraction with the highest amount of DNOM. Since mercury binds to DNOM, the HMW fractions are expected to contain the highest mercury levels.

Methyl mercury bound to LMW DNOM fractions is known to be more bioavailable due to their small size. Previous studies have found a strong link between DOC concentration and MeHg concentrations (Poste et al. 2015; Grigal 2002). HMW DNOM is quite refractory, and the bioavailability of methyl mercury is expected to be reduced when it is bound to HMW DNOM. This way, DNOM both contributes to the transport of mercury, as well as serving to detoxify mercury, because it is mainly associated with the HMW DNOM fractions.

2.5.1 Tangential flow filtration

Tangential flow filtration is a method of fractionating DNOM in water samples according to the molecular sizes of the DNOM. The water was separated into high and low molecular weight DNOM fractions with a cut-off of 100 kDa. Organic molecules larger than 100 kDa will not pass through the membrane, and are thus defined as high molecular weight (HMW) fractions. This fraction is called concentrate. Low molecular weight (LMW) fractions, called permeate, are able to pass through the membrane, which means that they are smaller than 100 kDa.

In TFF, the samples flows parallel (tangentially) to the membrane. This is in contrast to dead-end filtration, where the feed stream passes the membrane perpendicularly. An advantage of using TFF is that the accumulation of particles on the membrane is reduced compared to dead-end filtration (Krzeminski 2016). Both methods are illustrated in Figure 2.3.

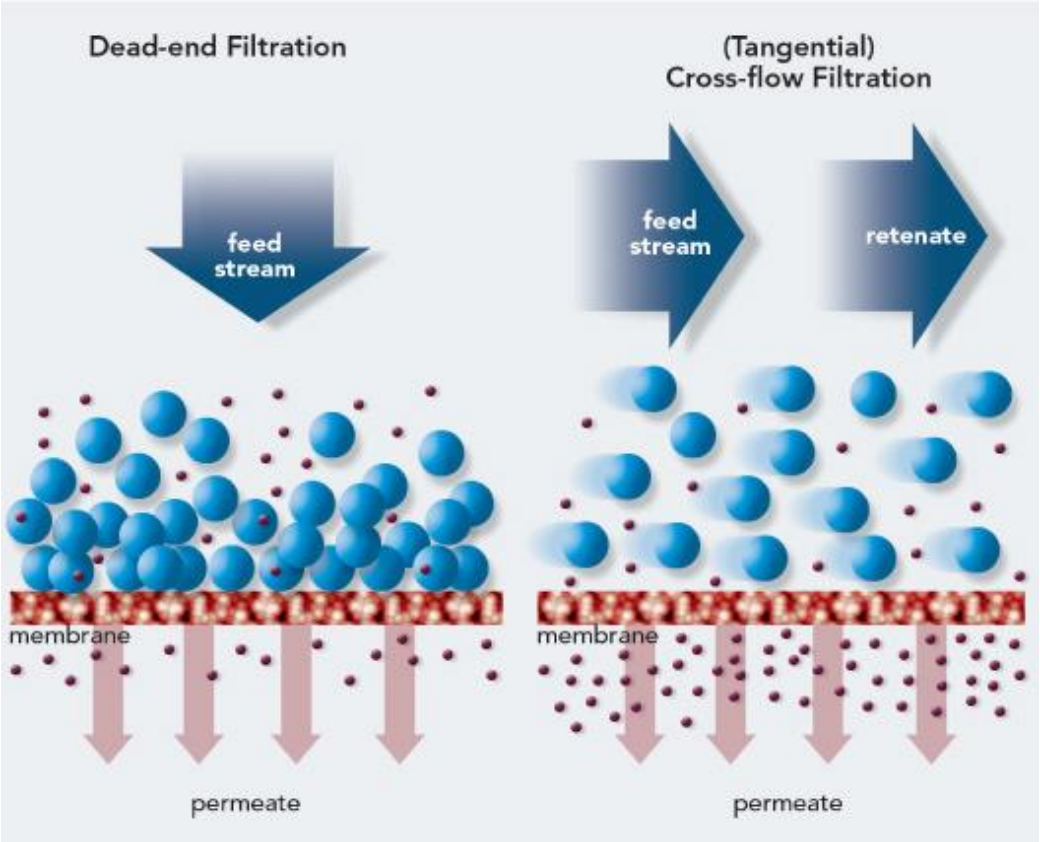

Figure 2.3: The concept of tangential flow filtration. The barrier between the dark blue and light blue part of the figure is the 100 kDa membrane. The arrows denote the transport of LMW organic compounds (winebusiness.com).

The system consists of a 50 L tank, an Alfa Laval GR40PP (100 kDa) membrane made of Polysulfone, and metal tubes directing the sample from the feed tank and around the system. The sample is pumped through the system by a Watson Marlow 701S peristaltic pump. Parameters such as conductivity, temperature and pH in the feed tank are monitored and the values are shown on a screen. The sample is transported from the feed tank to the membrane, which separates the sample into high and low molecular weight fractions. The fractions are then pumped through the tubes and can be collected separately. The instrument also has a recirculation mode, which recirculates the water back to the feed tank. This mode is mainly used for cleaning.

A great advantage of using TFF is that it allows for a large sample volume compared to e.g. ultrafiltration. In this case, however, the large volume needed is also a limitation, considering that the water must be manually carried from Langtjern. Another limitation of using TFF is the accumulation of material on the membrane surface, known as fouling. Fouling can disturb the measurement of compounds associated with colloids (Guéguen, Belin, and Dominik 2002).

2.6 Biodegradation

Natural organic matter is derived from plant and animal residues. When plants and animals die, their remains are decomposed and oxidized through biochemical processes, which are often facilitated by microorganisms. Microorganisms that are able to utilise pre-synthesised organic compounds, like DNOM, as a carbon source are called heterotrophs (vanLoon and Duffy 2011).

Biodegradation describes the process where organic matter is mineralised or partly oxidised and decomposed to smaller compounds by microorganisms. The term biodegradability describes to what extent the microorganisms are able to utilise the organic matter. Unfortunately, there is no standardised method for studying biodegradability of DNOM, and key parameters vary between studies. These parameters include incubation method and duration, nutrients added, temperature and initial DOC concentration (Marschner and Kalbitz 2003). Because of these different conditions, it is difficult to compare results from different studies.

Biodegradability can be determined by monitoring the bacteria's oxygen consumption using a PreSens 24-channel SensorDish® Reader (SDR), shown to the left in Figure 2.4. The 5 mL sensor vials are placed in the low-well plate on top of the SDR, as shown to the right in Figure 2.4. The vials are equipped with sensor spots at the bottom, allowing non-invasive oxygen monitoring. Figure 2.5 presents the basic principle of the sensors. The sensors contain luminescent dye that is excited and the luminescent lifetime, which depends on the partial pressure of oxygen, is then detected. The sensor response is converted to oxygen consumption by the software (PreSens 2016).

Figure 2.4: The 24-channel SensorDish Reader (SDR) is shown to the left. To the right, the SDR is shown fitted with a low-well plate and the 5 mL sensor vials (PreSens 2016).

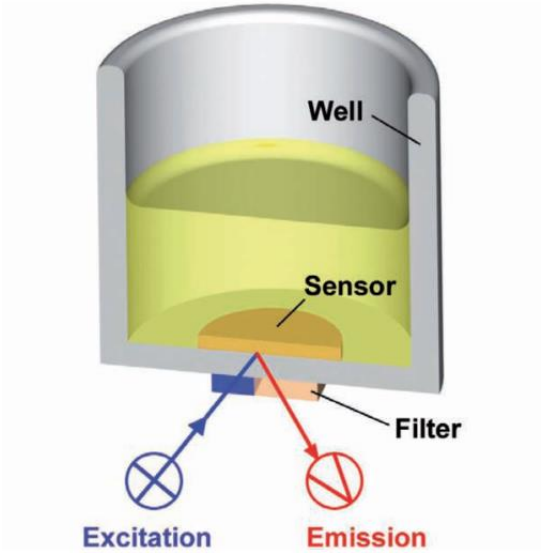

Figure 2.5: The sensor spots at the bottom of the sample vials contain luminescent dye that is excited (PreSens 2016)

DNOM can be classified into different groups based on how fast and easily they are biodegraded. There are three main groups: the labile pool, the slowly degraded pool and the recalcitrant pool. The labile pool of DNOM mostly consists of low molecular weight compounds, like simple carbohydrates and organic acids, amino acids and even small proteins. The slowly degraded pool contains larger carbohydrates (polysaccharides). The recalcitrant pool consists of compounds with more complex structures, like lignin degradation products, that are not easily cleaved by enzymes (Marschner and Kalbitz 2003).

A number of factors control biodegradability of DNOM. The most essential parameters are related to molecular size, structure and functional groups. Large compounds with a higher degree of aromatic character are generally known to be less biodegradable (Marschner and Kalbitz 2003). Availability of nutrients or toxic effects from present metals and other microorganisms can alter the ability of the microorganisms to biodegrade the DNOM. These factors can alter the chemical and physical environment in which the microorganisms facilitate biodegradation. Besides carbon, the most important nutrients are nitrogen and phosphate, in addition to sulphur and potassium (Marschner and Kalbitz 2003). Physical factors like temperature also influences biodegradability. These factors vary throughout the seasons, which thus causes the microbial activity to fluctuate and thereby also the production of DNOM.

2.7 Limnology

2.7.1 Turnover

Dystrophic lakes, such as Langtjern, have high inputs of refractory dissolved organic carbon (RDOC), and is characterised as humic. Because of this, less light penetrates the water and as a result, the primary production of the lake is low.

Lake water creates stable layers based on their temperature. The depth and temperature of the different layers vary among lakes with different climate and air temperature, depth and size of the lake (vanLoon and Duffy 2011).

The layer close to the surface is called epilimnion, and this water is heated up during the summer. At a certain depth the temperature decreases rapidly, and this middle layer is called metalimnion. Thermocline is the point in the metalimnion where the temperature changes the most. At Langtjern, the thermocline is usually found at a depth of 1-3 meters (de Wit et al. 2018). In the bottom layer (hypolimnion), the temperature is rather stable, although the temperature might decrease slightly toward the bottom. A figure showing the layers is shown in Figure 2.6.

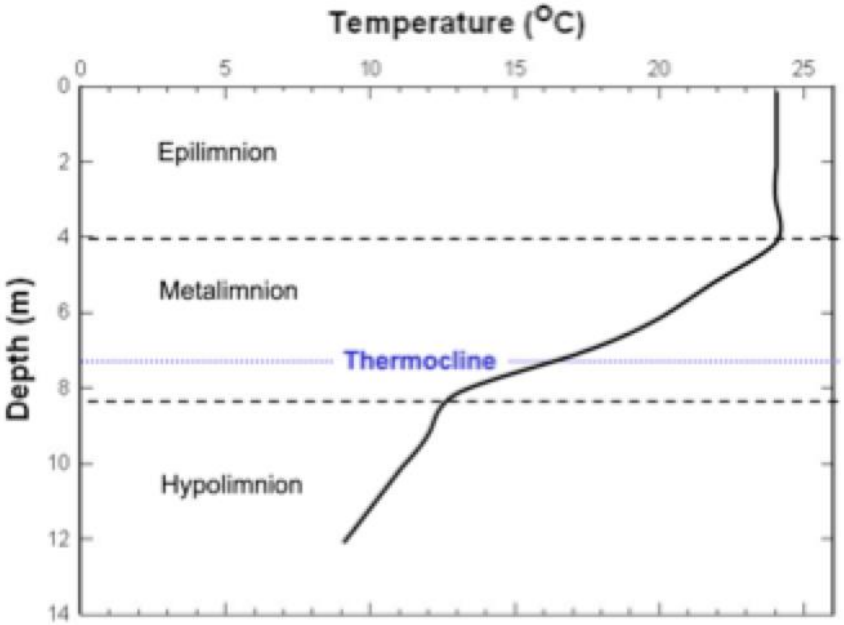

Figure 2.6: Temperature profiles in a lake. Although the main pattern in this figure is valid for Langtjern, it should be noted that Langtjern is a shallow lake and the depths on this figure are not correct. During the summer, the thermocline at Langtjern is usually at a depth of 1-3 meters (https://slideplayer.com/slide/8266865/).

During the summer, the surface water is warm and the temperature decreases towards the bottom. In the autumn, the temperature in the epilimnion decreases and the density increases. Water reaches its highest density at 4 °C. When the density of the surface water exceeds the density of the bottom water, the surface water sinks to the bottom, causing the bottom water to rise. This process is called the autumn turnover. After the turnover, the lake reaches a uniform temperature of 4 °C. Chemical and microbial activity is enhanced as a result of the turnover.

As winter approaches, the temperature in the epilimnion continues to decrease below the freezing point. Ice is formed on surface of the lake. The temperature right below the ice cover is close to 0 °C, and the temperature increases over a short depth downwards to 4 °C.

In the spring, the ice melts and the temperature in the epilimnion increases until it reaches the same temperature as the hypolimnion and the entire water mass is mixed again. The lake reaches a stable temperature of 4 °C, before the epilimnion is heated up by the sun. At this point, summer approaches and the cycle repeats.

2.8.3 Oxygen saturation

Oxygen saturation is high in the epilimnion during the summer because of a net high photosynthetic activity.

Figure 2.7 shows how the oxygen saturation (%) varies throughout the year of 2015 at depths of 1 and 8 meters in Lake Langtjern. The spring and autumn overturns are apparent around May 1st and October 1st, approximately, when the oxygen saturation at 8 meters (red dotted line) increases dramatically. This indicates that the water is mixed so that highly oxygen saturated water is moved from the surface to the bottom of the lake.

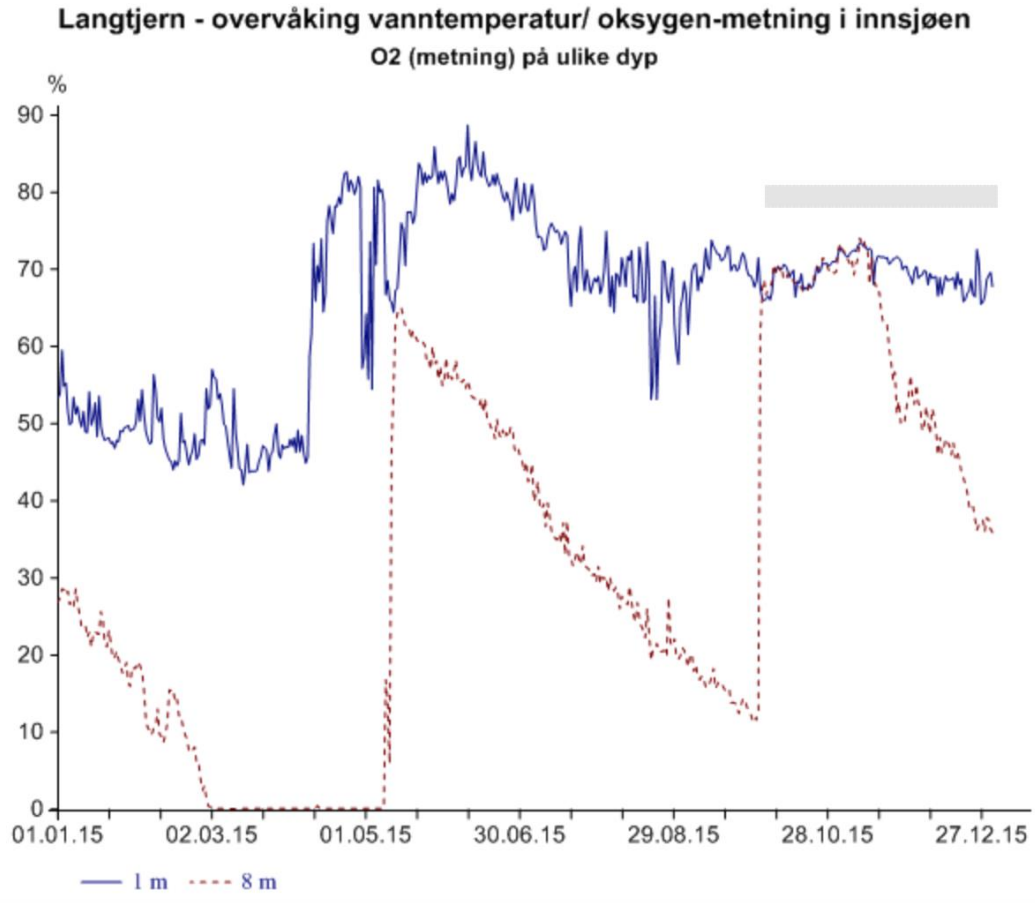

Figure 2.7: Oxygen saturation in Langtjern in 2015 (data from NIVAs monitoring station (aquamonitor.no/Langtjern)).

2.8 Data analysis

2.8.1 Analysis of variance

Analysis of variance (ANOVA) is, as the name indicates, analysis of the variances. A linear model is applied with experimental factors as input and an observed parameter as response. The variation related to each of the input factors are seen in relation to the residual variation, which is the variation that is not described by the input factors in the statistical model. ANOVA is a univariate method where one observed parameter at the time is tested. There may be multiple input factors, as in the present experiment, but one response parameter is tested at the time.

2.8.2 Multivariate analysis

Multivariate data analysis was performed by principal component analysis (PCA), which is a method that allows summarisation and visualisation of the information in a data set containing multiple inter-correlated quantitative variables (Kassambara 2017; Esbensen 2002). Important information can be extracted from a multivariate data table and be expressed as a set of few variables called principle components (or dimensions). These new variables correspond to a linear combination of the originals. The number of dimensions is less than or equal to the number of original variables.

The goal of PCA is to identify directions with the largest variances that describe the majority of the data with minimal loss of information.

An example of how PCA works is shown in Figure 2.8. Plot 1A shows two correlated variables in a coordinate system. PCA identifies the principal direction as the direction that shows the largest variance. This direction is called Principal Component 1 (PC1, also called Dimension 1). PC1 is then subtracted from the data, and the direction that captures the second most of the variation is identified as PC2. PC2 is always orthogonal to PC1. In plot 1B, the principal components are used as axes, and the original data is therefore rotated.

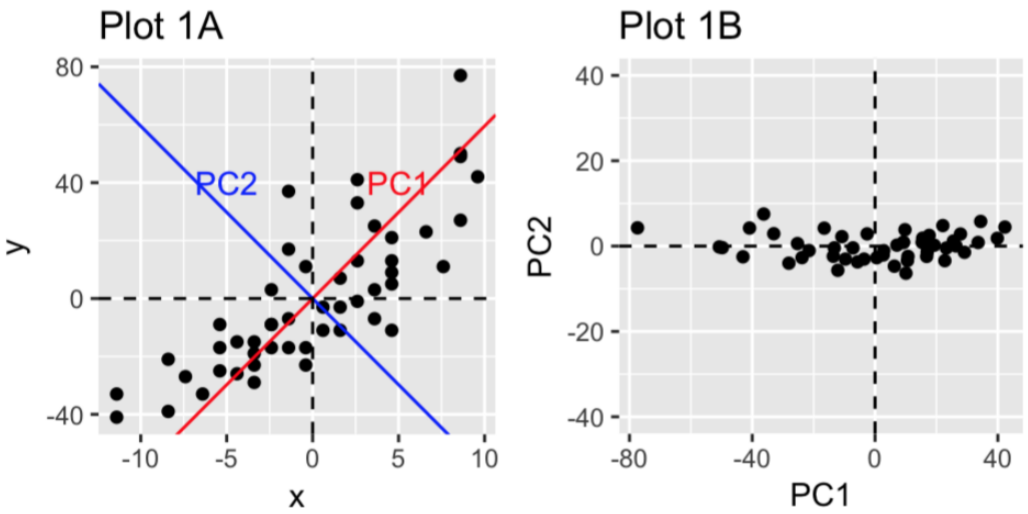

Figure 2.8: Illustration of Principle Component Analysis (PCA)(Kassambara 2017). A) Plot of two correlated variables. PCA first finds the direction in the data that shows the largest variance, called PC1. PC1 is then subtracted from the data, and the direction that captures the second most variation in the data is identified as PC2. B) The principle components are used as axes, which results in a rotation of the original data.

PCA compresses the variation so that it is easier to interpret the data, which is especially useful in data sets with many variables. In multivariate analysis, where several variables are correlated, the number of principal components that are relevant for interpretation is low compared to the number of original variables.

The results of PCA are graphically presented as plots of the samples (scores) and plots of the features (loadings). These plots are to be interpreted together. Features located in the loading plot in one direction are positively associated with samples located in the score plot in the same direction.

3. Materials and methods

3.1 Sample site

The samples were collected at the ecological monitoring site Langtjern, located in Buskerud (60°37'N; 9°73'E, 516 m a.s.l.). Figure 3.1 shows the catchment area, which has an area of 4.8 km^2 and consists of pine forest, wetlands and rock outcrop (NIVA 2017). Langtjern and the enclosing area have not been disturbed by human activities for more than 100 years, and is therefore an interesting study area. Lake Langtjern has a surface area of 0.227 km^2, a mean depth of 2 meters and a maximum depth of 12 meters.

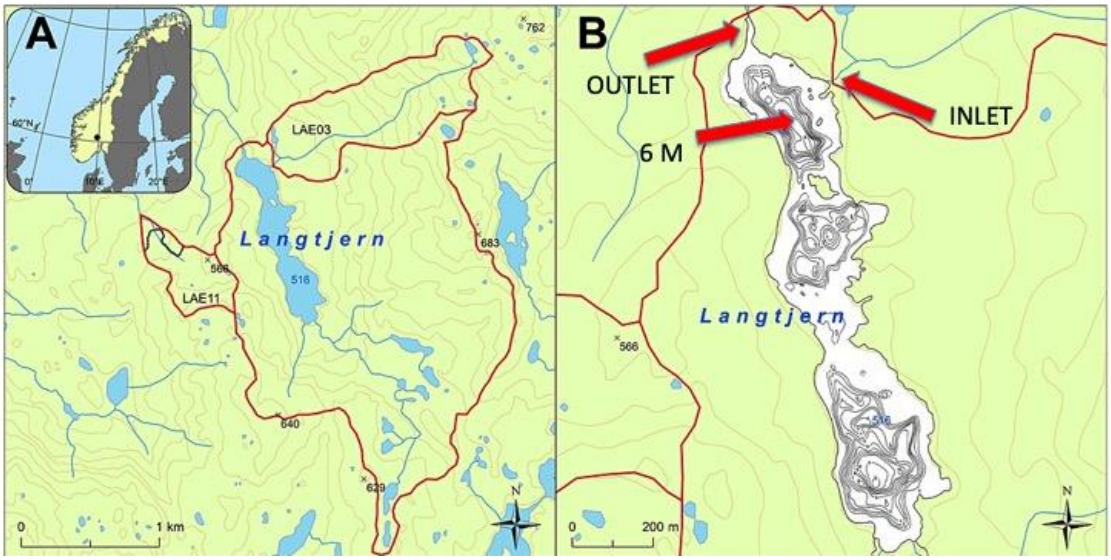

Figure 3.1: A) Overview of Langtjern catchment area. B) Lake Langtjern with contour lines indicating water depth (Couture et al. 2015). The red arrows indicate where the outlet, inlet and 6 m depth (hypolimnion) samples are collected.

Norwegian Institute of Water research (NIVA) has studied Langtjern since the 1970's. At that time, the effect of acid rain on water chemistry was the main aim of the studies. Since 2010, NIVA has extended the study site, and it is now a complete climate-monitoring site with monitoring instruments at the inlet, outlet and the middle of the lake, in addition a weather station (NIVA 2017).

Parameters that are monitored by NIVA at the inlet, outlet and by the buoy include water temperature at eight different depths, oxygen saturation, pH, conductivity, coloured dissolved organic matter

(CDOM), CO_2. The weather station measures water temperature, wind speed and direction, precipitation (mm), sunlight (W/m^2 per day) and humidity. The data presented as graphs can be accessed by anyone at www.aquamonitor.no/langtjern.

3.2 Sample collection

Three sets of samples were collected from Langtjern. The first set of samples was collected on May 30th, 2018. Late summer samples were collected on September 20th and fall samples were collected on October 17th, 2018, i.e. before and after the autumn turnover. In all three cases, 10 L were collected from the inlet, 10 L from the outlet, and 10 L from the middle of the lake at a depth of 6 meters. The latter is below the thermocline, and it was collected close to NIVAs monitoring buoy at the northern part of the lake. Weather conditions on the sampling collection dates can be found in Table 3.1. Pictures of the sample site can be found in the appendix, Section B.

Table 3.1: Weather conditions at Langtjern on the dates of sample collection. Data retrieved from http://www.aquamonitor.no/langtjern/.

Sampling date	Air temperature	Precipitation the preceding week	Sampling site	Water temperature
May 30th, 2018	15 °C	<1 mm	Inlet	7 °C
			Hypolimnion	5 °C
			Outlet	15 °C
September 20th	10 °C	23 mm	Inlet	9 °C
			Hypolimnion	7 °C
			Outlet	10 °C
October 17th	7 °C	1 mm	Inlet	7 °C
			Hypolimnion	6 °C
			Outlet	4 °C

For the sake of repeatability and comparison with previous results, the sample from the middle of the lake should have been collected at a depth of 8 meters. Unfortunately, the lake was not deep enough in May, and because of this, all the samples were collected at 6 meters, also in the late summer and fall. This is below the thermocline.

3.3 Sample pre-treatment

After collection, the samples were transported to the lab. Before and during transport, the samples were protected from sunlight and heat as much as possible, by keeping the samples in the shadow and inside a bag. The samples were stored overnight in a dark storage room with a temperature of 4 °C. Suction filtration was carried out the following three days, using a Büchner flask and Büchner funnel.

To remove the largest particles, the samples were first filtered using 0.7 μm glass microfibre filters from GE Healthcare Whatman™. Prior to filtration, any organic matter on the filters was burned off in a furnace for five hours at 450 °C. Approximately 2x50 mL of sample water was filtered first in order to remove any residue of carbon and to condition the filter. After throwing away this water, the rest of the 10 L sample water was filtered and collected in 10 L plastic containers, prewashed with a 10% HNO_3 solution. Due do gradual clogging of the filters, the filters were frequently replaced. Rinsing and conditioning of the filter were repeated for every new filter. Each filter was used to filtrate approximately 1 L of water, depending on the type of sample and filter. The outlet and hypolimnion samples were more highly coloured than the inlet sample, and the filters needed to be replaced more frequently.

After 0.7 μm filtration, the samples were filtered through a 0.2 μm cellulose acetate filters from Sartorius Stedim Biotech. This pore size was chosen because it sterilises the sample by removing the bacteria. Figure 3.2 presents the filters before and after filtration. Rinsing and frequent replacement of the filters resumed. Filtered water was collected in 10 L plastic containers prewashed with a 10% HNO_3 solution and rinsed thoroughly with type I water and sample.

Figure 3.2: Filters used to filter spring outlet samples. The filter to the right is a glass fibre filter before filtration. The filter in the middle is taken after filtering raw outlet water through 0.7 µm. The filter to the right is a cellulose acetate filter after filtration of 0.7 µm water through 0.2 µm.

After filtration, the samples were stored in a dark cold-room at 4 °C until analysis.

3.4 Tangential Flow Filtration

Tangential flow filtration (TFF) fractionates the dissolved organic natural matter (DNOM) in the water samples into high and low molecular weight DNOM compounds. Fractionation was conducted at NIVA using a KWR Watercycle Research Institute membrane testing apparatus.

In 2017, Francés conducted an experiment to find the optimal cut-off for Tangential Flow Filtration (TFF)(Francés 2017). According to her studies, a 10 kDa cut-off was too small for this purpose because the DOC analysis suggested that there was no significant amount of DNOM below 10 kDa. The DOC concentration was close to the limit of detection (LOD) and lower than the limit of quantification (LOQ). However, according to a review study by Perdue and Ritchie, approximately 50% of DOC should be smaller than 10 kDa (Perdue and Ritchie 2003). Francés continued with a cut-off of 100 kDa, which seemed more suitable according to her results. For that reason, 100 kDa cut-off was also used in this study. An Alfa Laval GR40PP (100 kDa) membrane made of Polysulfone was used.

The three sets of samples collected from the inlet, outlet and at 6 meters depth in the lake, respectively, were size fractionated after 0.2 µm filtration. For each of the three sample types (inlet, outlet and 6 meters), three biological replicates were collected. The first and third replicate had smaller volumes than the second, and were mainly used to check the system precision. For each of the two smaller replicates, approximately 0.35 L of permeate and concentrate are collected, while for the larger replicate (here called sample), 1 L of permeate and concentrate are collected. 0.5 L of the sample

water is also used to flush the system before fractionation, and this volume was discarded. DOC is measured in all of the three replicates, but all other analyses are only conducted on the 1 L sample.

As a part of installation of the membrane and starting a new fractionation, the system was first cleaned with a 0.2% Na-EDTA and NaOH alkaline wash. This procedure removes the protective coating material on the membrane surface, and the pH is adjusted to 8.5-10.5. The membrane was then physically compacted by running Reverse Osmosis (RO) water through the system at 10 bar for approximately 16 hours. The RO water used in this experiment is type II water, which is double filtered by ion exchange and reverse osmosis. After compaction, RO water was used to rinse the system before fractionation and between the replicates. The RO water was then flushed for half an hour in order to remove residual carbon in the system, followed by a membrane performance test to ensure optimal flow rates and high membrane performance. This test is carried out by running RO water through the system at different pressures using flush mode, and collecting both the “permeate” and “concentrate”. After collecting for 5 minutes, the volumes are measured, and the test is repeated once with the same pressure before testing with a different pressure. Usually, the pressures tested are 7, 5, 3 and 1 bar, subsequently.

Before each replicate, RO blanks were collected from the feed tank, permeate tube and concentrate tube and their carbon contents were analysed in order to detect any contamination in the system.

After the RO water was drained, sample was added to the feed tank. The system was flushed with the sample for 5 minutes at a pressure of 7 bar, which results in a waste volume of approximately 0.5 L. Flushing rinses the tubes and membrane by removing RO water remains. Ideally, the system should be flushed for 30 minutes, but due to a limited sample volume, recirculation mode was used to reduce the amount of waste. The system was allowed to recirculate for 30 minutes. After recirculation, the desired volumes of permeate and concentrate were collected. The remaining sample in the feed tank was drained and the waste volume was measured. Before fractionating a new replicate or sample, the system was cleaned again by adding new RO water, flushing and conducting a new membrane performance test.

After one whole sample (outlet, inlet or 6 m), the membrane was replaced and the membrane installation procedure was repeated. A used membrane is shown in Figure 3.3.

Figure 3.3: Alfa Laval GR40PP Polysulfone filter after filtration.

3.4.1 Investigating the effect of using different filtrate volumes.

Previous studies have indicated that the distribution of low and high molecular weight fractions, using a 10 kDa cut-off, is close to 50/50. Using a 100 kDa cut-off, the distribution is approximately 30/70 (Perdue and Ritchie 2003). In previous master studies using TFF as a fractionation method, no significant amount of DNOM was found below 10 kDa, and when using a 100 kDa membrane, the LMW counted for only 5.5% in the inlet and 14.3% in the outlet samples (Francés 2017). There has been considerable uncertainty related to the effect of this method used for filtrating a limited amount of sample. An experiment was thus conducted using water from lake Maridalsvannet, and the results are presented in this section as a control of the procedure. The purpose of the experiment was to investigate the effect of increasing the filtrate volume from 0.5 L to 1.0 L and 1.5 L, and to see whether the fractionation method itself affects the DOC results.

50 L of water was collected from the uppermost reaches of river Akerselven near Frysja in Oslo. This river flows from lake Maridalsvannet. Within hours after collection, the water was filtrated in the same manner as the Langtjern water, subsequently through 0.7 μm and 0.2 μm filters. Filtration took three days. After filtration, the water was bulked into a 50 L container and brought to NIVA. The experiment was conducted using an Alfa Laval GR40PP (100 kDa) membrane made of Polysulfone. This is the same type of membrane as used previously, as described in section 3.4. Section 3.4 also describes membrane pre-treatment, and the same method is used here.

Three different volumes of LMW (permeate) and HMW (concentrate) were tested: 0.5 L, 1.0 L and 1.5 L. Three replicates were made of each volume, so that each volume was tested three times. For all samples and replicates, the input volume was 4.5 L, and 0.5 L was used to flush the system before fractionation. After flushing, the desired volume (0.5, 1.0 or 1.5 L) was collected. The setup is presented in Figure 3.4.

Membrane pre-treatment, overnight compaction and a membrane performance test using RO water were performed as described in section 3.4, followed by collection of RO water samples from the feed tank for DOC analysis. The RO water was drained and the first 4.5 L sample was transferred to the feed tank. First, 0.5 L of sample was used to flush the system and this volume was discarded. The sample was then recirculated in the system for 30 minutes before sample collection started. 0.5 L of LMW and 0.5 L of HMW were collected in separate beakers and transferred to brown bottles. This procedure was repeated twice in order to obtain three replicates of 0.5 L filtrate. Between each replicate, the sample was drained and another 4.5 L sample was added directly without flushing with RO water.

Next, three replicates of 1.0 L samples and three replicates of 1.5 L samples were collected using the same procedure. However, the collection of the 1.5 L samples occurred the next day, so the system was flushed overnight with RO water. A membrane performance test was performed before collection of 1.5 L samples. RO water blanks were also collected to ensure a clean system.

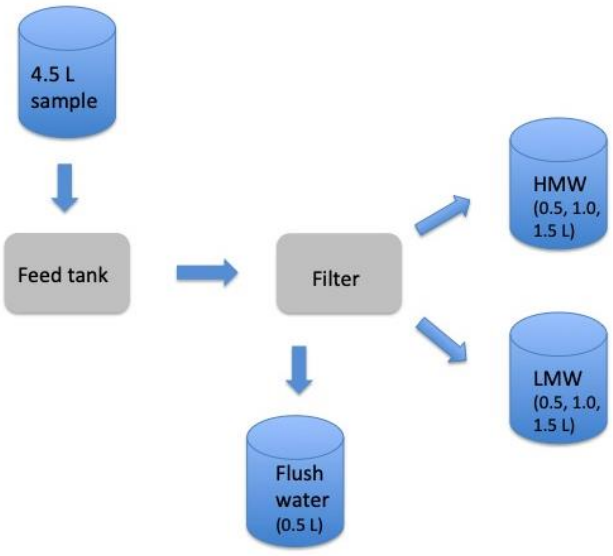

Figure 3.4: Sketch showing the principle of the fractionation method. For each of the three volumes being tested (0.5, 1.0 and 1.5 L), three replicates were run. In each case, 4.5 L of sample was added to the feed tank and 0.5 L was used to flush the system. After collecting the desired volume of LMW (permeate) and HMW (concentrate), the remaining sample was drained and discarded.

All blanks and samples were stored in a dark room with a temperature of 4 °C until analysis.

3.4.1.1 DOC

Dissolved organic carbon (DOC) was measured at the Institute of Biosciences, UiO, using the Shimadzu instrument TOC-V_{CPH} with an ASI-V automatic sampler. The analysis was conducted in accordance with the ISO 8245 method (1999). Potassium hydrogen phthalate standards were prepared and used to make a calibration curve, shown in the appendix, section B.

Non-Purgeable Organic Carbon (NPOC) was the instrument setting used in this analysis. The samples were first acidified by adding HCl, followed by combustion of DOC to CO_2 at 680 °C using a titanium oxide catalyst. This CO_2 is measured by a non-dispersive infrared (NDIR) detector.

KH-phthalate standards were used to create the calibration curve, and the preparation is described in the appendix, section B.1.

3.4.1.2 Spectrophotometric DNOM quality proxies

Absorbance was measured in order to detect structural changes in the DNOM of the filtrate when changing the filtrate volume. This was conducted at wavelengths 200-800 nm using a Shimadzu UV-1800 spectrophotometer with 1 cm quartz cuvettes. Instrument specifications can be found in the appendix, Section G. Two cuvettes containing type I water were used to perform background correction, and one of the cuvettes was kept as a reference during the analysis for the samples.

Based on the absorbances at 254 and 400 nm, as well as DOC concentrations, specific UV absorbance (sUVa), specific visible absorbance (sVISa) and specific absorption ratio (SAR) were calculated. These values reveal information about the collective size, structure and aromaticity of the DNOM material, as described in Equation 1, 2 and 3 show how these values are calculated.

$$sUVa = \frac{Abs(254\ nm)}{DOC} \cdot 100 \qquad (1)$$

$$sVISa = \frac{Abs(400\ nm)}{DOC} \cdot 100 \qquad (2)$$

$$SAR = \frac{Abs(254\ nm)}{Abs(400\ nm)} \cdot 100 \qquad (3)$$

In Figure 3.5, DOC concentrations are shown along with sUVa, sVISa and SAR values. sUVa and sVISa decreases with decreasing molecular size, while the SAR values show the opposite trend. However, there was no significant effect of volume. This indicates that although the volume increases, the structure of the DNOM remains stable.

The DOC concentration of HMW is higher than for LMW, but there is no significant effect of increasing the volume. Additionally, the amount of LMW is similar to the amount of HMW. This is in agreement with literature, and it indicates that for the water that is actually transported from the feed tank to the membrane, the separation method seems to works quite well.

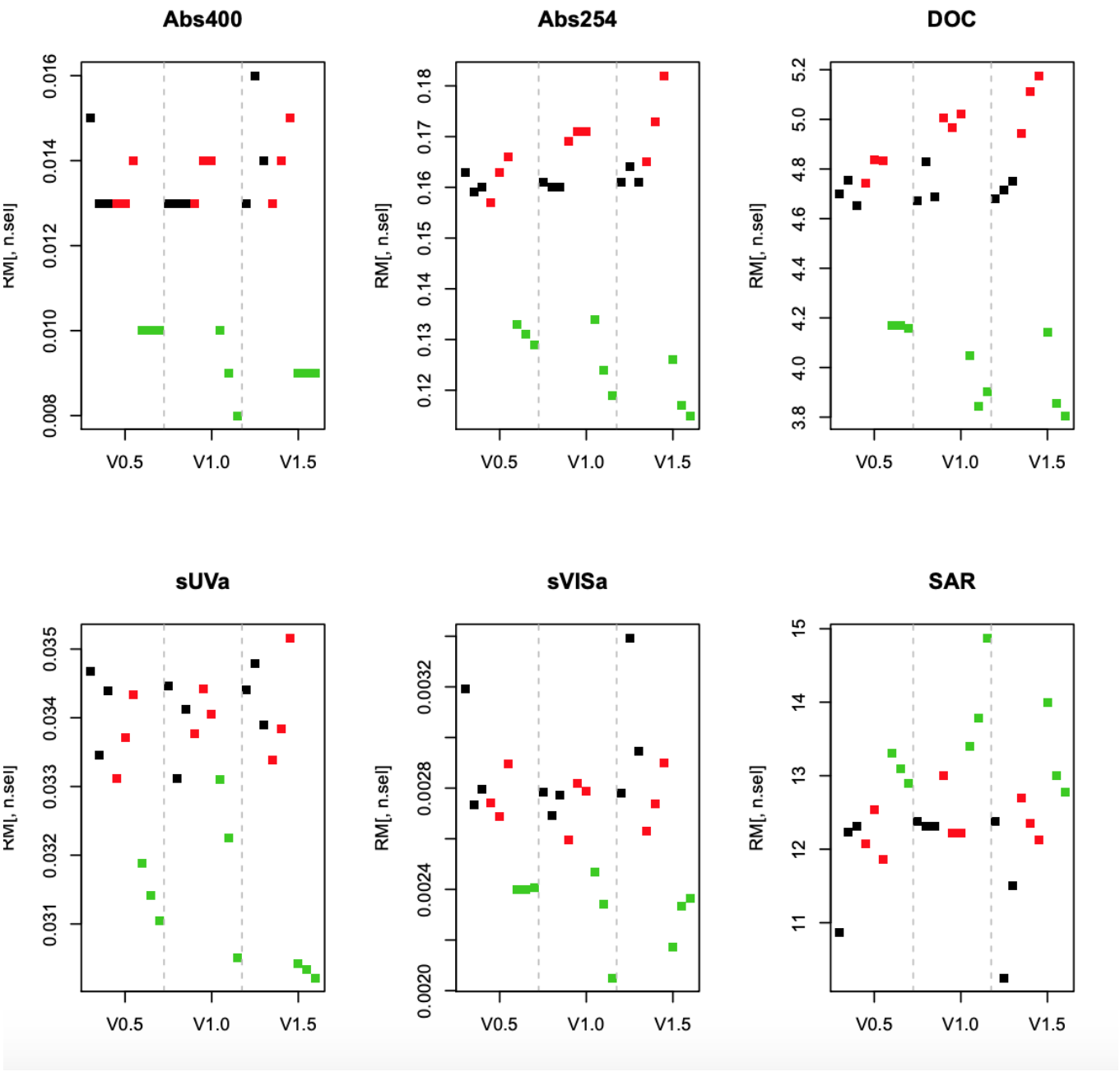

Figure 3.5: DOC concentration depends on the fraction. 0.2 µm (black) and HMW (red) fractions have higher concentrations than the LMW (green) fraction. sUVa and sVISa are lower for the LMW fraction than for the HMW and 0.2 µm fraction, while SAR increases with decreasing molecular weight of the DNOM.

DOC, sUVa, sVISa and SAR values all indicate that there are no significant differences in the DNOM structures or concentration as the filtrate volume changes, which indicates that the DNOM structure remains stable when the volume changes. This means that the data obtained from the Langtjern samples are representable for DNOM structure, and hence, they can be used to study the properties of DNOM.

3.5 Biodegradability

In a previous study (Håland 2017) different incubators and incubation methods were tested while the experiment was conducted at room temperature. After encountering problems reaching a stable temperature due to temperature variations during the day, the experiment was moved to an incubator in a cold-room. This method worked well, and therefore, this method is also used in this thesis.

Biodegradation was measured by monitoring oxygen consumption over time during sample incubation using a PreSens 24-channel SensorDish® Reader (SDR), as described in section 2.6. Immediately before the measurements of biodegradability, the sterilised sample (i.e. filtered through a 0.2 μm filter) was added an inoculum containing a nutrient stock solution and a culture of bacteria grown on the raw water sample. Glucose was used as a reference material.

Nutrient stock solution

Phosphorous and nitrogen were chosen as nutrients in this solution. Phosphorous has a key role and is usually the limiting nutrient in freshwater systems, in terms of limitation of primary production of the ecosystem (Correll 1999). It is essential in nucleic acids and in the metabolism, as adenosine triphosphate. Nitrogen is also of high importance as a limiting nutrient. Significant synergistic effects of nitrogen and phosphorous combined, as well as addition of nitrogen or phosphorous alone, have strong effects on freshwater systems (Elser et al. 2007).

Phosphorous and nitrogen were added as K_2HPO_4 and NH_4NO_3, and a 10 mM stock solution was prepared (Appendix, H.1). 10 mM is the concentration used in previous master studies after different concentrations and nutrient ratios were tested (Håland 2017). The nutrient stock solution was added both to the inoculum and to the sample solutions, as presented in Table 3.1.

Inoculum

Inoculum was prepared using raw water (not filtered) from Langtjern, containing the lake's original bacteria. Approximately 125 mL raw water was suction filtered through a Merck Isopore™ 2.0 μm membrane filter. The purpose of using this pore size was to sterilise the samples by removing microorganisms larger than bacteria. The filtered water was transferred to a 250 mL Erlenmeyer flask.

This volume is double the volume of the water, which leaves enough oxygen in the flask for the bacteria to grow. 250 μL nutrient solution was added to the flask to enhance bacterial growth. Aluminium foil was used to cover the flask in order to avoid algae growth. The flask was then left on a shaker at moderate speed for 48 hours at room temperature.

Glucose solution

A 10 mg $C \cdot L^{-1}$ glucose solution is used as reference. Its chemical properties are thoroughly documented and it has a high and predictable bioavailability (Maier and Pepper 2015).

Sample vials and PreSens

Four 50 mL volumetric flasks were used to prepare the solutions. The four bottles contain the same amount of inoculum and nutrient solution, but differ in the type of sample they contain: glucose (reference), inlet, outlet and 6 m, respectively. The contents of the flasks are presented in Table 3.1.

Table 3.1: Content of the four volumetric flasks used to prepare the biodegradation solutions.

Flask 1	**Flask 2**	**Flask 3**	**Flask 4**
500 μL inoculum			
500 μL nutrient solution			
49 mL glucose	49 mL inlet	49 mL outlet	49 mL 6 m

Each solution was transferred to four 5 mL sample vials to create four replicates. Also, four replicates of Type I water were used as blanks. The blanks are used to account for instrumental drift and to monitor temperature fluctuations or other factors that will affect all vials.

The 5 mL vials were over-filled to create a convex meniscus to make sure there was no air in the vial. Caps were put on and parafilm was used to seal the gap between the cap and the vial. After sealing, the vials were placed on the SDR and placed in the incubator.

Incubation

During the experiment, the samples were kept in a VWR INCU-line IL 56 Prime incubator, The incubator and the computer running the software were kept in a storage room with a temperature of 4 °C to ensure a stable temperature. The 5 mL vials containing samples were fitted on top of the SDRs and the software was started up. Parameters such as time interval, oxygen unit and incubator temperature were set according to section H.2 in the appendix, and the experiment was started. A time interval of 15 seconds was used. The experiment was allowed to run for approximately five days with the incubator temperature set to 25 °C.

After the biodegradation experiment, the data was processed using R to obtain the respiration rates. The R script was the same script as used in previous master studies (Ong 2018; Francés 2017). It is assumed that respiration rate is concentration dependent, and the respiration rates were therefore divided by the DOC concentrations in order to account for the differences in respiration rates in DNOM with different structure and aromaticity. The HMW fractions have higher DOC concentrations, and this fraction is less easily biodegraded by bacteria than the LMW fraction (Guggenberger, Zech, and Schulten 1994; Qualls and L. Haines 1992; Marschner and Kalbitz 2003).

3.6 DOC

DOC was measured in accordance with the ISO 8245 method (1999), using the same procedure as described in section 3.4.1.1. The calibration curves of the spring, late summer and fall samples are shown in section C in the appendix.

DOC was measured as a proxy fro DNOM in all samples, all replicates and all blanks, including all size fractions (0.2 μm, LMW and HMW). Only the large volume replicates were used for other analyses. Limit of detection (LOD) was calculated as 0.307 and limit of quantification (LOQ) was calculated as 1.02.

3.7 Total mercury

Total mercury (totHg) was analysed at NIVA using cold-vapour atomic fluorescence spectroscopy (CVAFS), according to EPA 1631 protocol (2002). Brooks Rand Labs MERX automated system with model III atomic fluorescence detector is the instrument that was used.

All mercury in the sample was oxidized to Hg^{2+} with BrCl, as shown in the reaction in Equation 4.

$$Hg^{2+} + Br^{+} \rightarrow Hg^{2+} + Br^{-} \qquad (4)$$

Hydroxylamine hydrochloride (NH2OH·HCl) was then added to destroy free halogens, which can interfere with the analysis (EPA 2002). In the next step, Hg^{2+} was reduced to volatile Hg^{0} with $SnCl_2$, shown in Equation 5.

$$Hg^{2+} + Sn^{2+} \rightarrow Hg^{0} + Sn^{4+} \qquad (5)$$

Hg^{0} was then separated from solution by purging with purified N_2, and it was then collected in the sample trap at room temperature. The sample trap contains gold-coated silica sand, and Hg^{0} binds to the gold. To release Hg^{0}, the sample trap was heated to 450 □C, and Hg^{0} was transferred to and collected in the second gold trap, i.e. the analytical trap. Heating of the analytical trap caused Hg^{0} to be released and carried by argon gas to the cell of cold-vapour atomic fluorescence spectrometer, where it was detected at 253.7 nm (Harris and Lucy 2016).

3.8 Major anions

The concentration of fluoride (F^-), chloride (Cl^-), phosphate (PO_4^{3-}) and sulphate (SO_4^{2-}) and nitrate (NO_3^-) were determined by ion chromatography at the Department of Chemistry, UiO, using a Thermo Fisher Scientific Dionex Integrion HPIC™ instrument with a Dionex™ AS-DV autosampler, a Dionex™AG18 guard column and AS18 separation column. The instrument was operated using the Thermo Fisher Scientific software Chromeleon 7.

An eluent is pumped through the system in order to separate the sample ions. The autosampler injects the sample into the eluent stream and is pumped through the column, where the ions are separated based on their charge, radius and interaction with the ion exchange sites (Thermo-Fisher 2016). The stationary phase in the column is positively charged and can interact with the negatively charged anions. Stronger interaction results in a longer retention time. After moving through the column, the eluent and sample move through a suppressor, which decreases background noise and enhances sample detection. Ions are identified based on their retention time, and the chromatogram peak areas

and heights are compared to the peaks produced by the standard solution. Peak areas are used to determine ion concentration.

Calibrations curves for each ion were created by preparing calibration solutions from a Dionex Seven Anion Standard solution. The calibration curves are presented in the appendix, Section D.

Charge contributions from organic acid (DNOM-A^-) was determined using a model from 1983 (Oliver, Thurman, and Malcolm 1983).

3.9 Major cations

Calcium (Ca^{2+}), magnesium (Mg^{2+}), sodium (Na^+) and potassium (K^+) concentrations were analysed at the Department of Chemistry, UiO, using Inductively Coupled Plasma Optical Emission Spectrometry (ICP-OES). The analysis was carried out according to ISO 22036 (2008) using a Varian Vista AX CCD simultaneous ICP-AES instrument with axial viewing. The instrument is equipped with a cone spray nebuliser and a Sturman-Masters spray chamber.

The sample is introduced to the instrument through a narrow tube, and a peristaltic pump transports the liquid to the nebuliser. The nebuliser converts the liquid sample into mist, while the mist droplets that are too large are removed in the spray chamber. The mist is then introduced to the plasma created by argon gas, which holds a temperature of 6000 K. The sample mist collides with the ions and electrons in the plasma, and the sample is thereby converted to ions. Their electrons reach an excited state, and they emit photons at specific wavelengths when they return to their ground state. This emission is detected by the instrument.

All samples and blanks were nitric acid and caesium. Nitric acid is added to preserve the samples, and caesium works as an electron donor. 0.2 mL of a solution containing 65% nitric acid and 5% caesium was added to the samples and blanks to a total volume of 20 mL. Nitric acid and caesium were also added to the standards so that they contained the same percentage by volume as the samples and blanks.

Prior to analysis, standards with increasing cation concentrations were prepared in order to create a calibration curve. The standard concentrations and calibration curves are presented in the appendix, Section E, in addition to the instrument settings. After creating a calibration curve, three blanks were analysed in order to ensure a clean system. Blanks were also analysed between every third sample throughout the whole sample sequence to ensure that there is neither carry-over nor drift in the

baseline of the signal from the instrument. In addition to the blanks that were analysed, the system was rinsed between every sample by placing the tube in Type I water and pumping water through the system for approximately 30 seconds. This rinsing process was not analysed.

3.10 Spectrophotometry

Absorbance was measured using a Shimadzu UV-1800 UV-VIS spectrophotometer, according to the procedure described in section 3.4.1.2.

Based on the obtained absorbance and DOC values, specific UV absorbance (sUVa), specific visible absorbance (sVISa) and specific absorption ratio (SAR) were calculated. Equation 1, 2 and 3 in section 3.4.1.2 were used to calculate these values.

3.11 pH and conductivity

The pH of the raw water, filtered water (0.2 μm), concentrate and permeate were measured according to ISO 10523. A Thermo Scientific Orion™ DualStar™ pH/ISE Dual Channel Benchtop Meter with an Orion™ ROSS Ultra™ pH electrode were used for this purpose. This electrode is a combination electrode that combines the glass electrode and the reference electrode. pH is measured by measuring the potential differences between the two electrodes.

Conductivity was measured using a Mettler-Toledo FiveGo™ conductivity meter and an LE703 conductivity probe, according to ISO 7888 (1985). Prior to measurement, the instrument was calibrated using an 84 $\mu S \cdot cm^{-1}$ calibration solution. Conductivity is a measure of the current conducted by ions in the sample of interest.

3.12 Data analysis

3.12.1 Experimental design

In the present thesis, three effects were studied: collection season (spring, late summer and fall), lake position (inlet, outlet and hypolimnion (6 m)) and DNOM size fraction (0.2 μm, HMW and LMW). All combinations of these three factors were included, which leads to a full factorial three-way factorial

experimental design. There were no replicates of the sampling in the lake. The total number of samples were 3*3*3=27 samples.

3.12.2 Univariate analysis

Statistical validation is performed by analysis for variance (ANOVA) where the experimental factors, season, sampling site and fraction and their interaction terms, are used as input in the model. The statistical interaction effects imply a test to validate if the effect of one factor is different for different levels of another factor. The residual of the model is used as estimation of the experimental error by ANOVA.

Replicates were taken for the laboratory analysis and used for quality assessment of the quality of the laboratory test. As these replicates were not sampling replicates taken as new samples in the lake these replicates can not be used for validation of the effects of the experimental factors.

The p-value obtained from ANOVA was adjusted for multiple comparisons by false discovery rate (FDR) adjusted p-value, which imply that the number of false positives is limited to a given percentage of the features claimed to be significant. The ANOVA with adjustment of the p-values were performed for all ions simultaneously and for the other parameters. Results are presented as the topic are presented in the text.

For visualisation of the results, line plots with whiskers are plotted of significant observations. The whiskers in the plot are one standard deviation of the variation within each data point. The line plots display means of two of the experimental factors. One series of plots display the season (Spring, Late Summer and Fall) along the x-axis with the fractions (o.2µm, HMW and LMW) as different lines in the plot. Whiskers are in this plot displayed as the standard deviation across the three sampling sites in each data points. Similarly, a series of plots display the sampling site along the x-axis with the fractions as different lines in the plots. Whiskers are in these plots displayed as the standard deviation across the three seasons in each data points. ANOVA was performed

Principal component analysis (PCA) were performed where all observations were standardised by mean cantering and standardised to unit variance to allow all variables to have the same impact on the model. All data analysis were performed using R, version 3.5.2 and R studio, version 1.0.153.

4. Results and discussion

4.1 pH

pH of the raw samples compared to the pH values of the samples filtered through a 0.2 μm membrane filter are presented in Figure 4.1. The pH values of the filtrated samples were lower than expected. This indicates contamination of the samples, likely as a result of inadequate rinsing of the sample containers. A 10% nitric acid solution was used to clean the sample containers. Although the containers were thoroughly rinsed with type I water, followed by rinsing with sample multiple times, the obtained pH values suggest that some nitric acid was still remaining in the container. This is confirmed by the high nitrate values obtained in the ion chromatography analysis, as further discussed in Section 4.2. Based on the pH and nitrate values, it appears that the late summer (September) samples are more contaminated than the other samples. The raw samples showed pH values close to the expected values and to the values reported by NIVAs AquaMonitor (aquamonitor.no/langtjern/). According to the AquaMonitor, the pH was 5.3 on the sampling day in the spring, 4.8 in the late summer and 5.1 in the fall. Raw samples were kept in fluoropolymer bottles. These bottles were also cleaned with nitric acid, but the bottles are smaller and easier to rinse. This will be further assessed in Section 4.2.

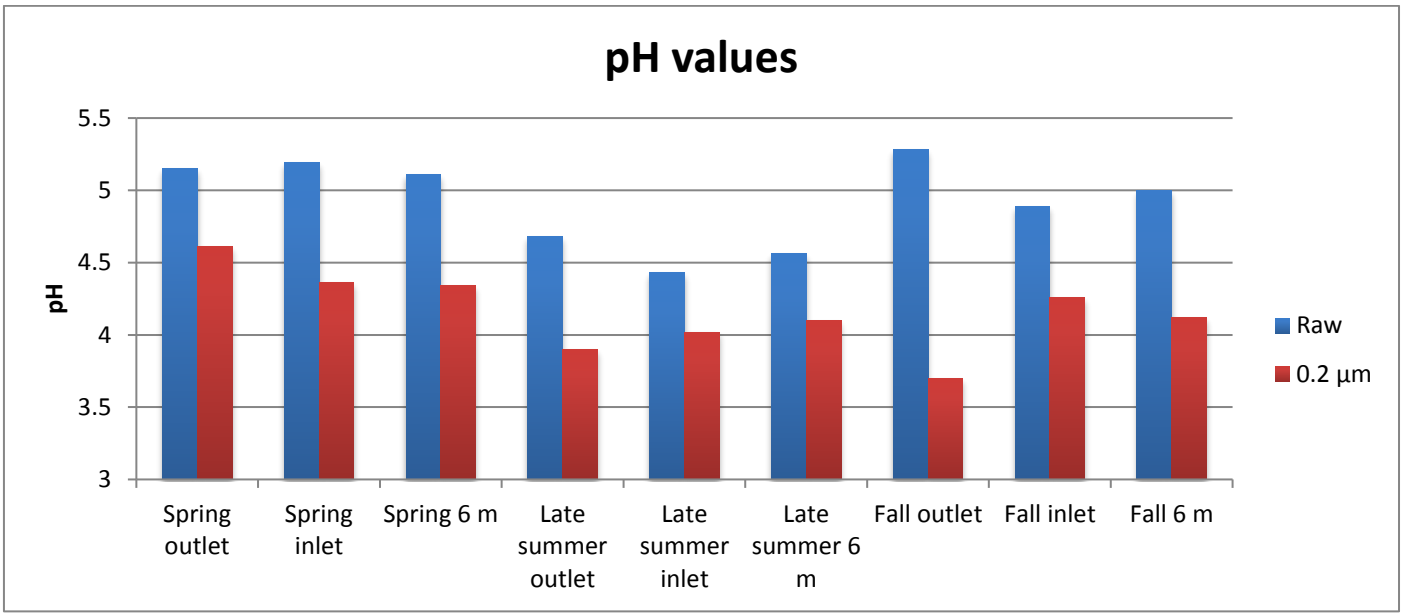

Figure 4.1: pH values of the raw samples compared to the 0.2 µm samples.

In Figure 4.2, the pH values of the 0.2 µm fractions are compared to the pH in the low molecular weight (LMW) fractions. Generally, the LMW pH values are slightly higher than the 0.2 µm fraction pH values, but this difference is not significant ($p>0.05$). It was suggested that humic acids are removed from the sample, which may be the cause for the higher pH value in the filtrate.

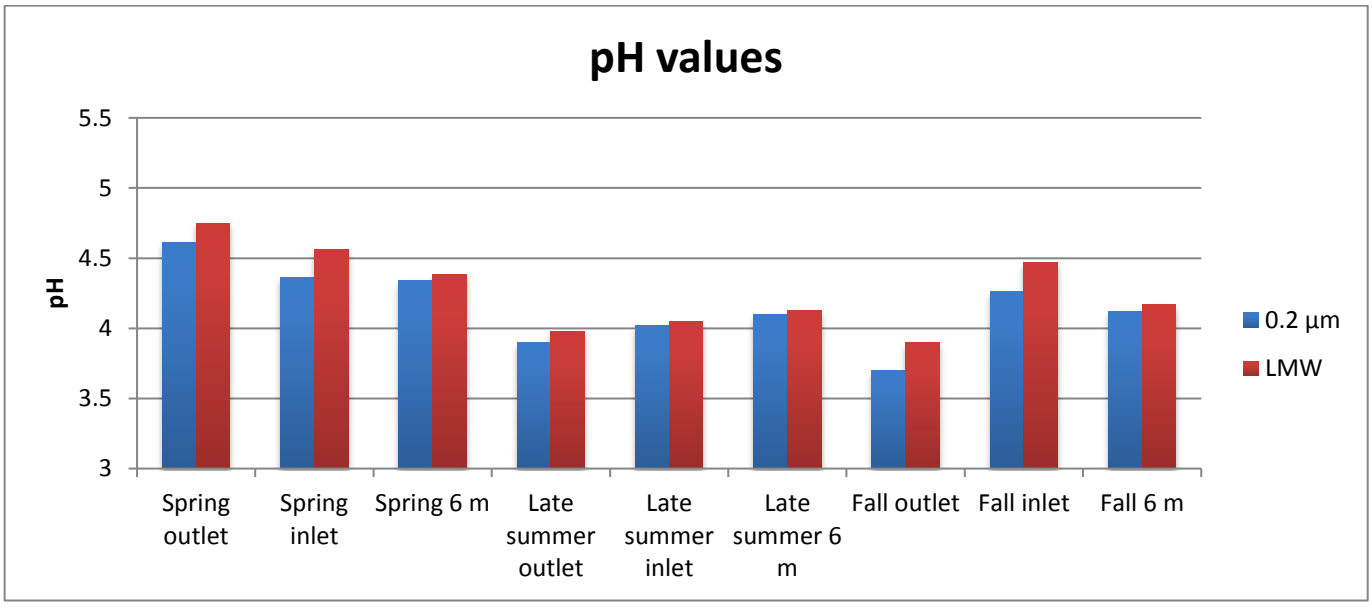

Figure 4.2: pH values of the 0.2 µm samples compared to the LMW samples.

Conductivity and pH data can be found in the appendix, Section F.

4.2 Major cations and anions

4.2.1 Charge distribution

For quality control of the data, the equivalent charge of major cations and anions are stacked side by side to check if there is charge balance (Figure 4.3-4.5). For all sampling seasons, the sum of equivalent charge of major inorganic anions in the 0.2 µm filtrated samples is lower than the sum of equivalent charge of major inorganic cations. This difference is balanced by organic anions (A^-) using a model calculation based on pH and DOC concentration (Oliver, Thurman, and Malcolm 1983).

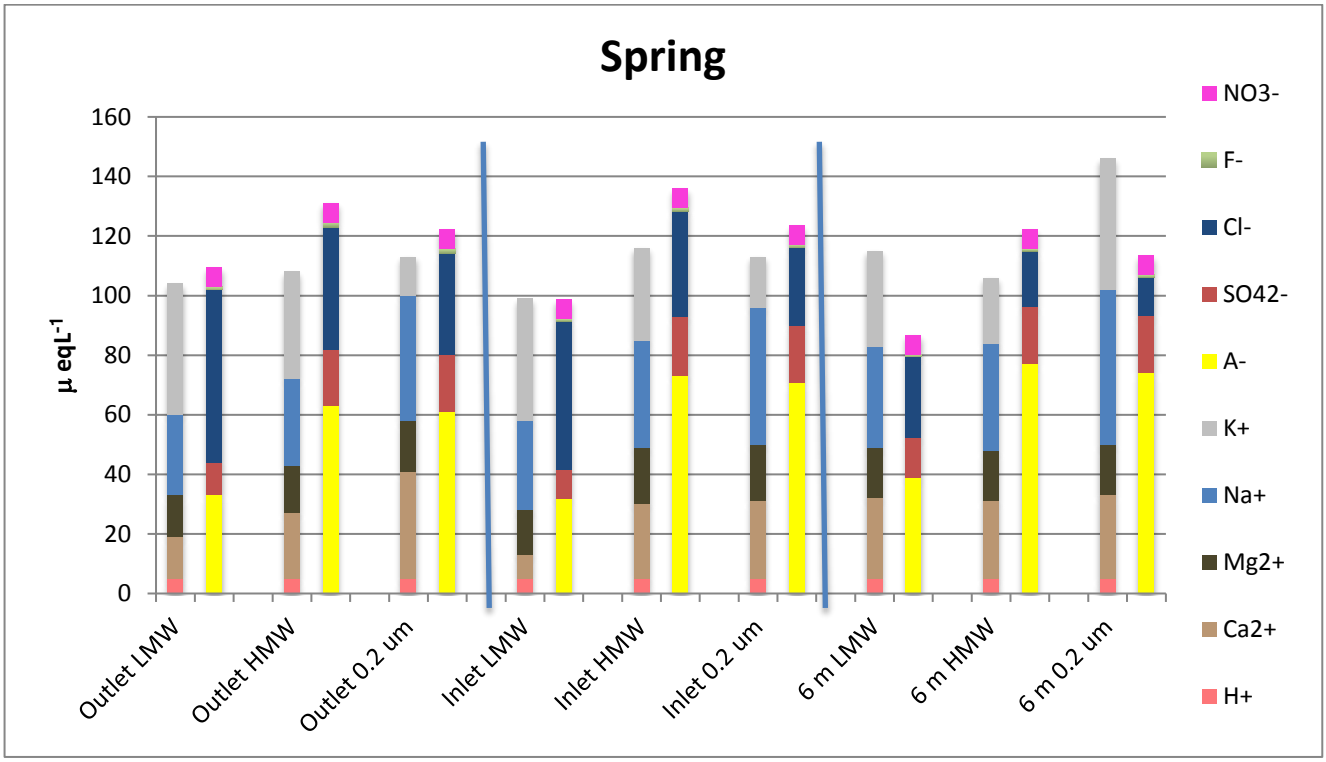

Figure 4.3: Charge distribution of the major cations and anions of the spring samples. The data are corrected for NO_3^- and H^+.

Sulphate values are missing from the 6 m HMW fraction due to an analytical error in the ion chromatography analysis. Therefore, an imputed value based on the average values of outlet and inlet HMW is used.

As addressed in Section 4.1, the pH values in the filtrated samples were lower than expected due to contamination from the nitric acid that was used to wash the sample containers. This was further confirmed by high nitrate concentrations described in this section. Because of the high nitrate concentrations, the nitrate values are replaced with nitrate values obtained in previous studies conducted at NIVA (Braaten 2015) and previous master studies (Francés 2017; Håland 2017; Ong 2018). The average nitrate value, 6.4 μeqL^{-1}, was applied to all seasons and fractions. Additionally, the H^+ concentrations were replaced by values obtained by the AquaMonitor.

Sodium (Na^+) and chloride (Cl^-), as well as organic acid (A^-), show the highest concentrations in the spring samples (Figure 4.3). Potassium (K^+) also showed high values in the spring, which was surprising considering that potassium is an important nutrient, and the concentration is therefore expected to be low. One possible explanation for this could be that the spring samples were collected before the growing season started and in that case, K^+ is present at higher concentrations.

Na^+ and Cl^- are expected to have relatively high concentrations compared to other ions because of the proximity to the ocean. In dystrophic lakes found in regions with poorly weatherable mineral soil, ions such as Ca^{2+} and Mg^{2+} and bicarbonate are usually found in low concentrations. This includes Langtjern. Bicarbonate is also found in low concentrations because at pH 5, it is protonated to form carbonic acid.

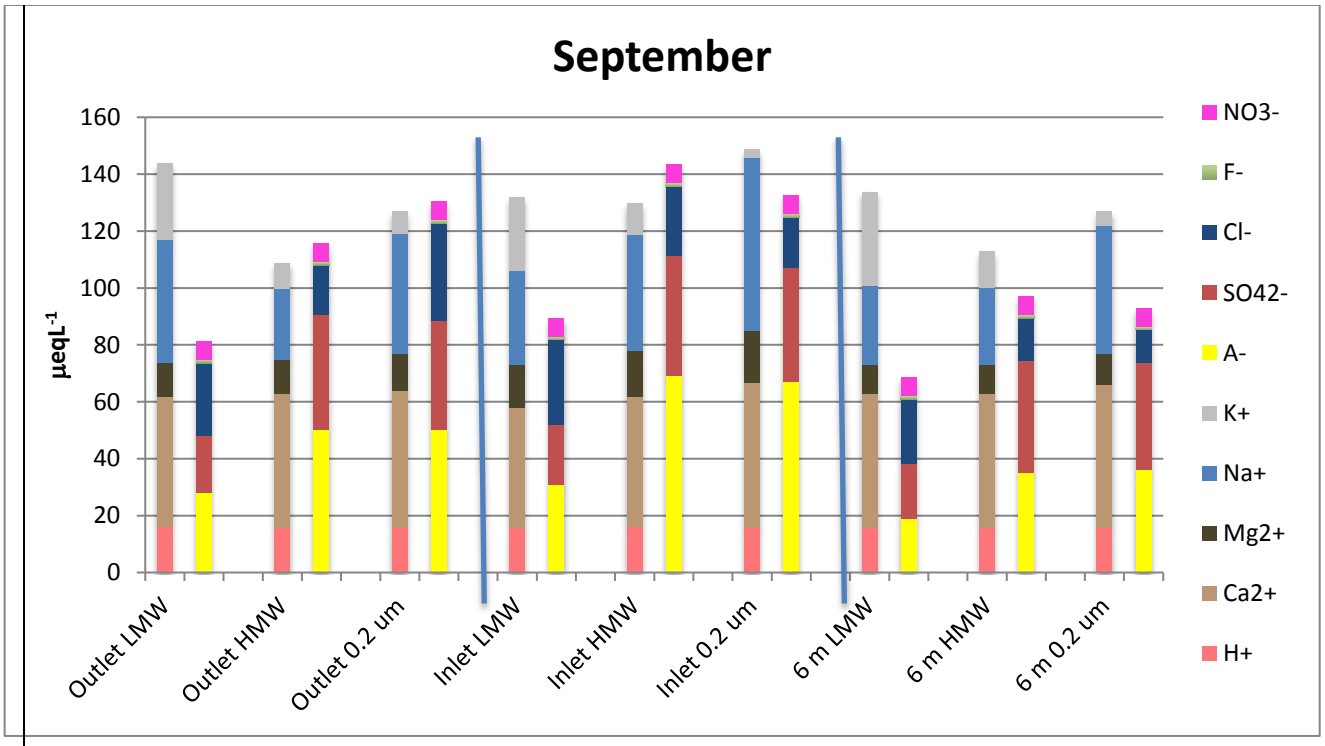

Figure 4.4: Charge distribution of the major cations and anions of the fall samples. The data are corrected for NO_3^- and H^+.

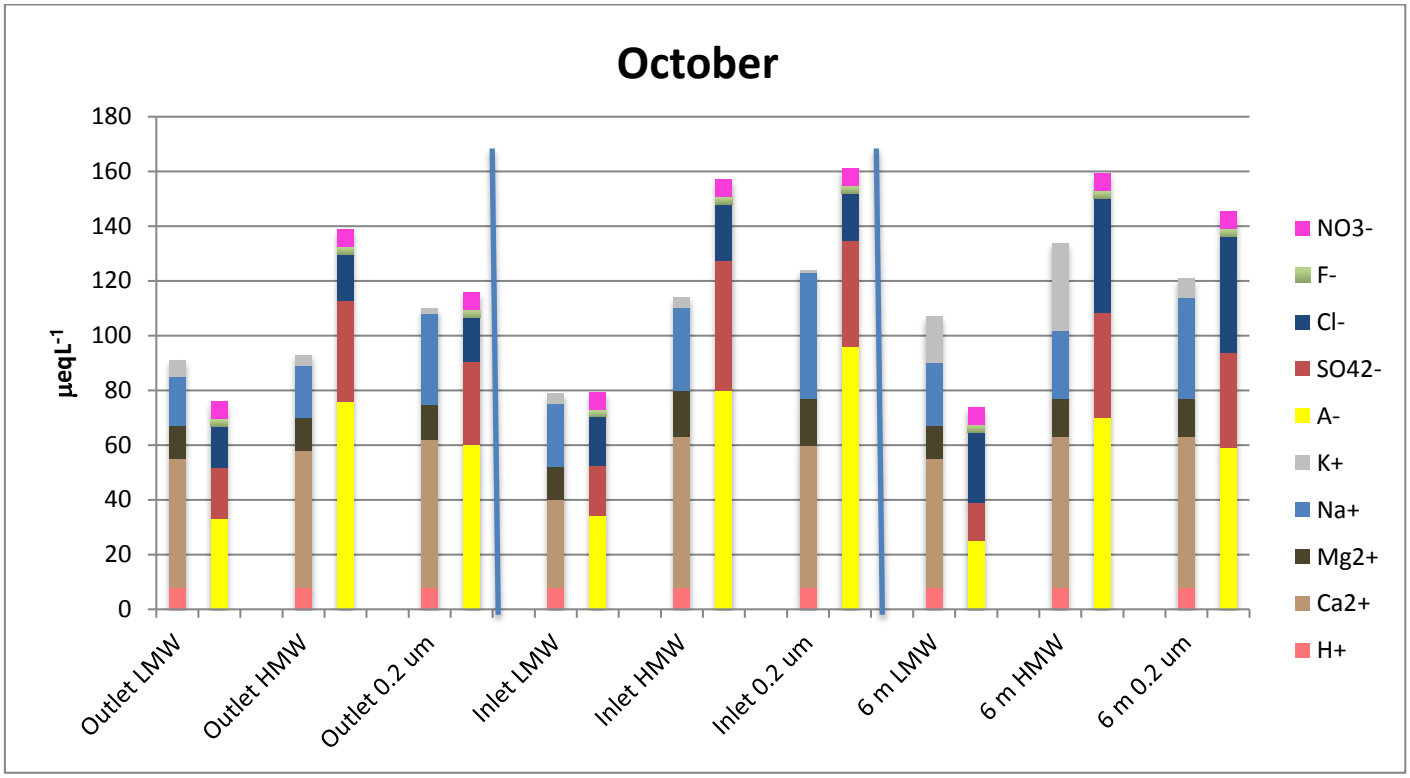

Figure 4.5: Charge distribution of the major cations and anions of the fall samples. The data are corrected for NO_3^- and H^+.

There are some large deviations in the charge balances, especially in the late summer and fall samples, but overall, most samples seem sufficiently balanced for interpretation of the data, while taking cautions into consideration.

Using a 100 kDa cut-off, the major ions are small enough to pass the membrane. In order to sustain charge balance, however, the cations that are associated to the HMW DNOM do not pass the membrane. This is mainly polyvalent cations such as aluminium, iron, calcium and magnesium.

4.2.2 Statistical analysis of major anions and cations

Results of all ion data are validated univariately by analysis of variance (Table 4.1), and a multivariate overview is provided by principal component analysis (Figure 4.6).

Table 4.1: FDR-adjusted p-values of the ions from three-way ANOVA. The p-values of the main effects of sampling season, sampling site and fraction, as well as all the two-ways interaction are presented.

		Ca^{2+}	Mg^{2+}	Na^{+}	K^{+}	F^{-}	Cl^{-}	SO_4^{2-}	A^{-}
Main effects	**Season**	0.000	0.000	0.002	<0.001	<0.001	0.003	0.000	0.000
	Sampling site	0.117	0.000	0.037	0.323	0.021	0.271	0.063	0.003
	Fraction	0.004	0.002	<0.001	0.347	0.080	0.080	0.000	0.000
Interaction effects	**Season*Sampling site**	0.826	0.012	0.140	0.826	0.104	0.006	0.104	0.013
	Season*Fraction	0.347	0.347	0.600	0.347	0.347	0.041	0.005	0.015
	Sampling site* Fraction	0.236	0.143	0.309	0.598	0.449	0.449	0.427	0.143

Sampling season had a significant main effect ($p < 0.05$) on the concentrations of all major ions. Significant ($p<0.05$) effects of sampling site were observed for Mg^{2+}, Na^{+} and $F^{-}$and A-. SO_4^{2-} had a p-value of 0.054. Ca^{2+}, Mg^{2+}, Na^{+} and SO_4^{2-} showed a significant ($p<0.05$) effect of fraction.

The sample and parameter loading plots of a PCA performed on all the cations and anions (Figure 4.6) shows that the largest difference in the ion composition is between the seasons and size fractions along the two first principal components (Dim1 and Dim2). These two principal components account for 42% and 26%, respectively, of the total variation. Seasons and fractions are positioned in diagonal directions in the plot. The spring samples (Sp) are located in the upper left of the score plot and the fall samples are found in the lower right. The LMW fractions are located in the lower left, and the 0.2 μm and HMW fractions are located in the upper right. In the corresponding loading plot, the spring samples are associated with relatively high Mg^{2+} values. The spring samples are also associated with the highest concentration of K^{+} and Cl^{-}, while the fall samples are associated with the highest concentration of Ca^{2+}, SO_4^{2-} and F^{-}.

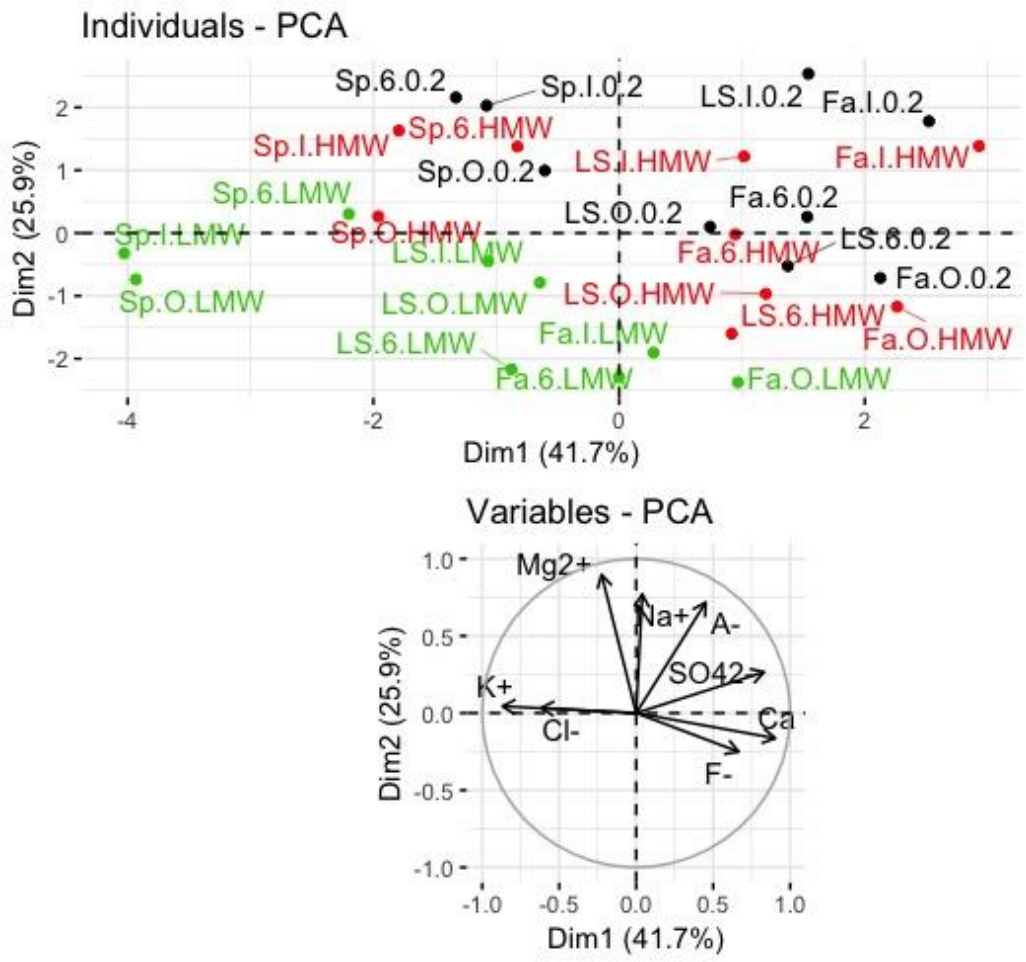

Figure 4.6: Principal Component 1 (horizontal direction) and 2 (vertical direction) of Principal Component Analysis of the measured ions. The plot of the samples ("Individuals") display LMW fractions (in green), HMW fractions (in red), and the 0.2 µm fraction (in black) for samples collected at the Spring (LS), Late summer (LS) and the Fall (Fa), at the lake position Outlet (O), Inlet (I) and at 6 m depth (6). The corresponding plot of the variables displays how the different observed features relate to the samples.

Spatial variations in the cation and anion concentrations are displayed in Figure 4.7 and Figure 4.8, respectively, of all main effects with FDR-adjusted p-values below 0.05 (Table 4.1). Both Mg^{2+} and Na^{+} have higher concentrations in the inlet compared to the outlet. A preceding master study (Francés 2017) found higher concentrations of Ca^{2+} and Mg^{2+} in the outlet compared to the inlet, which was explained by groundwater seepage into Langtjern from other sources than the inlet. Although Mg^{2+} was higher in the inlet also in this study, calcium showed no significant ($p>0.05$) difference between the inlet and the outlet.

Polyvalent ions are greatly associated to DNOM. As will be presented in in Section 4.3, the majority of DNOM is HMW, and it is therefore assumed that the majority of the anionic charge is found in the

HMW fraction. This will be balanced mainly by di- and polyvalent cations. For that reason, the monovalent Na^+ is not expected to be found at higher concentrations in the HMW fraction. In this case, the 0.2 μm fraction is significantly ($p<0.001$) higher than the LMW and HMW fractions, which is unexpected.

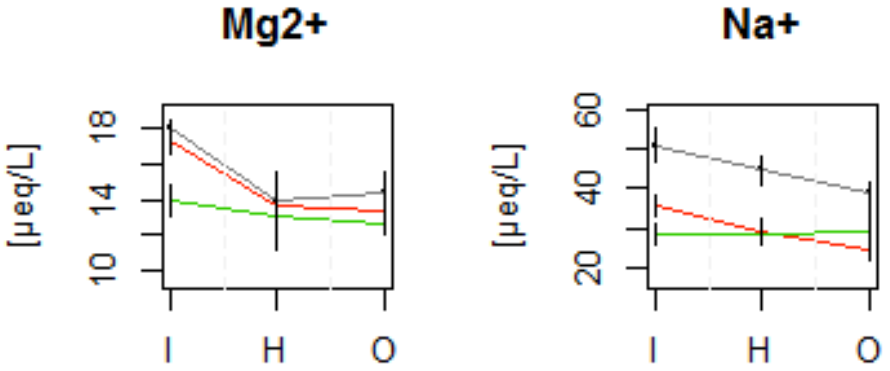

Figure 4.7: Cation concentrations show a significant effect of sampling site by FDR-adjusted p-values ($p < 0.05$) for 0.2 μm (grey), HMW (red) and LMW (green) fractions. In each figure, outlet samples are shown to the left (O), inlet samples are shown in the middle (I) and hypolimnion samples are shown to the right (H).

Cation concentrations are significantly ($p<0.05$) affected by season (Figure 4.8). The Ca^{2+} concentration increases over the summer, while Mg^{2+}, Na^+ and K^+ decrease ($p<0.05$) Increased calcium concentration in the autumn might be charge balanced by increased sulphate concentrations.

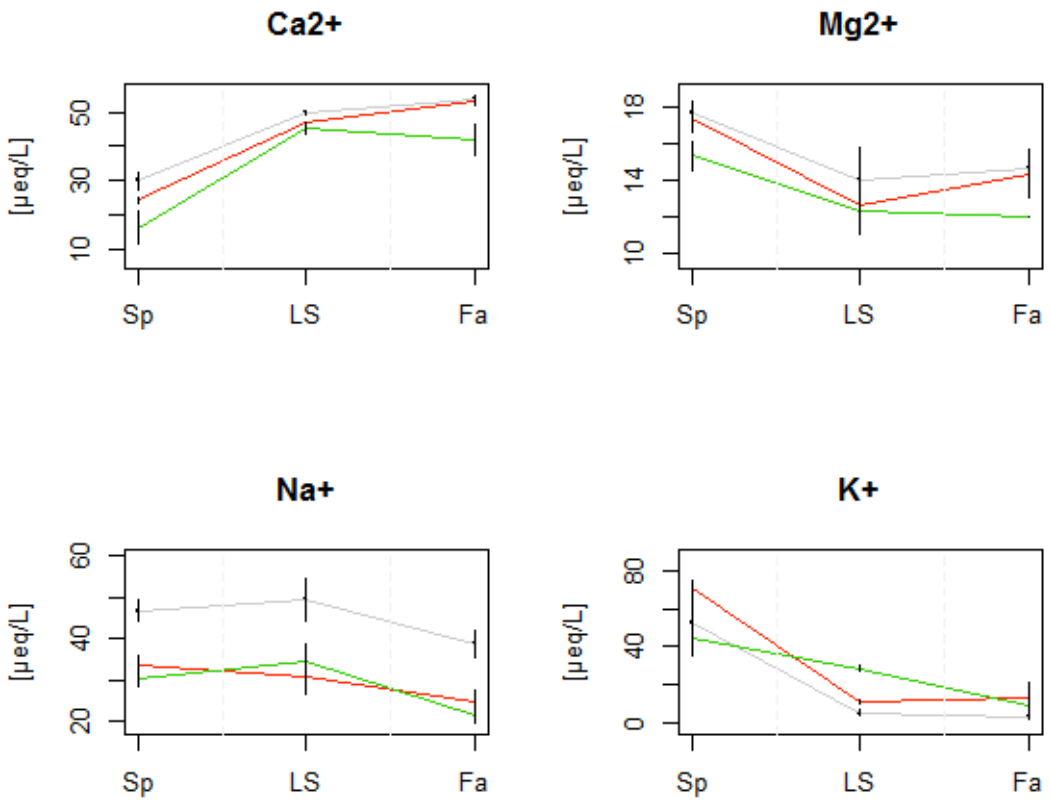

Figure 4.8: Cation concentrations show a significant effect of season by FDR-adjusted p-values ($p < 0.05$) for 0.2 µm (grey), HMW (red) and LMW (green) fractions. In each figure, spring samples are shown to the left (Sp), late summer samples are shown in the middle (Ls) and fall samples are shown to the right (Fa).

Anion concentrations (Figure 4.9) show that the sulphate concentration increases over the summer ($p<0.01$). The summer of 2018 was particularly dry. Increased sulphate concentration following a warm and dry summer is a widely recognised phenomenon in regions with water-saturated soils, such as peats and fens. Water saturated soil is anoxic, but during dry periods, the soil is exposed to oxygen, which leads to oxidation of sulphide to sulphate (Eimers and Dillon 2002; Bayley, Behr, and Kelly 1986). Sulphate is therefore present at higher concentrations in the late summer and fall samples compared to the corresponding spring samples. Increased calcium concentrations in the autumn might be charge balanced by sulphate (Vangenechten, Bosmans, and Deckers 1981). This occurs when H^+ from the sulphuric acid is exchanged for Ca^{2+} on the soil cation exchanger. This could contribute to high calcium concentrations in the late summer and fall. SO_4^{2-} in the HMW fractions increase more strongly during the season than the LMW fraction. Difference in SO_4^{2-} between the size fractions is smaller in the spring than in the late summer and fall.

The sulphate concentration is higher in the HMW and 0.2 μm fraction compared to the LMW fraction. This is unexpected because sulphate is not bound to DNOM, and it should therefore not be affected by fraction size.

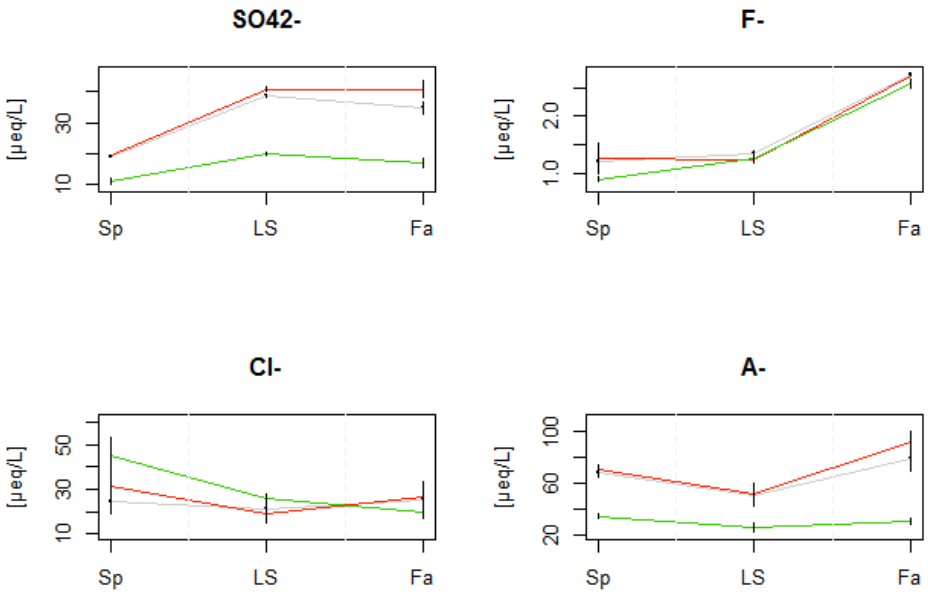

Figure 4.9: Anion concentrations show a significant effect of season by FDR-adjusted p-values ($p < 0.05$) for 0.2 μm (grey), HMW (red) and LMW (green) fractions. In each figure, spring samples are shown to the left (Sp), late summer samples are shown in the middle (Ls) and fall samples are shown to the right (Fa).

4.3 Size fractionation

Tangential flow filtration (TFF) was used to size fractionate the DNOM in the Langtjern samples. DOC was measured as a proxy for DNOM in all samples, all replicates and all blanks, including all size fractions (0.2 μm, LMW and HMW).

DOC concentrations in the 0.2 μm size fraction, and back-calculated DOC concentrations of HMW and LMW in the outlet, inlet and at 6 meters are presented in Figure 4.10. The estimations assume that the 0.2 μm sample accounts for 100% of the DOC, and the DOC concentration of the LMW and HMW in the 0.2 μm samples are then back-calculated based on the percentage of DOC in this sample.

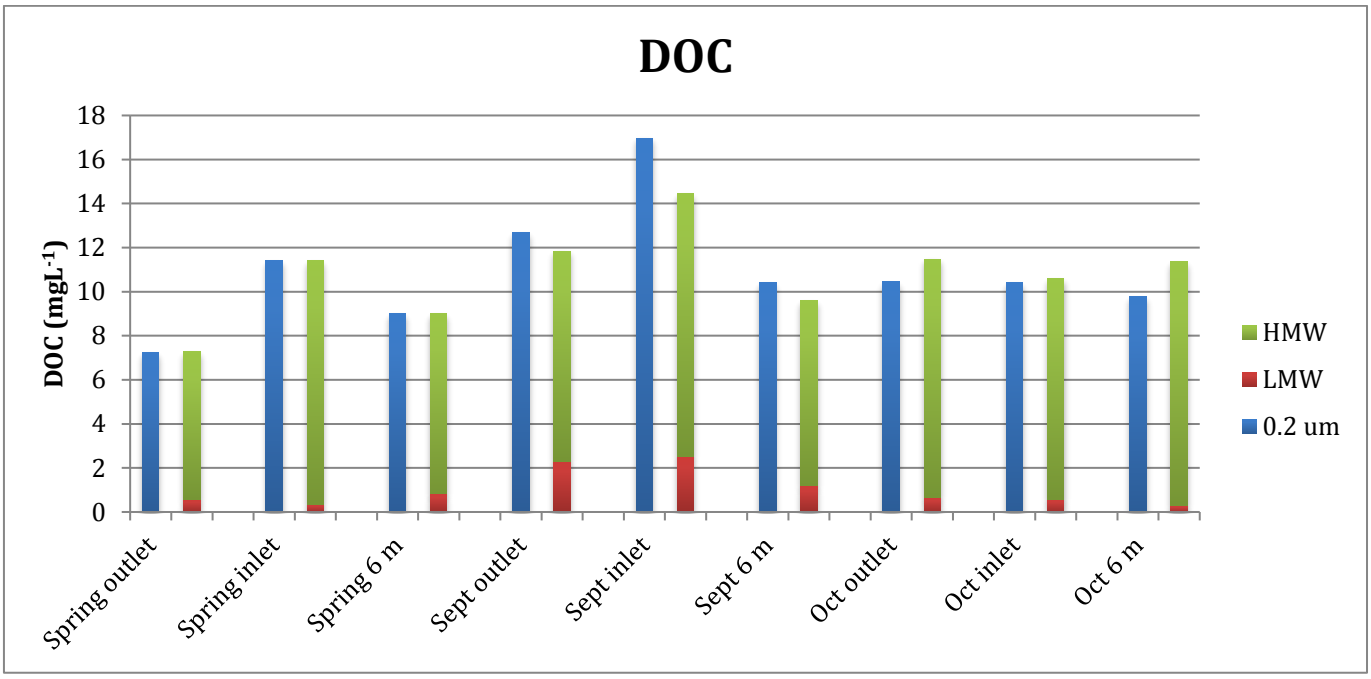

Figure 4.10: DOC in the different size fractions. The calculations are based on the total volume of 0.2 µm sample that passed the membrane. The 0.2 µm sample is assumed to account for 100% of the mass, and the LMW and HMW are calculated as percentages of the 0.2 µm.

On average the LMW fraction accounted for 14% of the DOC in the 0.2 µm samples. The average relative amount of LMW compared to HMW was 0.19**.** The Inlet had lower relative amount of LMW DOC (average 0.16), the outlet was intermediate (0.19), and the lake water at the hypolimnion had the highest contribution of LMW DOC (0.21), although the outlet and hypolimnion samples were similar. This indicates that LMW DNOM is produced in the lake, which is in agreement with literature in that autochthonous DNOM is more LMW than allochthonous. The highest relative amount of LMW DOC was found in the late summer (average 0.22) and lowest (0.17) in the fall season.

DOC concentration is significantly ($p < 0.001$) affected by all the main effects: season, lake position and size fraction, as well as interaction effects (Table 4.2, Figure 4.11).

Table 4.2: FDR-adjusted p-values of DOC from the three-way ANOVA. The p-values of the main effects of sampling season, sampling site and fraction, as well as all the two-ways interaction are presented.

		DOC (mg C/L)
Main effects	**Season**	<0.001
	Sampling site	<0.001
	Fraction	<0.001
Interaction effects	**Season*Sampling site**	0.001
	Season*Fraction	0.004
	Sampling site*Fraction	0.001

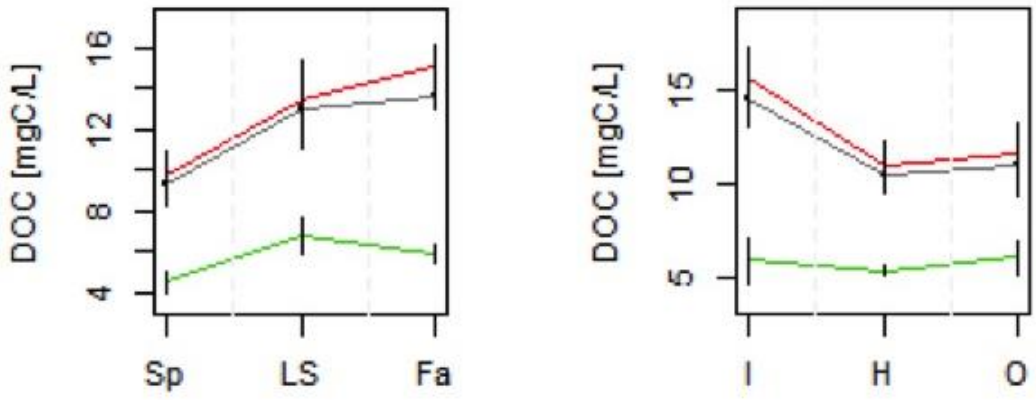

Figure 4.11: Average temporal and spatial variation in DOC concentrations, as well as distribution between size fractions (0.2 μm: Grey, HMW: red, LMW: green). The effect of season is presented to the left (Sp: spring, LS: late summer, Fa: fall), and the effect of sampling site is presented to the right (Inlet: I, Hypolimnion: H, Outlet: O)

The highest amount of DOC was found in the HMW fractions. The DOC concentration increases from the spring to the late summer and fall sampling campaigns. A possible explanation for the low concentration in the summer could be dilution as a result of snow melting in the spring. NIVAs AquaMonitor (http://aquamonitor.no/langtjern/) reported precipitation in August and September, which brings more DNOM into the lake. In a previous master study, however, it was found that the rainwater also leads to dilution, which minimises the effect of DNOM transportation to the lake (Håland 2017).

DOC concentration is also significantly ($p<0.001$) affected by sampling site, and the inlet has a significantly ($p<0.001$) higher DOC content than the outlet and hypolimnion samples. During biodegradation, the smallest molecules are expected to be broken down first because they are more biodegradable. This will reduce the amount of LMW DNOM in the lake water. Photo-oxidation, on the other hand, will break down HMW DNOM to LMW DNOM. HMW DNOM has a higher content of chromophores and is therefore more susceptible to photo-oxidation (Rajakumar 2018). This may lead to the higher amount of LMW in the outlet compared to the inlet. Additionally, autochthonous produced DNOM is mainly LMW (Al-Reasi, Wood, and Smith 2011). This can be heterotrophic as well as autotrophic from algae photosynthesis. This production will also contributes to more LMW DNOM in the lake than in the inlet.

There is less HMW DNOM in the outlet compared to the inlet, and a slightly higher amount of LMW DNOM in the outlet and hypolimnion sample. This could indicate that photo-oxidation in the lake has broken down large molecules so that there is less HMW DNOM remaining. The corresponding increase in LMW DNOM is small, and this can be explained by biodegradation of DNOM, which breaks down smaller molecules more easily. These findings are supported by sUVa and sVISa values presented in Section 4.5, which show the same tendency of higher molecular weight DNOM in the inlet compared to the outlet.

4.4 DNOM physicochemical characteristics

Both sUVa and sVISa were significantly ($p<0.05$) affected by sampling season, sampling site and size fraction as well as interaction between season and position (Table 4.3). SAR was significantly affected by all the three main effects, but none of the interaction terms.

Table 4.3: FDR-adjusted p-values from three-way ANOVA of the physiochemical properties. Black values indicate p-values < 0.05, while grey values indicate p-values > 0.05.

		Abs254	Abs400	sUVa	sVISa	SAR
Main effects	**Season**	<0.001	<0.001	0.011	0.001	<0.001
	Sampling site	<0.001	<0.001	0.025	0.013	0.013
	Fraction	<0.001	<0.001	<0.001	<0.001	<0.001
Interaction effects	**Season*Sampling site**	0.008	0.035	0.039	0.036	0.190
	Season*Fraction	0.004	0.004	0.473	0.177	0.106
	Sampling site*Fraction	0.001	0.001	0.248	0.248	0.248

sUVa, sVISa and SAR values all show a significant ($p<0.001$) effect of fraction (Figure 4.12). The higher molecular weight fractions had higher sUVa and sVISa values and lower SAR values than low molecular weight fractions, which is consistent with the conceptual understanding. The lower degree of aromatic character and smaller size in the LMW fraction is in agreement with previous studies (Weishaar et al. 2003; Vogt and Gjessing 2008) and master studies (Francés 2017; Ong 2018).

sUVa, sVISa and SAR values are also significantly ($p<0.05$) affected by sampling season (Figure 4.13). As a significant main effect, sUVa and sVISa values decrease from the spring to the late summer, and increase again the fall, while the SAR values show the opposite trend. An explanation for this could be structural changes in DNOM that might occur during the summer as a result of DNOM degradation by solar radiation. Additionally, as previously mentioned, the spring samples were collected during a dry

period. The absence of rain could lead to a build-up of DNOM, leading to increased molecular size and aromaticity. This could explain the high spring values.

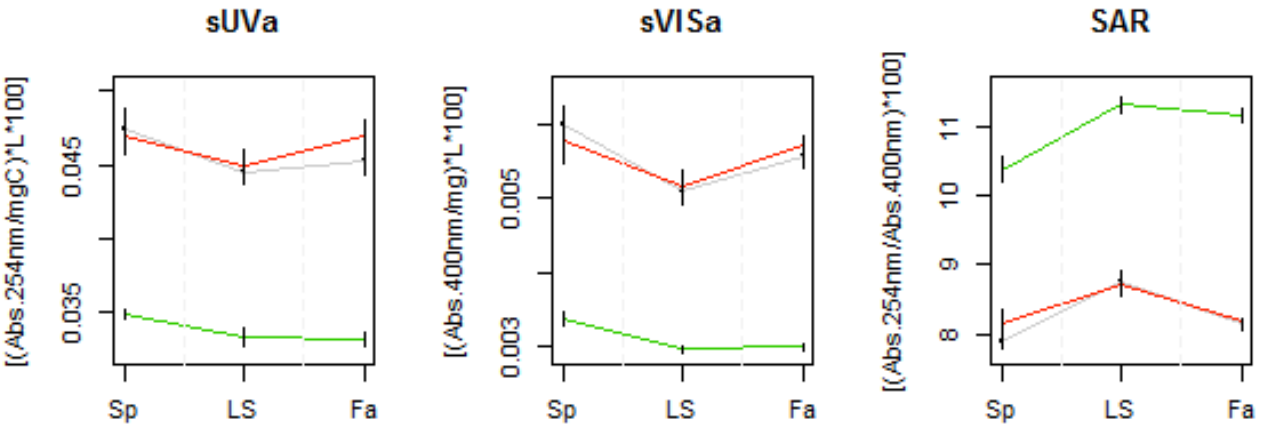

Figure 4.12: sUVa, sVISa and SAR values vary with season. Spring values are presented in blue, late summer are presented in grey and fall values are presented in black.

In Figure 4.13, the effects of sampling site (outlet, inlet or 6 m) on the sUVa, sVISa and SAR values are presented. The sVISa and sUVa values are significantly ($p<0.05$) higher in the lake and in the inlet compared to the outlet, while the SAR values show the opposite trends. This might suggest that DNOM has been degraded in the lake, which results in lower sUVa and sVISa values in the outlet compared to the inlet. Lower sUVa and sVISa values in the outlet can also be due to production of autochthonous material in the lake, which has lower molecular weight and thereby lower sUVa and sVISa values. Langtjern has several inlets originating from different sub-catchments, as well as groundwater seepage into the lake, meaning that the inlet investigated in this thesis is not representative for all the influx of water to the lake. Furthermore, lake flowing into the lake is mixed with epilimnion water. Epilimnion water may have arrived during the previous season, and may have DNOM characteristics that are different from the incoming water, which can explain the differences between the inlet and the outlet water. Flow differences might also account for the differences in sUVa and sVISa. A previous master study (Håland 2017) found that sUVa varied with flow in the inlet, and the degree of aromaticity in the DNOM decreased during a discharge period.

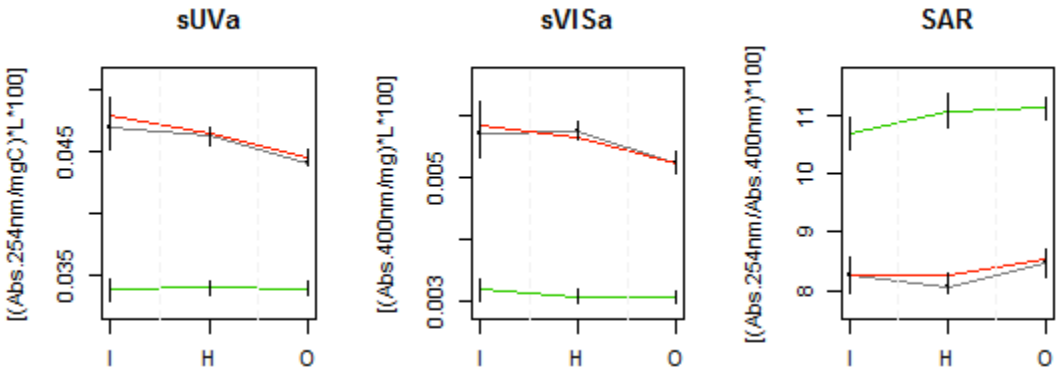

Figure 4.13. sUVa, sVISa and SAR vary with position in the lake (Inlet: I, Hypolimnion: H, Outlet: O). The effect of fraction is also included (0.2 µm: grey, HMW: red, LMW: green).

Absorbency data can be found in the appendix, Section G.

4.5 Biodegradability

The rate of oxygen consumption by bacteria was measured during DNOM biodegradation as a measure for the biodegradability of DNOM. Biodegradability differs from biodegradable DNOM in that it is the rate rather than the amount of biodegradable DNOM (BDOM) that is measured. Biodegradability is conceived to be a more relevant parameter than BDOM in natural dynamic systems. One hypothesis in this thesis is that the low molecular weight (LMW) fractions will show more rapid oxygen consumptions.

Table 4.3: FDR-adjusted p-values of RR and RR/DOC.

		RR	RR/DOC	RR/Abs400
Main effects	**Season**	0.273	0.400	0.213
	Sampling site	0.647	0.450	0.450
	Fraction	0.532	0.052	0.002
Interaction effects	**Season*Sampling site**	0.493	0.493	0.493
	Season*Fraction	0.709	0.709	0.636
	Sampling site*Fraction	0.626	0.650	0.725

RR/DOC had an adjusted p-value of 0.052 for the main effect of fractions (Table 4.3).

The respiration rate is higher in the LMW fractions compared to the HMW fractions (Figure 4.14). The results from RR/DOC and RR/Abs400 show similar patterns and suggest that the LMW fractions are more bioavailable, which is in accordance with the hypothesis. Furthermore, there seems to be a higher respiration rate in the inlet compared to the other sampling sites. This difference was not found to be significant in this experiment.

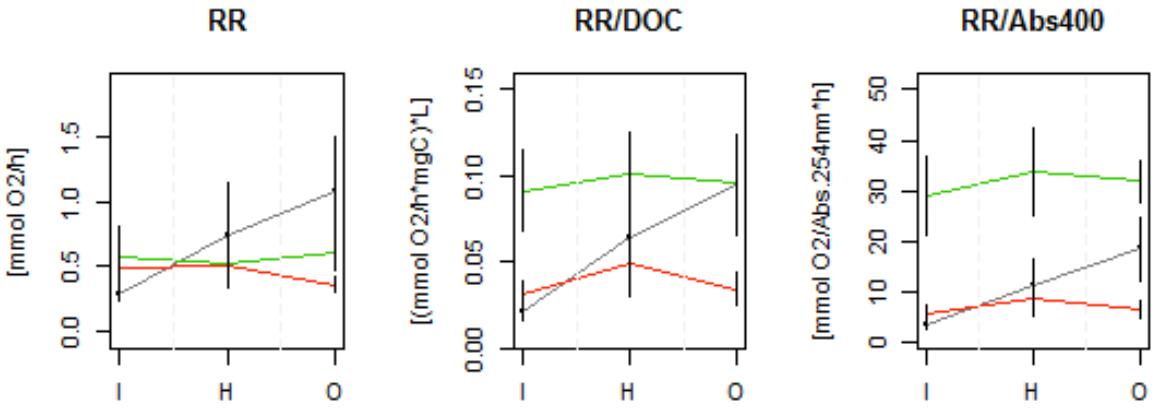

Figure 4.14: Respiration rates relative to the DOC concentration and Abs400, respectively. Outlet samples are shown to the left (O), inlet samples are shown in the middle (I) and hypolimnion samples are shown to the right (H). The mean value of each fraction is shown (0.2 μm (grey), HMW (red) and LMW (green)), and the error bars represent the uncertainty in the sampling site.

In Figure 4.15, a 2D scatterplot of RR/DOC plotted against the proxies of DNOM quality (SAR, sUVa and sVISa) is presented, where only the HMW and LMW fractions are included. All three proxies showed differences related to the size fraction (Table 4.2), so plots primarily show the relation between two groups of data points.

Differences in the respiration rate between the size fractions were not observed between the sampling sites or between the seasons, as there were no significant interaction effects for this parameter (Table 4.2). Furthermore, there were no significant main effects of position or season.

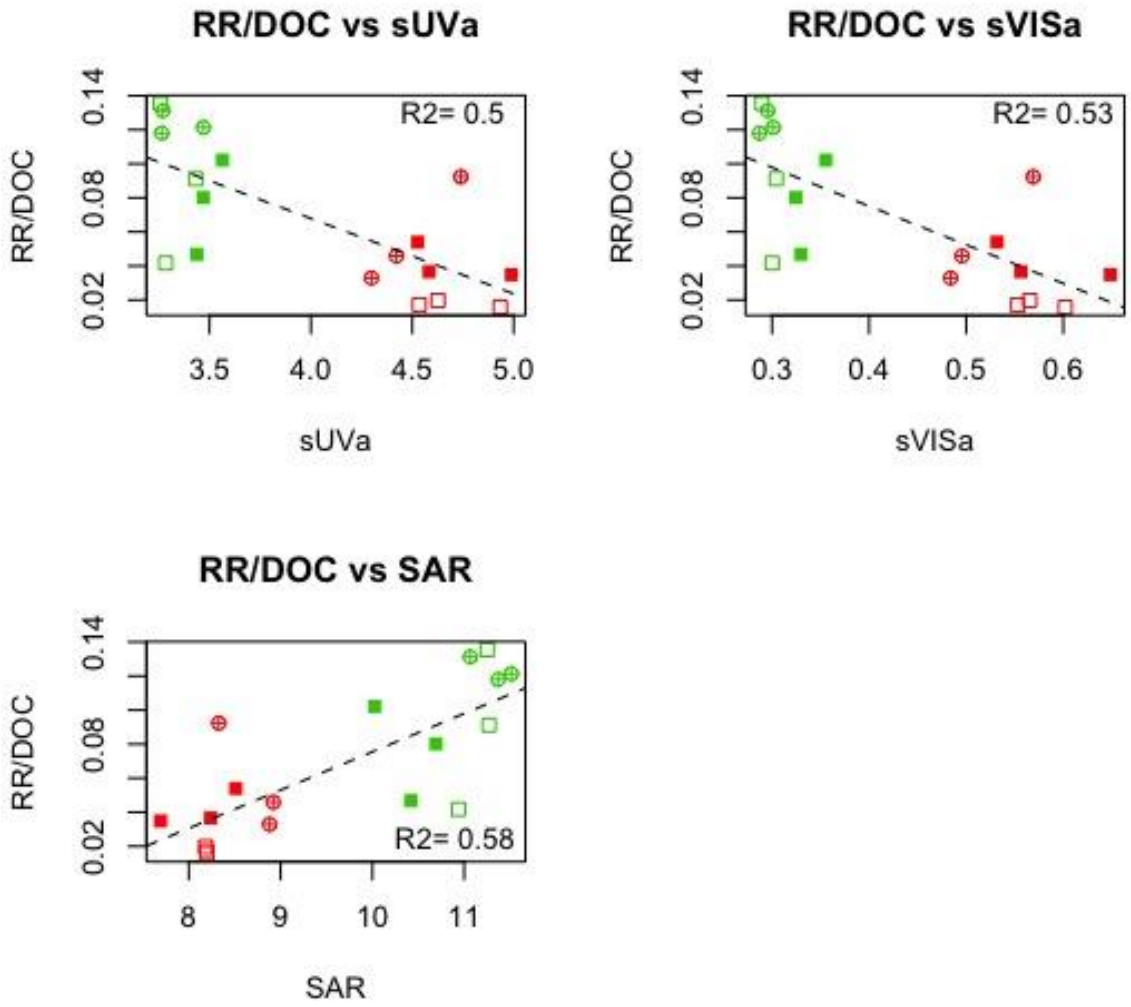

Figure 4.15: Respiration rates (RR/DOC) vs SAR, sUVa and sVISa, respectively. LMW (green) and HMW (red), spring samples (open squares), late summer samples (crossed circles) and fall samples (filled squares).

As seen in Figure 4.14 and 4.15, LMW DNOM has the highest respiration rate (RR)/DOC of the fractions, which indicates that it is more easily degraded by bacteria than the HMW DNOM. This would be in

accordance with the hypothesis raised in the present thesis and this is further supported by the corresponding sUVa, sVISa and SAR values obtained in Section 4.4. The fractions that have the smallest size or lowest degree of aromaticity are observed to have the highest respiration rate.

Biodegradation graphs can be found in the Appendix, Section H.4. The graphs showing all the RR/DOC values, ordered by season and fraction type, are also included in the Appendix, Section H.3.

It is assumed that the rate of biodegradation depends on the concentration of DNOM. The respiration rates were therefore divided by the DOC concentrations in order to account for the differences in respiration rates in DNOM with different structure and aromaticity. For this assumption to be valid, the amount of bacteria cannot be a limiting factor. In this experiment, bacteria are added to the sample vials along with nutrients in order to provide optimal conditions for bacteria to break down DNOM.

4.5.1 Differences in VIS absorbency before and after biodegradation

Absorbance was measured before and after biodegradation in order to detect any changes in the quality of DNOM. Differences in Abs_{400} values were calculated and are presented in Figure 4.16.

After incubation, the samples contain large amounts of bacteria. These bacteria adsorb UV radiation and scatter the visible radiation. This will thus interfere with the absorbency measurements of DNOM. In this experiment, a glucose solution was used as a reference. The glucose solution is the only solution in this experiment that contains bacteria from the inoculum, but not DNOM. Considering that the glucose solution with bacteria is colourless, it is likely that bacteria do not absorb visible light. There may be some scattering due to the colloidal bacteria particles, though this is conceived as insignificant. Therefore, changes in absorptivity at 400 nm are assumed to occur solely due to changes in the DNOM. The changes in relative absorptivity (sVISa) can thus provide information about structural changes of DNOM during biodegradation. Molecules with large conjugated systems absorb visible light, while smaller molecules with less conjugation do not.

During biodegradation, the DOC decreases because DNOM molecules are digested by bacteria and the most bioavailable DNOM molecules are digested first. As a result, mainly the largest molecules, with higher degree of aromaticity, in each size fraction remain after biodegradation. These molecules absorb more visible light, resulting in an increased Abs400. DOC decreases more than the 400 nm absorbency, and as a result, it is expected that the sVISa values will increase as a results of biodegradation.

The results show that absorptivity at 400 nm as a result of biodegradation (Figure 4.16) increases in the LMW fractions for all seasons. This indicates that the aromaticity has increased. An explanation for this is that small molecules in the LMW fractions are more easily broken down than the smallest molecules of the larger fractions. Although most of the HMW and 0.2 μm fractions increase, some absorbency values decrease, which is unexpected. Additionally, the 0.2 μm spring outlet and spring inlet samples are very high. This is the bulk sample, and it contains a heterogeneous mixture of molecules of all sizes below 0.2 μm. Therefore, if one particular sample contains a large amount of small DNOM molecules, these will be broken down easily, resulting in a large Abs400 increase. Interpretation of the 0.2 μm graph is therefore not possible in the same way as for the HMW and LMW fractions.

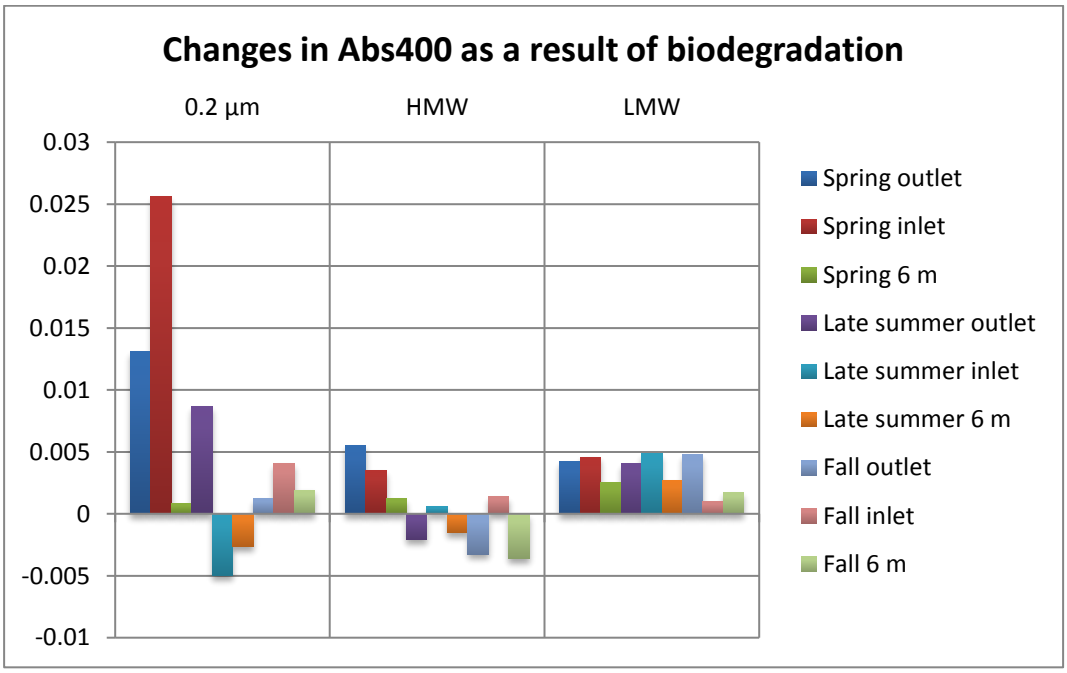

Figure 4.16: Difference in Abs400 (visible light) values as a result of biodegradation, based on measured absorptivity before and after biodegradation. The value obtained before biodegradation is subtracted from the value obtained after biodegradation, so that a positive value indicates that the absorbance at 400 nm has increased during biodegradation.

Bacteria absorb UV radiation, which means that the changes in Abs254 values are caused by the increased amount of bacteria. For that reason, only changes in Abs400 are discussed here.

4.6 Mercury

4.7.1 Quality control of the data

A boxplot of all the Hg values for each fraction, from all season and lake positions are shown in Figure 4.17.The Hg value obtained for spring outlet HMW was 9.9 ngL^{-1}. This was considerably higher than the other HMW values obtained. Therefore, a two-sided Grubb's test was performed, which identified this data point as an outlier ($p < 0.001$). The value is therefore not included in further data analyses. The value of this identified outlier was replaced with the mean of the two values of same fraction (0.2 µm), but different sampling site (inlet and hypolimnion).

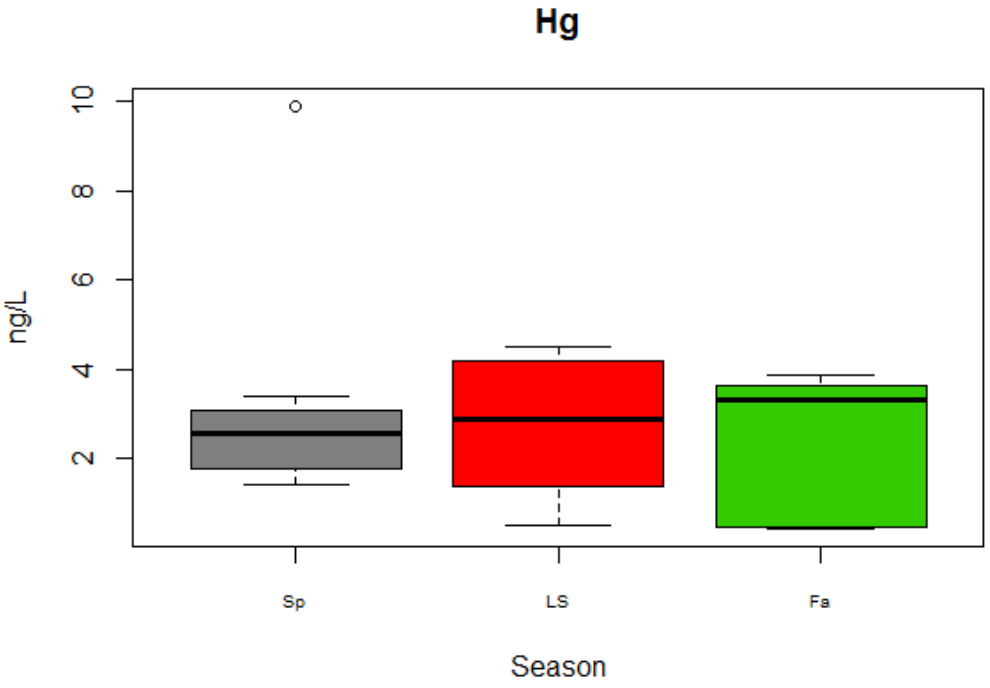

Figure 4.17: Boxplot of the mercury values. For each of the fractions presented in the figure (0.2 µm, HMW and LMW), all seasons and lake positions are included. The highest Hg value of 9.9 ngL^{-1} is presented as a dot at the top of the figure, and it is removed as an outlier in the data analysis.

4.7.2 Results of the mercury data analysis

Percentage distribution of totHg mass in the HMW and LMW fractions were calculated in the same manner as for DOC, assuming that the volume of 0.2 µm fraction that passed the membrane contains 100% of the mass of totHg (Figure 4.22). Only three of the samples (spring inlet, spring and late summer hypolimnion) have a percentage distribution of LMW and HMW that adds up to approximately 100%. The other samples do not add up to 100%, which suggests that some mercury is lost to the membrane. Nevertheless, the overall trend shows that the majority of totHg is found in the HMW fraction. Within each sample, the LMW makes up 3-18% of HMW+LMW. This is consistent with previous studies (Francés 2017; Ong 2018). The spring samples have the highest percentage of totHg in the LMW fraction (average 16.4%), compared to the late summer samples (average 6.10%) and fall samples (average 3.70%).

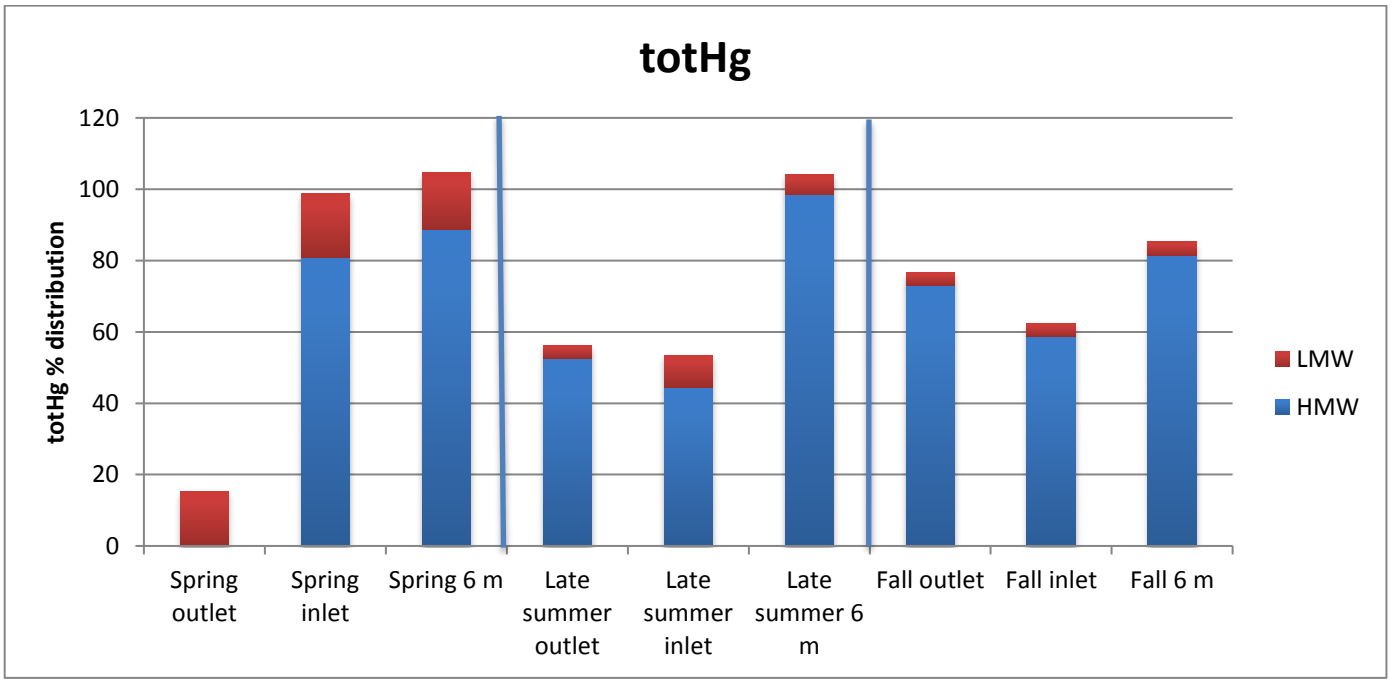

Figure 4.18: Distribution of totHg between LMW and HMW. The calculation is based on the total volume of 0.2 µm sample that passed the membrane. This volume was used to obtain the mass of totHg in the 0.2 µm sample, and the LMW and HMW fractions are calculated as percentages of 0.2 µm, assuming that the 0.2 µm fraction accounts for 100% of the mass. The HMW fraction of the spring outlet sample is removed as an outlier.

The p-values presented in Table 4.4 show that the size fraction has a significant main effect on the total Mercury concentration, while there is no significant difference in the totHg levels between the sampling season or sites. On the other hand, the density of Mercury on the DNOM (i.e. Hg/DOC) showed significant differences between both sampling season and size fraction. The main effects are presented as line plots in Figure 4.19.

Table 4.4: FDR-adjusted p-values for the ANOVA of mercury.

		totHg (ng/L)	DOC (mg C/L)	totHg/DOC (ng Hg/mg C)
Main effects	**Season**	0.464	<0.001	**0.001**
	Sampling site	0.796	<0.001	0.450
	Fraction	**0.000**	<0.001	**0.002**
Interaction effects	**Season*Sampling site**	0.493	0.001	0.257
	Season*Fraction	0.042	0.004	0.011
	Sampling site*Fraction	0.248	0.001	0.040

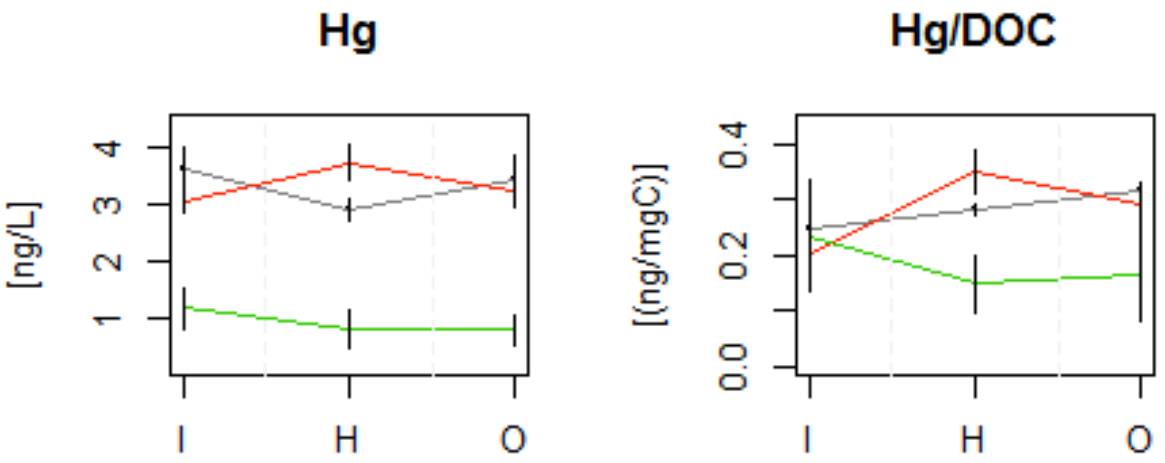

Figure 4.19: Line plot with whiskers of the main variations in Hg, Hg/DOC and DOC. Size fraction has a significant main effect on the total Hg conc., while all the main effects and interaction effects are significant on Hg/DOC.

The concentration of total Hg is significantly affected by size fraction. The main part of totHg is bound to the HMW DNOM fractions. Hg/DOC is also significantly lower in the LMW fraction. The Hg/DOC decreases over the summer, which can be explained by structural changes of DNOM.

A boxplot of all the totHg, DOC and Hg/DOC values is presented in Figure 4.20. The totHg boxplot shows that the levels of Hg in the LMW fraction is lower than in the to other size fractions in all seasons, and as previously stated, there is no significant ($p>0.05$) difference between seasons or between sampling sites. In the DOC boxplot, the concentrations of DNOM in the LMW fractions are also significantly lower then in the two other size fractions.

As mentioned, there is no significant variation in totHg concentrations during the summer.

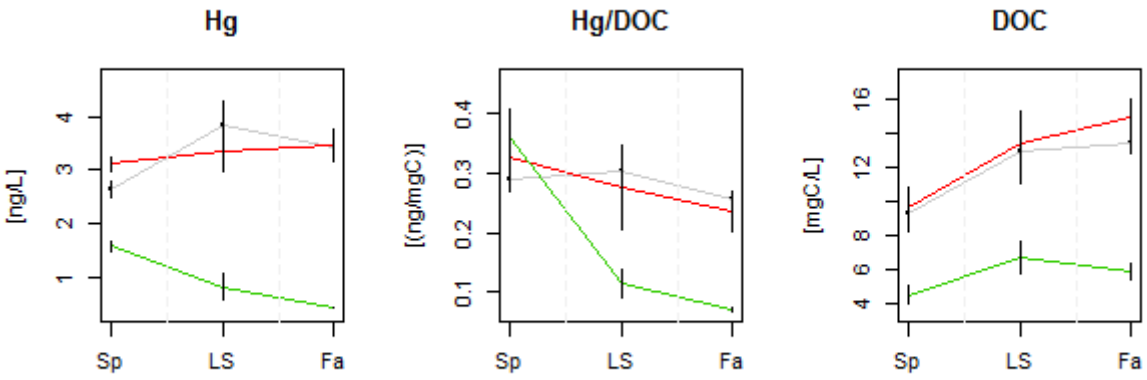

Figure 4.20: Line plot of Hg (ng/L), Hg/DOC (ng/mg C) and DOC (mg C/L). Grey lines are 0.2 µm samples, red lines are HMW fractions and green lines are LMW fractions. In each figure, spring values are presented to the left (Sp), late summer samples in the middle (LS) and fall samples to the right (Fa).

Both for DOC and Hg, the concentration is lower in the LMW fraction. During the season, the concentration of DOC increases in the 0.2 µm and HMW fractions. This increase may be related to the precipitation that was observed in August and September, according to NIVAs AquaMonitor. Interestingly, mercury decreases during the season in the LMW fraction, but not in the HMW fractions. This results in large changes in Hg/DOC for the LMW fraction during the season. The purpose of dividing totHg by DOC is to relate the amount of totHg to the content of the DNOM.

In Figure 4.21, the total Mercury concentration is plotted against sVISa, SAR, sUVa and DOC, respectively. We find strong correlations between totHg and the sVISa, sUVa and SAR. This is because there is a significant effect of size fraction on the totHg concentration and these proxies for the DNOM quality. This is thus co-correlations between the totHg and the DNOM quality proxies because all the parameters are strongly influenced by fraction size. This is consistent with the hypothesis and previous studies (Francés 2017; Ong 2018). Within each size fraction, however, there is no clear correlation with mercury.

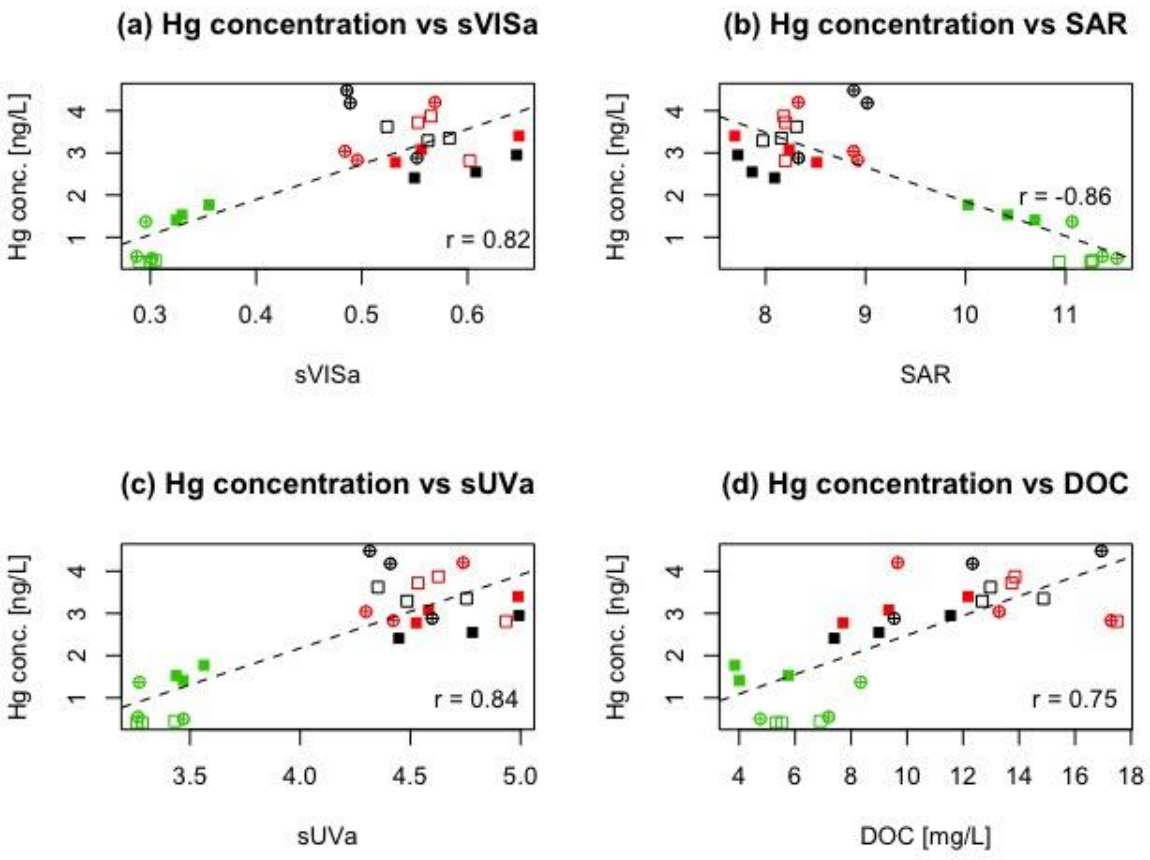

Figure 4.21: Scatter plots of a) totHg concentration vs sVISa, b) totHg concentration vs SAR, c) totHg concentration vs sUVa and d) totHg concentration vs DOC concentration. In all plots: LMW fractions (green), HMW fractions (red) and 0.2 μm (black), spring samples (open squares), late summer (crossed circles) and fall samples (filled squares).

4.7 Summary of data analysis

An overview over the main results of this study is presented by explorative multivariate data analysis by Principle Component Analysis (PCA), Figure 4.22 and 4.23. The three first components, explaining approximately 75% of the total variation, are related to the experimental design.

The main variation in these data, reflected by the score plot, is the differences related to the size fractions accounting for 40.1% of the total variation along the first principle component. The corresponding loading plot of this first principal component shows that both SAR and RR/DOC are located towards the same directing in the loading plot as the LMW fraction is located in the corresponding scoring plot. On the other hand, sVISa, sUVa, Hg and DOC are negatively correlated to SAR and RR/DOC and located opposite to LMW. Mg^{2+}, Ca^{2+}, and SO_4^{2-} are located towards the HMW fractions.

The second principle component separates samples taken in the spring from the samples taken in the late summer and fall, accounting for 23.5% of the total variation. The third principle component separates samples in the fall from the late summer, accounting for 7.8% of the total variation.

The PCA shows that the main variation between the data is between the size fractions. The second most important variation is between the seasons, separating spring from the two other seasons.

Relative biodegradability (RR/DOC) is positively correlated with SAR, which is a measure for the amount of LMW compounds. This is in accordance with the hypothesis. Specific absorptivity is relatively low in the LMW fraction and high in the HMW fraction.

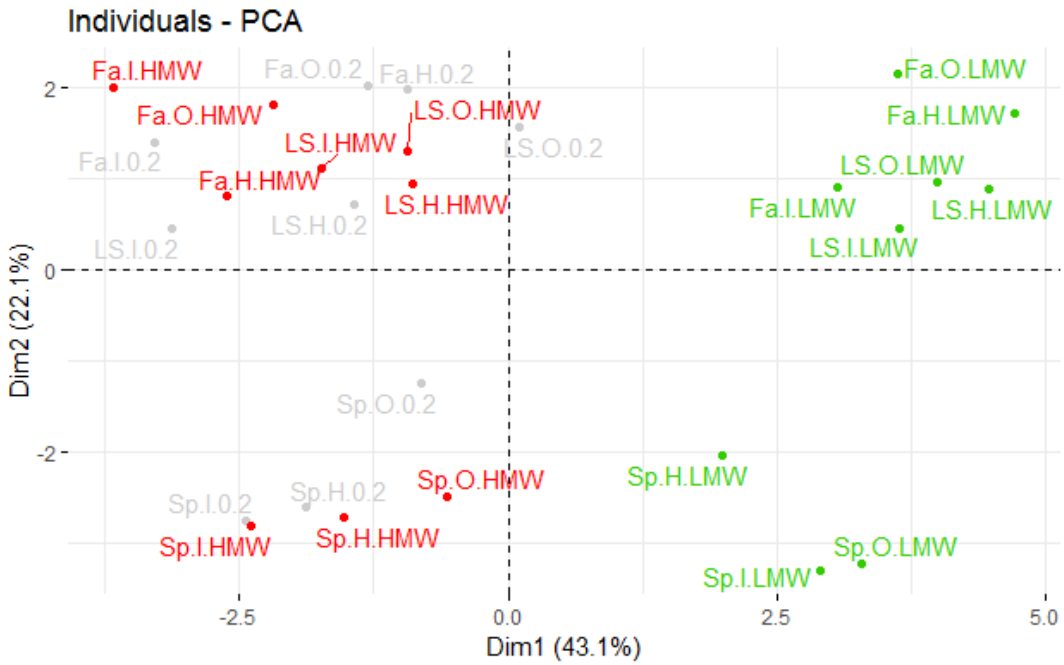

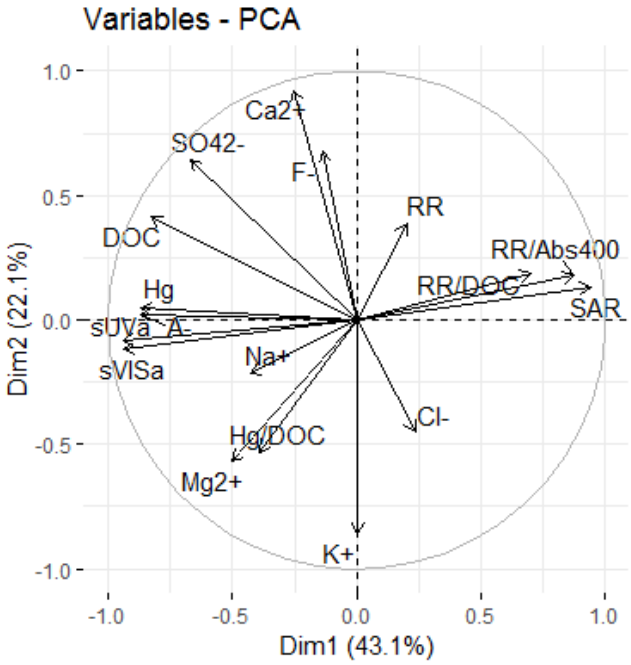

Figure 4.22: Principal Component 1 (horizontal direction) and 2 (vertical direction) of Principal Component Analysis of presented features. The score plot of the samples ("Individuals") display LMW fractions (in green), HMW fractions (in red), and the 0.2 µm fraction (in black) for samples collected at the Spring (LS), Late summer (LS) and the Fall (Fa), at the lake position Outlet (O), Inlet (I) and at the hypolimnion depth (6). The corresponding loading plot of the variables displays how the different observed features relate to the samples.

5. Conclusion

The main hypothesis for this thesis was that mercury (totHg) is mainly bound to high molecular weight (HMW) DNOM, and that this fraction is less bioavailable than the low molecular weight (LMW) DNOM. Furthermore, because LMW DNOM is smaller and less aromatic, it was expected to have lower sUVa and sVISa values, and higher SAR values than HMW DNOM.

Spectrophotometry confirmed that the LMW fractions were smaller and less aromatic than the HMW fractions. The sVISa value was 0.006 in the HMW fraction and 0.003 in the LMW fraction in the unit [(Abs.400nm/mgC)*L*100]. sUVa was 0.046 in the HMW fraction and 0.034 in the LMW fraction [(Abs.254nm/mgC)*L*100], and their ratio SAR was 8.4 in the HMW fraction and 11.0 in the LMW fraction. This is reflected by biodegradation experiments, which showed that the LMW fractions were also significantly more bioavailable pr unit DOC than HMW fractions, the ratio RR/DOC was 0.039 [(mmol O2/h*mgC)*L] in the HMW fraction and 0.096 in the LMW fraction.

The concentration of DNOM was lower in the LMW fraction, as means across all sampling time points and sites. The DOC concentration was 12.7 in the HMW fraction and 5.74 in the LMW fraction. Additionally, the inlet had higher DNOM concentrations compared to the outlet and hypolimnion across all seasons and fractions. Photo-oxidation and microbial processes in the lake breaks down DNOM, which could explain the reduction in concentration from the inlet to the outlet. Furthermore, the DNOM concentrations increased during the summer in all fractions and lake positions. Snow melting during the spring could contribute to a dilution of DNOM during the spring, and thereby lower concentrations. Following a dry summer, precipitation in August and September could transport DNOM from soil to surface water, and thereby increasing the DNOM concentration in the late summer and fall samples.

Results from the mercury analysis showed that across all seasons and sampling sites, the majority of totHg was bound to the HMW fractions of DNOM. When considering totHg/DOC, there was no significant difference between the fractions. In the late summer and fall samples, the density of mercury in the LMW DNOM was significantly lower than in the spring samples, whereas minor changes were observed for the HMW fractions.

There were no significant seasonal differences between the size fractions in the inlet, but totHg/DOC in LMW DNOM decreased strongly from the inlet to the hypolimnion and outlet, whereas minor changes were observed for the HMW fractions across these sampling sites. These observations suggest that microbial and abiotic processes in the lake lead to breakdown and structural changes in DNOM, mainly LMW, which may lead to uptake of mercury in the nutrient chain. This would be in accordance with the observed higher biodegradation of the LMW fraction.

6. Recommended future work

During TFF size fractionation, collection of HMW and LMW started at the same time. HMW is fractionated roughly twice as fast, and after the desired volume of HMW was collected, the rest of the HMW was directed back into the feed tank while the LMW was still being collected. That means that the collection conditions of LMW changed during collection: the first half of LMW was collected while HMW is also collected, while the second half of LMW was collected while HMW was being recirculated back into the feed tank. In future experiments, this should be avoided. One possible way of doing this is to first collect LMW alone while HMW is being recirculated, and then collect HMW. Another possibility is to start collection of both fractions at the same time, but when the desired volume of HMW is collected, the HMW should not be recirculated, but rather transferred to a graduated cylinder. That way, the volume can be measured.

In this thesis, the method to calculate the amount of the different fractions of the studied constituents in the 0.2 µm sample has been modified from what has been done previously. In order to obtain a comprehensive data set with results from several years of master studies, the old results should be re-calculated so that the results from many years of master studies are possible to compare.

Knowledge about the number and types of bacteria in the sample would be helpful in order to understand differences in respiration rates. In this study, bacteria are first removed by filtrating the samples through a 0.2 µm filter. In the biodegradation experiment, indigenous bacteria from raw Langtjern water are then added to the samples along with nutrients. Although this method serves to control the amount of bacteria, there could be seasonal and temporal changes in the bacterial community that are not taken into account.

References

Al-Reasi, Hassan A., Chris M. Wood, and D. Scott Smith. 2011. 'Physicochemical and spectroscopic properties of natural organic matter (NOM) from various sources and implications for ameliorative effects on metal toxicity to aquatic biota', *Aquatic Toxicology*, 103: 179-90.

Bayley, S. E., R. S. Behr, and C. A. Kelly. 1986. 'Retention and release of S from A freshwater wetland', *Water, Air, and Soil Pollution*, 31: 101-14.

Braaten, H. F. V. 2015. 'Mercury in boreal freshwater fish - Factors and processes governing increasing concentrations', University of Oslo.

Braaten, H. F. V., Heleen A. de Wit, Eirik Fjeld, Sigurd Rognerud, Espen Lydersen, and Thorjørn Larssen. 2014. 'Environmental factors influencing mercury speciation in Subarctic and Boreal lakes', *Science of The Total Environment*, 476: 336-45.

Braaten, H. F. V., Steffan Åkerblom, Helen A. de Wit, Gunnar Skotte, Martti Rask, Jussi Vuorenmaa, Kimmo K. Kahilainen, Tommi Malinen, Sigurd Rognerud, Espen Lydersen, Per-Arne Amundsen, Nicholas Kashulin, Tatiana Kashulina, Petr Terentyev, Guttorm Christensen, Leah Jackson-Blake, Espen Lund, and Bjørn Olav Rosseland. 2017. "Spatial and temporal trends of mercury in freshwater fish in Fennoscandia (1965-2015)." In *ICP Waters report*, edited by Heleen de Wit and Raoul-Marie Couture. Oslo: NIVA.

Braaten, Hans Fredrik Veiteberg, Eirik Fjeld, Sigurd Rognerud, Espen Lund, and Thorjørn Larssen. 2014. 'Seasonal and year-to-year variation of mercury concentration in perch (Perca fluviatilis) in boreal lakes', *Environmental Toxicology and Chemistry*, 33: 2661-70.

"The case for Calcium Chloride." In.: Occidental Chemical Corporation.

Chakraborty, Parthasarathi, Koffi Marcellin Yao, Kartheek Chennuri, Krushna Vudamala, and Peddinti Venkata Raghunadh Babu. 2014. *Interactions of mercury with different molecular weight fractions of humic substances in aquatic systems*.

Correll, D. L. 1999. *Phosphorus: A Rate Limiting Nutrient in Surface Waters*.

Couture, Raoul-Marie, Heleen A. de Wit, Koji Tominaga, Petri Kiuru, and Igor Markelov. 2015. 'Oxygen dynamics in a boreal lake responds to long-term changes in climate, ice phenology, and DOC inputs', *Journal of Geophysical Research: Biogeosciences*, 120: 2441-56.

de Wit, Heleen, Raoul-Marie Couture, Leah Jackson-Blake, Martyn Futter, Salar Valinia, Kari Austnes, Jose-Luis Guerrero, and Yan Lin. 2018. *Pipes or chimneys? For carbon cycling in small boreal lakes, precipitation matters most: Lakes: pipes or chimneys?*

Driscoll, Charles T., Robert P. Mason, Hing Man Chan, Daniel J. Jacob, and Nicola Pirrone. 2013. 'Mercury as a Global Pollutant: Sources, Pathways, and Effects', *Environmental Science & Technology*, 47: 4967-83.

EFSA. 2018. 'Scienticic Opinion on the risk for public health related to the presence of mercury and methylmercury in food.', *EFSA Journal*, 10.

Eimers, M. Catherine, and Peter J. Dillon. 2002. 'Climate effects on sulphate flux from forested catchments in south-central Ontario', *Biogeochemistry*, 61: 337-55.

Elser, James J., Matthew E. S. Bracken, Elsa E. Cleland, Daniel S. Gruner, W. Stanley Harpole, Helmut Hillebrand, Jacqueline T. Ngai, Eric W. Seabloom, Jonathan B. Shurin, and Jennifer E. Smith. 2007. 'Global analysis of nitrogen and phosphorus limitation of primary producers in freshwater, marine and terrestrial ecosystems', *Ecology Letters*, 10: 1135-42.

EPA. 2002. "Method 1631, Revision E: Mercury in Water by Oxidation, Purge and Trap, and Cold Vapour Atomic Fluorescence Spectrometry." In.
Esbensen, K. H. 2002. *Multivariate Data Analysis - in practice. An introduction to multivariate data analysis and experimental design.* (CAMO Software AS: Aalborg University).
Evans, C. D., Monteith, D. T., Cooper, D. M. 2005. 'Long-term increases in surface water dissolved organic carbon: Observations, possible causes and environmental impacts', *Environmental Pollution*, 137: 55-71.
Finstad, Anders G., Tom Andersen, Søren Larsen, Koji Tominaga, Stefan Blumentrath, Heleen A. de Wit, Hans Tømmervik, and Dag Olav Hessen. 2016. 'From greening to browning: Catchment vegetation development and reduced S-deposition promote organic carbon load on decadal time scales in Nordic lakes', 6: 31944.
Fitzgerald, William F., Daniel R. Engstrom, Robert P. Mason, and Edward A. Nater. 1998. 'The case for atmospheric mercury contamination in remote areas', *Environmental Science & Technology*, 32.
Folkehelseinstituttet. 2016. "Metaller i mat." In *Miljø og helse - en kunnskapsbase*.
Francés, Elena Martínez. 2017. 'Biodegradability and Spectroscopic Properties of Dissolved Natural Organic Matter Fractions Linked to Hg and MeHg Transport and Uptake', University of Oslo.
Fukuda, Naomichi, Masaki Takaoka, Shingo Doumoto, Kazuyuki Oshita, Shinsuke Morisawa, and Tadao Mizuno. 2011. *Mercury emission and behavior in primary ferrous metal production*.
Gaffney, Jeffrey S., Nancy A. Marley, and Sue B. Clark. 1996. 'Humic and Fulvic Acids and Organic Colloidal Materials in the Environment.' in, *Humic and Fulvic Acids* (American Chemical Society).
Gilmour, Cynthia C., Dwayne A. Elias, Amy M. Kucken, Steven D. Brown, Anthony V. Palumbo, Christopher W. Schadt, and Judy D. Wall. 2011. 'Sulfate-Reducing Bacterium Desulfovibrio desulfuricans ND132 as a Model for Understanding Bacterial Mercury Methylation', *Applied and Environmental Microbiology*, 77: 3938.
Gjessing, E. T., P. K. Egeberg, and J. Håkedal. 1999. 'Natural organic matter in drinking water — The "NOM-typing project", background and basic characteristics of original water samples and NOM isolates', *Environment International*, 25: 145-59.
Grigal, D. F. 2002. 'Inputs and outputs of mercury from terrestrial watersheds: a review', *Environmental Reviews*, 10: 1-39.
Guéguen, C., C. Belin, and J. Dominik. 2002. 'Organic colloid separation in contrasting aquatic environments with tangential flow filtration', *Water Research*, 36: 1677-84.
Guggenberger, Georg, Wolfgang Zech, and Hans-Rolf Schulten. 1994. 'Formation and mobilization pathways of dissolved organic matter: evidence from chemical structural studies of organic matter fractions in acid forest floor solutions', *Organic Geochemistry*, 21: 51-66.
Harmens, Harry, David A. Norris, Georgia R. Koerber, Alan Buse, Eiliv Steinnes, and Åke Rühling. 2008. 'Temporal trends (1990–2000) in the concentration of cadmium, lead and mercury in mosses across Europe', *Environmental Pollution*, 151: 368-76.
Harris, Daniel C., and Charles A. Lucy. 2016. *Quantitative Chemical Analysis* (W. H. Freeman and Company: USA).

Hautala, Kimmo, Juhani Peuravuori, and Kalevi Pihlaja. 2000. 'Measurement of aquatic humus content by spectroscopic analyses', *Water Research*, 34: 246-58.
Hollis, L., L. Muench, and R. C. Playle. 1997. 'Influence of dissolved organic matter on copper binding, and calcium on cadmium binding, by gills of rainbow trout', *Journal of Fish Biology*, 50: 703-20.
Hong, Young-Seoub, Yu-Mi Kim, and Kyung-Eun Lee. 2012. 'Methylmercury Exposure and Health Effects', *Journal of Preventive Medicine and Public Health*, 45: 353-63.
Håland, A. 2017. 'Characteristics and Bioavailability of Dissolved Natural Organic Matter in a Boreal Stream during Storm Flow', University of Oslo.
Kassambara, A. 2017. *Practical Guide to Principal Component Methods in R, PCA, (M)CA, FAMD, MFA, HCPC, factoextra* (STHDA).
Krzeminski, P. 2016. "Tangential Flow FIltration & Size Fractionation of Organic Matter." In *CLIMER project meeting*. NIVA.
Leenheer, Jerry A., and Jean-Philippe Croué. 2003. 'Peer Reviewed: Characterizing Aquatic Dissolved Organic Matter', *Environmental Science & Technology*, 37: 18A-26A.
Maier, Raina M., and Ian L. Pepper. 2015. 'Chapter 3 - Bacterial Growth.' in Ian L. Pepper, Charles P. Gerba and Terry J. Gentry (eds.), *Environmental Microbiology (Third Edition)* (Academic Press: San Diego).
Marschner, Bernd, and Karsten Kalbitz. 2003. 'Controls of bioavailability and biodegradability of dissolved organic matter in soils', *Geoderma*, 113: 211-35.
McKnight, Diane M., Elizabeth W. Boyer, Paul K. Westerhoff, Peter T. Doran, Thomas Kulbe, and Dale T. Andersen. 2001. 'Spectrofluorometric characterization of dissolved organic matter for indication of precursor organic material and aromaticity', *Limnology and Oceanography*, 46: 38-48.
Monteith, Donald T., John L. Stoddard, Christopher D. Evans, Heleen A. de Wit, Martin Forsius, Tore Hogasen, Anders Wilander, Brit Lisa Skjelkvale, Dean S. Jeffries, Jussi Vuorenmaa, Bill Keller, Jiri Kopacek, and Josef Vesely. 2007. 'Dissolved organic carbon trends resulting from changes in atmospheric deposition chemistry', *Nature*, 450: 537-40.
Munthe, John, Ingvar Wängberg, Sigurd Rognerud, Eirik Fjeld, Matti Verta, Petri Porvari, and Markus Meili. 2007. "Mercury in Nordic ecosystems." In.
NIVA. 2017. 'Langtjern - long term ecological monitoring', NIVA.
Oliver, Barry G., Earl M. Thurman, and Ronald L. Malcolm. 1983. 'The contribution of humic substances to the acidity of colored natural waters', *Geochimica et Cosmochimica Acta*, 47: 2031-35.
Ong, S. H. L. 2018. 'Biodegradability and Mercury Fractions in Dissolved Natural Organic Matter Size Fractions', University of Oslo.
Pacyna, E. G., J. M. Pacyna, K. Sundseth, J. Munthe, K. Kindbom, S. Wilson, F. Steenhuisen, and P. Maxson. 2010. 'Global emission of mercury to the atmosphere from anthropogenic sources in 2005 and projections to 2020', *Atmospheric Environment*, 44: 2487-99.
Parks, Jerry M., Alexander Johs, Mircea Podar, Romain Bridou, Richard A. Hurt, Steven D. Smith, Stephen J. Tomanicek, Yun Qian, Steven D. Brown, Craig C. Brandt, Anthony V. Palumbo, Jeremy C. Smith, Judy D. Wall, Dwayne A. Elias, and Liyuan Liang. 2013. 'The Genetic Basis for Bacterial Mercury Methylation', *Science*, 339: 1332.
Perdue, E. M., and J. D. Ritchie. 2003. *Dissolved Organic Matter in Freshwaters* (Elsevier).

Peuravuori, Juhani, and Kalevi Pihlaja. 1997. 'Molecular size distribution and spectroscopic properties of aquatic humic substances', *Analytica Chimica Acta*, 337: 133-49.
Pirrone, N., S. Cinnirella, X. Feng, R. B. Finkelman, H. R. Friedli, J. Leaner, R. Mason, A. B. Mukherjee, G. B. Stracher, D. G. Streets, and K. Telmer. 2010. 'Global mercury emissions to the atmosphere from anthropogenic and natural sources', *Atmos. Chem. Phys.*, 10: 5951-64.
Poste, Amanda E., Hans Fredrik Veiteberg Braaten, Heleen A. de Wit, Kai Sørensen, and Thorjørn Larssen. 2015. 'Effects of photodemethylation on the methylmercury budget of boreal Norwegian lakes', *Environmental Toxicology and Chemistry*, 34: 1213-23.
Poulain, Alexandre J., and Tamar Barkay. 2013. 'Cracking the Mercury Methylation Code', *Science*, 339: 1280.
PreSens. 2016. "SDR SensorDish Reader manual." In.
Qualls, Robert, and Bruce L. Haines. 1992. *Biodegradability of Dissolved Organic Matter in Forest Throughfall, Soil Solution, and Stream Water*.
Rahman, Mohammad Arifur, Md. Abu Hasan, Rahim Abdur, and A. M. Shafiqul Alam. 2010. 'Characterization of Humic Acid from the River Bottom Sediments of Burigonga: Complexation Studies of Metals with Humic Acid', *2010*, 11.
Rajakumar, Janaki. 2018. 'Factors Explaining the Effect of Photo-oxidation on Dissolved Natural Organic Matter', University of Oslo.
Ravichandran, Mahalingam. 2004. 'Interactions between mercury and dissolved organic matter––a review', *Chemosphere*, 55: 319-31.
Skjelkvåle, B. L. 2003. "The 15-year report: Assessment and monitoring of surface waters in Europe and North America acidification and recovery, dynamic modelling and heavy metals." In *ICP Waters report (73/2003)*. Norwegian Insititute for water research.
Skjelkvåle, B. L., T. Andersen, G. A. Halvorsen, G. G. Raddum, E. Heegaard, J. Stoddard, and R. F. Wright. 2000. "The 12-year report: Acidification of Surface Water in Europe and North America; Trends, biological recovery and heavy metals." In *ICP Waters 52/2000*. Norwegian Institute for Water Research.
Thermo-Fisher. 2016. 'Dionex Integrion HPIC System Operator's manual'.
Ullrich, Susanne M., Trevor W. Tanton, and Svetlana A. Abdrashitova. 2001. 'Mercury in the Aquatic Environment: A Review of Factors Affecting Methylation', *Critical Reviews in Environmental Science and Technology*, 31: 241-93.
UN. 2013. "Minamata convention on mercury." In. Kumamoto, Japan: United Nations Environment.
———. 2017. "The 50-ratification milestone required for the Minimata Convention on Mercury to enter into force was reached on 18 May 2017!" In.: United Nations Environment, Minamata Convention on Mercury.
UNEP. 2002. "Global Mercury Assessment." In, edited by United Nations Environment Programme. Geneva, Switzerland: UNEP Chemicals.
Vangenechten, J. H. D., F. Bosmans, and H. Deckers. 1981. 'Effects of short-term changes in rain water supply on the ionic composition of acid moorland pools in the Campine of Antwerp (Belgium)', *Hydrobiologia*, 76: 149-59.
vanLoon, Gary W., and Stephen J. Duffy. 2011. *Environmental chemistry, a global perspective* (Oxford University Press Inc: USA).
Vogt, Rolf, and Egil Gjessing. 2008. "Correlation between optical and chemical properties of DNOM. From molecular understanding to innovative applications of humic

substances." In *The 14th International Meeting of the International Humic Substances Society*. Moscow, Russia.
Weishaar, James L., George R. Aiken, Brian A. Bergamaschi, Miranda S. Fram, Roger Fujii, and Kenneth Mopper. 2003. 'Evaluation of Specific Ultraviolet Absorbance as an Indicator of the Chemical Composition and Reactivity of Dissolved Organic Carbon', *Environmental Science & Technology*, 37: 4702-08.
Zhang, Yanxu, Daniel J. Jacob, Hannah M. Horowitz, Long Chen, Helen M. Amos, David P. Krabbenhoft, Franz Slemr, Vincent L. St. Louis, and Elsie M. Sunderland. 2016. 'Observed decrease in atmospheric mercury explained by global decline in anthropogenic emissions', *Proceedings of the National Academy of Sciences of the United States of America*, 113: 526-31.

Appendix

A. Data analysis

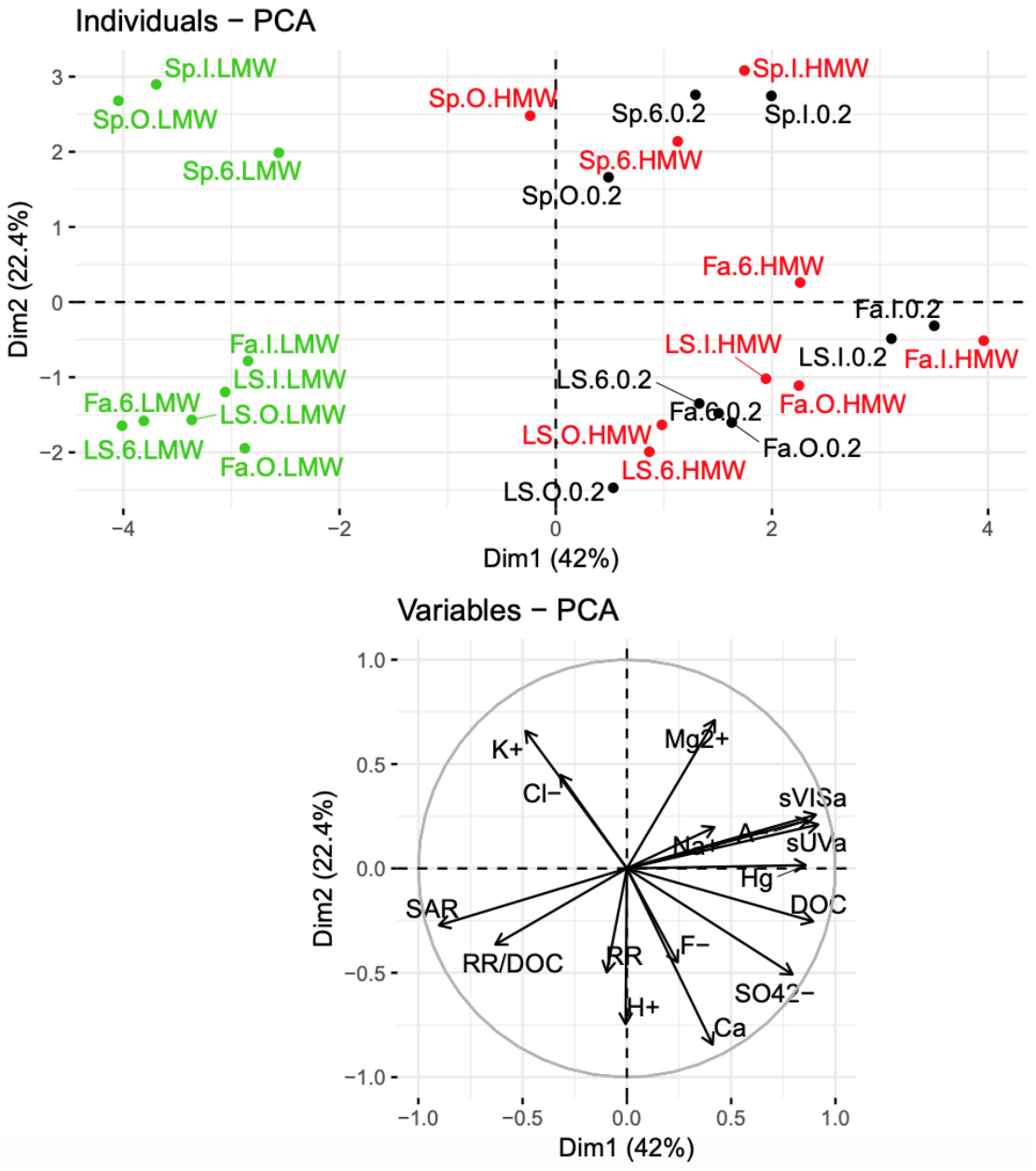

Figure A.3: PCA dimension 1 and 2 Principal Component 1 (horizontal direction) and 2 (vertical direction) of Principal Component Analysis of presented features. The score plot of the samples ("Individuals") display LMW fractions (in green), HMW fractions (in red), and the 0.2 µm fraction (in black) for samples collected at the Spring (LS), Late summer (LS) and the Fall (Fa), at the lake position Outlet (O), Inlet (I) and at the hypolimnion depth (6). The corresponding loading plot of the variables displays how the different observed features relate to the samples.

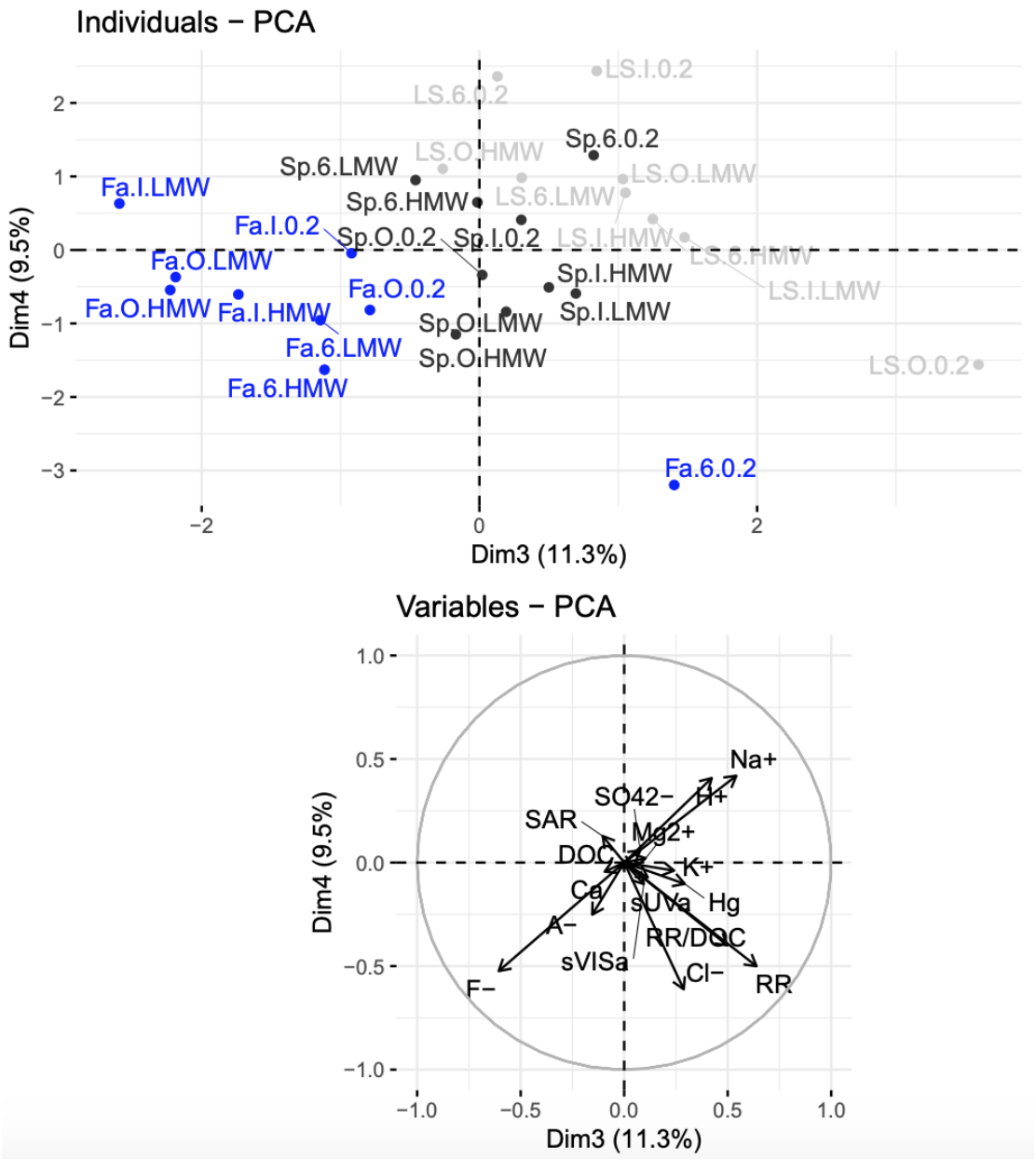

Figure A.4: PCA dimension 3 and 4. Principal Component 1 (horizontal direction) and 2 (vertical direction) of Principal Component Analysis of presented features. The score plot of the samples ("Individuals") display LMW fractions (in green), HMW fractions (in red), and the 0.2 µm fraction (in black) for samples collected at the Spring (LS), Late summer (LS) and the Fall (Fa), at the lake position Outlet (O), Inlet (I) and at the hypolimnion depth (6). The corresponding loading plot of the variables displays how the different observed features relate to the samples

B. Sample collection

Samples were collected at lake Langtjern. Figure A.1 and A.2 shows the inlet in May and September, respectively.

Figure A.3: The inlet of Langtjern at the first sampling, May 30th, 2018. The inlet was unusually dry, which made sample collection challenging.

Figure A.4: The inlet of the lake on September 20th, 2018. The water stream was normal this time.

C. DOC

C.1 Calibration curves

A 1000 ppm KH-phthalate stock solution was made by drying KH-phthalate in the oven for one hour at 100 °C, dissolving 2.125 g of the dried material in type I water and diluting to 1000 mL in a volumetric flask. From the stock solution, standards with the concentrations 0, 3, 5, 10, 20 and 30 ppm were prepared. The calibration curves for analysing the spring, September and October samples are presented in Figure A.3, A.4 and A.5, respectively.

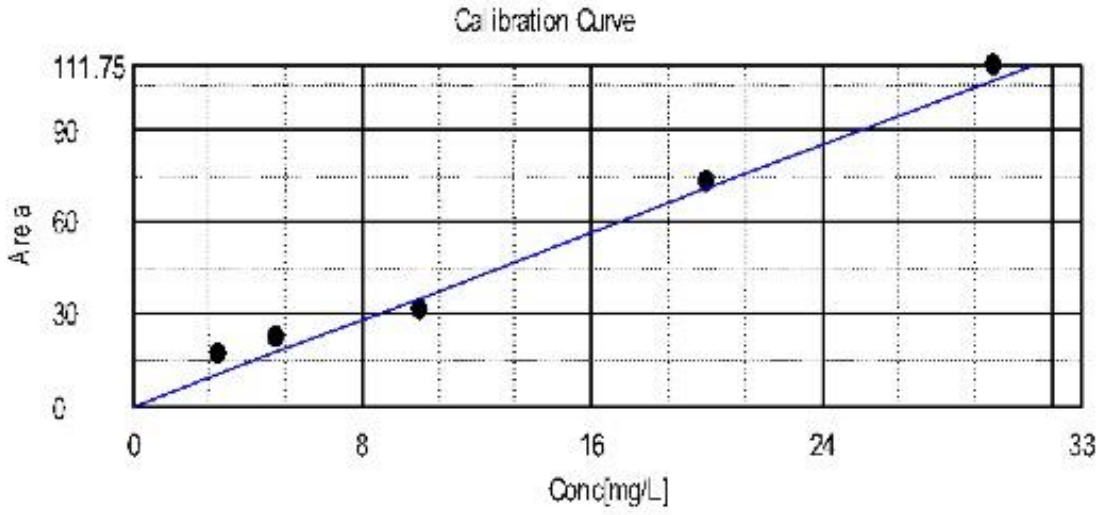

Figure A.5: Calibration curve for DOC measurements of the spring samples. The standards were made from potassium hydrogen phthalate solutions.

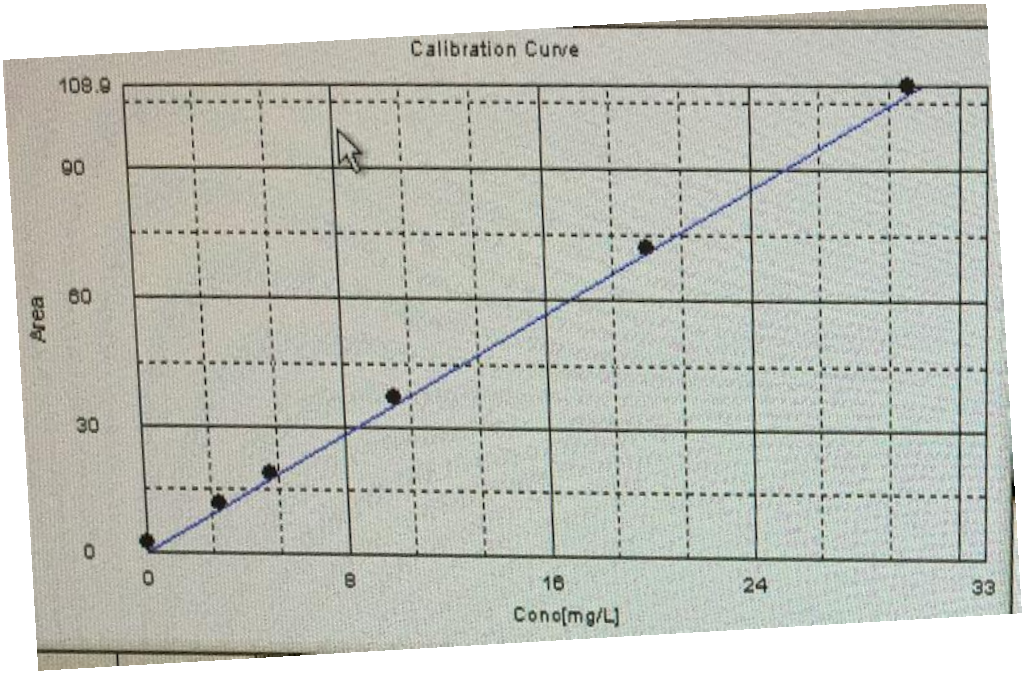

Figure A.6: Calibration curve for DOC analysis of the September samples.

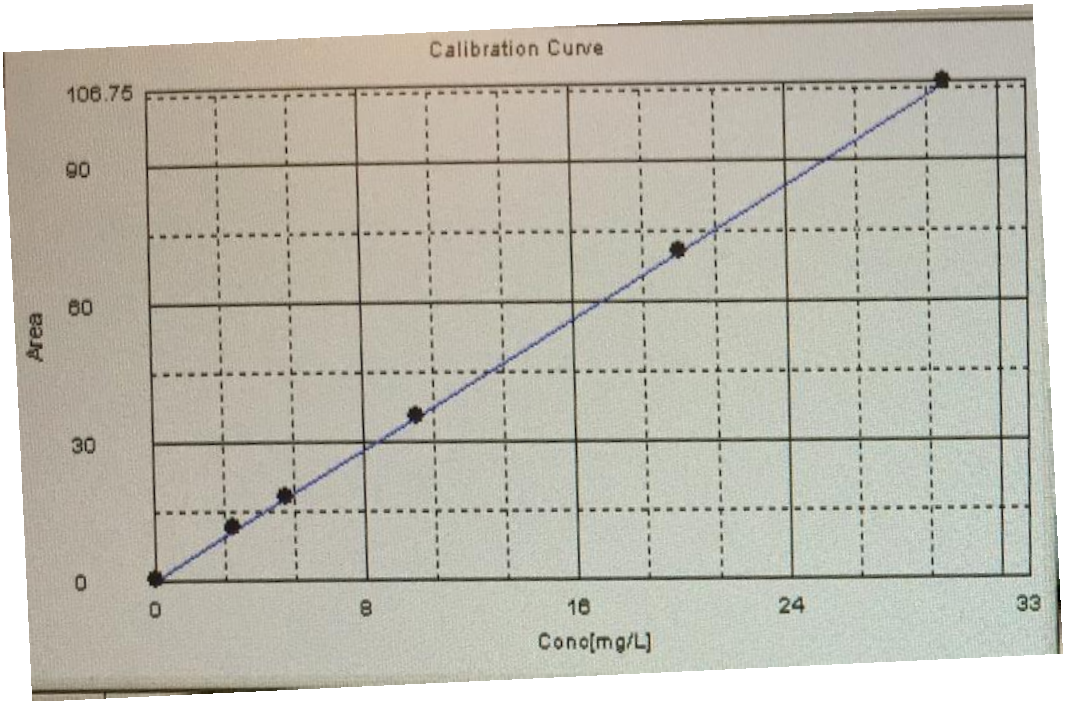

Figure A.7: Calibration curve for the DOC analysis of the October samples.

C.2 DOC results

DOC results are presented in table A.1.

Table A.2: DOC data of the spring samples from the outlet, inlet and at 6 meters.

			DOC (mgL^{-1})	Sample volume (L)	DOC mass (mg)	DOC dist (%)	DOC gain/loss (mg)	DOC gain/loss (%)
Outlet	Rep 1	Feed	7.45	1.06	7.90			
		Concentrate	7.29	0.81	5.90	84	-0.9	-11
		Permeate	4.41	0.25	1.10	16		
	Sample	Feed	7.24	3.92	28.36			
		Concentrate	7.88	2.92	23.02	86	-1.5	-5.0
		Permeate	3.89	1.00	3.89	14		
	Rep 2	Feed	7.50	1.50	11.25			
		Concentrate	7.96	1.11	8.83	86	-1.0	-9.0
		Permeate	3.72	0.39	1.45	14		
Inlet	Rep 1	Feed	11.27	1.18	13.24			
		Concentrate	11.77	0.825	9.71	88	-2.1	-16
		Permeate	3.957	0.35	1.38	12		
	Sample	Feed	11.41	3.96	45.13			
		Concentrate	12.20	3.00	36.54	91	-4.8	-11
		Permeate	3.77	1.00	3.77	9		
	Rep 2	Feed	11.97	1.86	22.26			
		Concentrate	12.57	1.51	18.98	93	-1.9	-9.0
		Permeate	3.81	0.35	1.33	7		
6 m depth	Rep 1	Feed	9.10	0.93	8.46			
		Concentrate	9.42	0.58	5.46	71	-0.8	-9.0
		Permeate	6.39	0.35	2.23	29		
	Sample	Feed	9.02	4.14	37.35			
		Concentrate	9.66	3.14	30.36	85	-1.5	-4.0
		Permeate	5.48	1.00	5.48	15		
	Rep 2	Feed	8.86	1.52	13.47			
		Concentrate	8.96	0.92	8.24	72	-2.0	-15
		Permeate	5.42	0.60	3.25	28		

B.3 Percent distribution and estimated DOC

Table A.3: Estimated DOC, spring.

	SPRING	FEED	HMW	LMW
OUTLET	Measured DOC (mg/L)	7.24	7.88	3.89
	% Distribution	100	85.56	14.44
	Estimated DOC (mg C/L)	7.24	6.74	0.56
INLET	Measured DOC (mg/L)	11.41	12.20	3.77
	% Distribution	100	90.66	9.34
	Estimated DOC (mg C/L)	11.41	11.06	0.35
6 M	Measured DOC (mg/L)	9.02	9.66	5.48
	% Distribution	100	84.72	15.28
	Estimated DOC (mg C/L)	9.02	8.18	0.84

Table A.4: Estimated DOC, September.

	SEPTEMBER	FEED	HMW	LMW
OUTLET	Measured DOC (mg/L)	12.69	14.22	7.004
	% Distribution	100	67.00	33.00
	Estimated DOC (mg C/L)	12.69	9.53	2.31
INLET	Measured DOC (mg/L)	16.97	17.45	7.979
	% Distribution	100	68.62	31.38
	Estimated DOC (mg C/L)	16.97	11.97	2.50
6 M	Measured DOC (mg/L)	10.42	11.55	4.36
	% Distribution	100	72.60	27.40
	Estimated DOC (mg C/L)	10.42	8.39	1.19

Table A.5: Estimated DOC, October.

	OCTOBER	FEED	HMW	LMW
OUTLET	Measured DOC (mg/L)	10.47	12.37	5.28
	% Distribution	100	87.49	12.51
	Estimated DOC (mg C/L)	10.47	10.82	0.6605
INLET	Measured DOC (mg/L)	10.42	11.55	4.36
	% Distribution	100	86.72	13.28
	Estimated DOC (mg C/L)	10.42	10.02	0.5790

6 M	Measured DOC (mg/L)	9.79	12.11	3.40
	% Distribution	100	91.43	8.57
	Estimated DOC (mg C/L)	9.79	11.07	0.2914

D. Anions

Major anions were analysed using the instrument shown in Figure A.6.

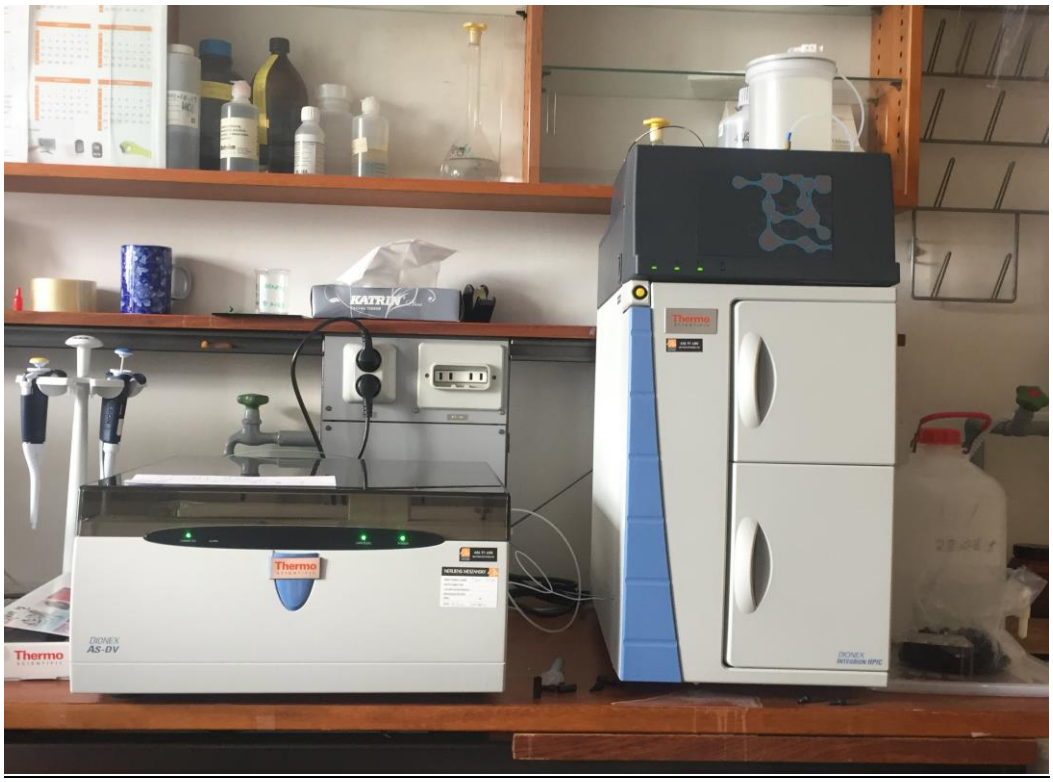

Figure A.8: Major anions were analysed using this Thermo Scientific Dionex Integrion HPIC instrument with a Dionex AS-DV autosampler. A computer connected to the instrument is used to run the software Chromeleon

D.1 Calibration curves

Calibrations curves for each ion were created by preparing calibration solutions from a Dionex Seven Anion Standard solution. 10x, 20x, 100x, 200x, 500x and 1000x dilutions were made. Calibration curves for each anion are presented in figure A.7.

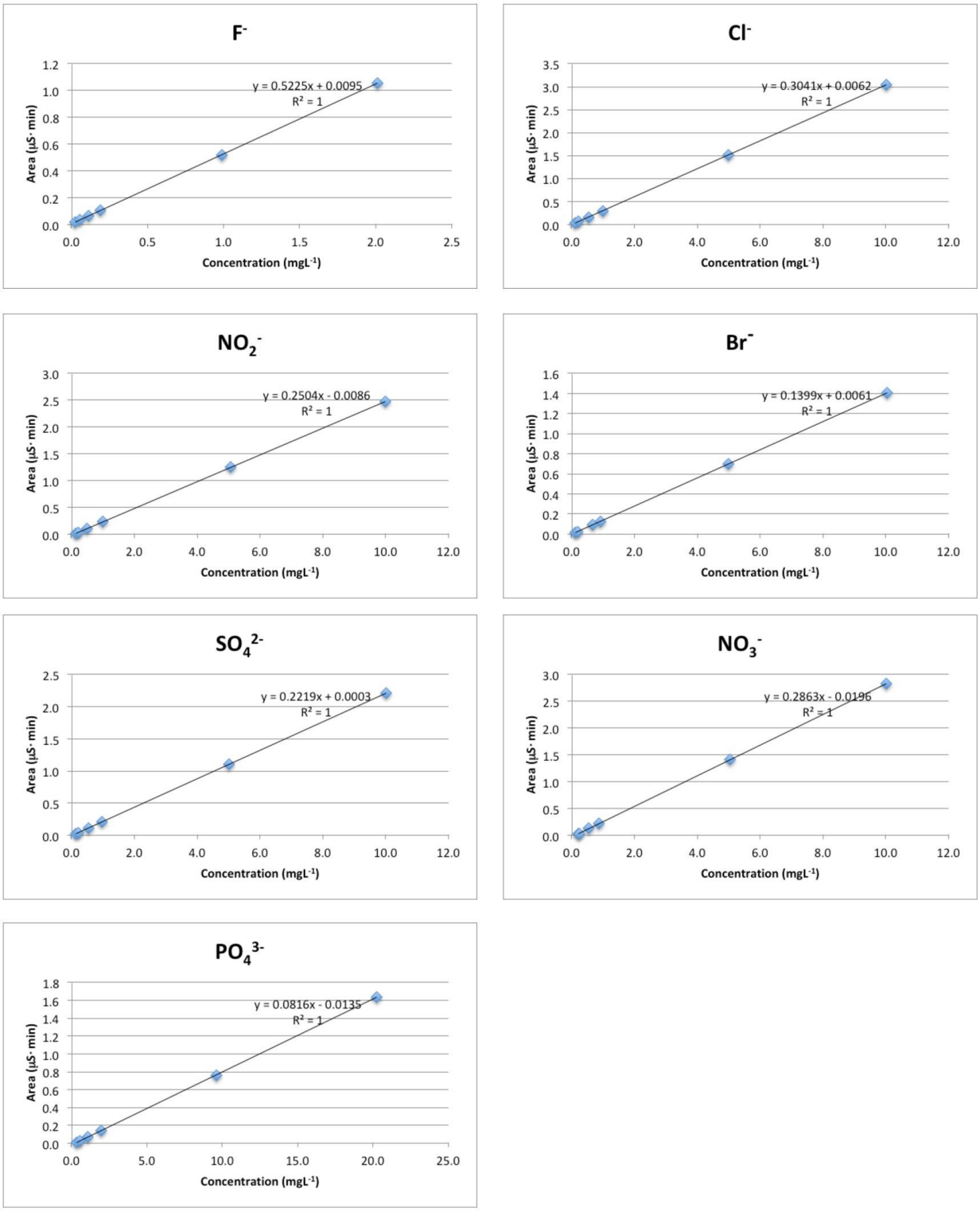

Figure A.9: Calibration curves for the anions of the spring samples. (MAKE AXES LARGER)

D.2 Dionex standard

The calibration curve was made using Thermo Fisher Scientific Dionex Seven Anion standard solution. The ion concentrations in the original solution are presented in table 7.

Table A.5: The ion concentrations in the Dionex seven anion standard solution.

Element	**Concentration (mgL^{-1})**
Fluoride (F^-)	20
Chloride (Cl^-)	100
Nitrite (NO_2^-)	100
Bromide (Br^-)	100
Nitrate (NO_3^-)	100
Phosphate (PO_4^{3-})	200
Sulphate (SO_4^{2-})	100

D.3 Instrument settings

The Dionex instrument settings are presented in table A.3.

Table A.6: IC instrument settings

Parameters	**Setting**
IC column	AS18
Run time per sample	22 minutes
Type of flow	Isocratic
Flow rate	0.25 $mLmin^{-1}$
Pump pressure	200 psi
Pump column and compartment temperature	25 °C
Electrolytic suppressor type	AERS 2 mm
Electrolytics suppressor hydroxide	23 mM
Electrolytics eluent generator concentration	25 M

E. Cations

Figure A.10 shows instrument being used for cation analysis. Concentrations of the cations in the standard solutions are presented in Table A.4 (spring) and A.5 (September and October).

Figure A.10: Major cations were analysed using this Varian Vista AX CCD simultaneous ICP-AES instrument.

Table A.7: Concentrations of the cations in the standard solutions used in the first ICP-OES experiment (spring samples).

	Std. 1 (mgL^{-1})	**Std. 2 (mgL^{-1})**	**Std. 3 (mgL^{-1})**	**Std. 4 (mgL^{-1})**	**Std. 5 (mgL^{-1})**	**Std. 6 (mgL^{-1})**	**Std. 7 (mgL^{-1})**
Na^+	0.96	2.4	60	12	20	40	64

K^+	0.96	2.4	60	12	20	40	64
Mg^{2+}	0.96	2.4	60	12	20	40	64
Ca^{2+}	0.96	2.4	60	12	20	40	64
Al^{3+}	0.096	0.24	0.60	1.2	2.0	4.0	6.4
Fe^{3+}	0.096	0.24	0.60	1.2	2.0	4.0	6.4

The first ICP-OES experiment was conducted using the standards presented in Table A.4. However, these concentrations were too high, and therefore, new standard solutions were prepared. The new concentrations are presented in Table A.5. These standards were used to create a calibration curve for the September and October samples.

Table A.8: Concentrations of the standard solution used in the second and third ICP-OES experiment (September and October samples).

	Std. 1 (mgL^{-1})	**Std. 2 (mgL^{-1})**	**Std. 3 (mgL^{-1})**	**Std. 4 (mgL^{-1})**	**Std. 5 (mgL^{-1})**	**Std. 6 (mgL^{-1})**	**Std. 7 (mgL^{-1})**
Na^+	0	0.5	1.0	1.5	2.0	2.5	3.0
K^+	0	0.5	1.0	1.5	2.0	2.5	3.0
Mg^{2+}	0	0.2	0.4	0.6	0.8	1.0	1.2
Ca^{2+}	0	0.2	0.4	0.6	0.8	1.0	1.2
Al^{3+}	0	0.2	0.4	0.6	0.8	1.0	1.2
Fe^{3+}	0	0.2	0.4	0.6	0.8	1.0	1.2

Table A.9: Limit of detection and limit of quantification, spring.

	Limit of detection (LOD)(mgL^{-1})	**Limit of quantification (LOQ)(mgL^{-1})**
Ca^{2+}	0.145	0.484
K^+	0.0183	0.0611
Mg^{2+}	0.0170	0.0565
Na^+	0.194	0.646

Table A.10: Limit of detection and limit of quantification, late summer.

	Limit of detection (LOD)(mgL^{-1})	**Limit of quantification (LOQ)(mgL^{-1})**
Ca^{2+}	0.116	0.385
K^+	0.0413	0.138

Mg^{2+}	0.0115	0.0384
Na^{+}	0.0361	0.120

F. pH and conductivity

The pH meter was calibrated using calibration solutions of pH 4.0, 7.0 and 10.0**.** The measured pH values are presented in table A.6, A.7 and A.8.

The conductivity meter was calibrated using an 84 $\mu S \cdot cm^{-1}$ calibration solution.

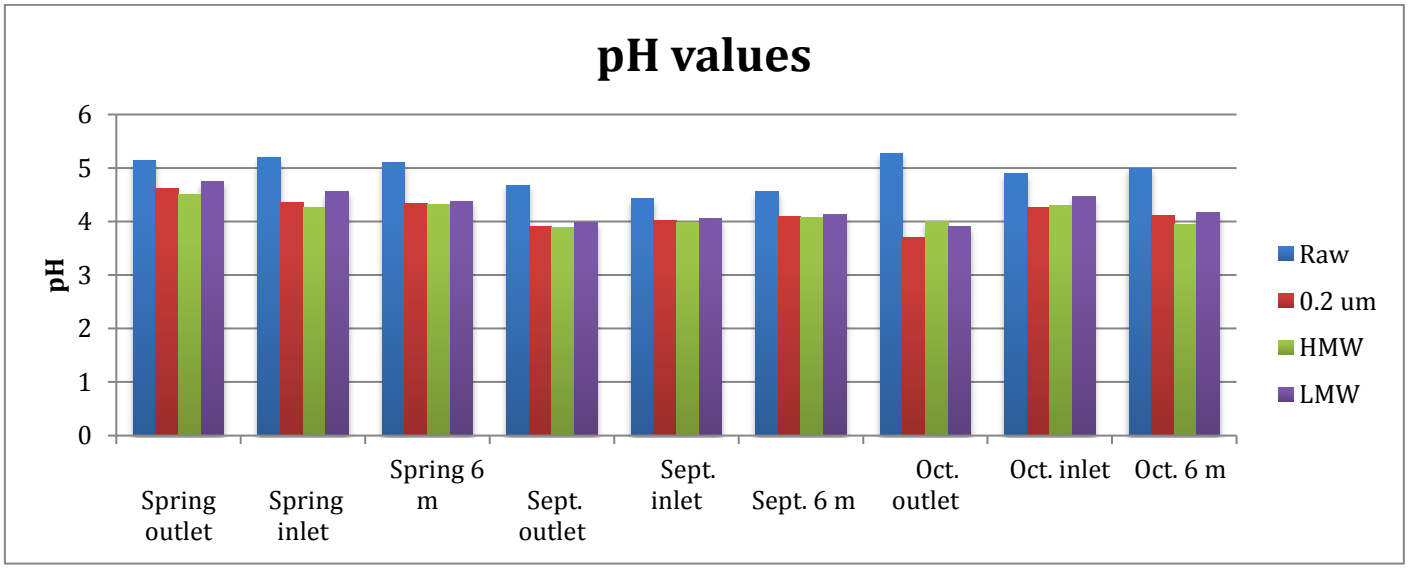

Figure A.11: pH values.

Table A.11: pH, conductivity and temperature for the size fractions of the spring samples.

SPRING		pH	Temperature (°C)	Conductivity (μScm^{-1})	Temperature (°C)
Outlet	Raw	5.15	20.6	10.32	21.0
	Influent	4.61	19.0	12.06	21.4
	Concentrate	4.51	17.5	16.75	18.02
	Permeate	4.75	17.3	10.29	19.1
Inlet	Raw	5.19	20.2	10.21	21.1
	Influent	4.36	18.0	17.25	21.3
	Concentrate	4.27	18.3	23.4	19.1
	Permeate	4.56	18.0	16.13	18.9

6 m depth	Raw	5.11	21.8	8.15	22.3
	Influent	4.34	19.0	12.88	21.0
	Concentrate	4.31	19.1	15.36	18.2
	Permeate	4.38	19.0	12.12	20.2

Table A.12: pH, conductivity and temperature for the size fractions of the September samples.

SEPTEMBER		pH	Temperature (°C)	Conductivity (μScm^{-1})	Temperature (°C)
Outlet	Raw	4.68	16.0	10.56	19.5
	Influent	3.90	14.2		
	Concentrate	3.89	11.8		
	Permeate	3.98	11.7		
Inlet	Raw	4.43	15.0	11.42	18.1
	Influent	4.02	14.7		
	Concentrate	3.99	12.1		
	Permeate	4.05	12.5		
6 m depth	Raw	4.56	16.8	13.94	21.1
	Influent	4.10	15.6		
	Concentrate	4.08	13.0		
	Permeate	4.13	13.5		

Table A.13: pH, conductivity and temperature of the size fractions of the October samples.

OCTOBER		pH	Temperature (°C)	Conductivity (μScm^{-1})	Temperature (°C)
Outlet	Raw	5.28	17.6	9.22	19.7
	Influent	3.70	15.3	37.9	15.3
	Concentrate	4.01	13.6	29.9	16.1
	Permeate	3.90	14.1	33.6	14.9
Inlet	Raw	4.89	17.9	11.09	15.8
	Influent	4.26	15.2	19.75	15.2

	Concentrate	4.30	13.5	25.5	14.8
	Permeate	4.47	13.7	13.58	15.0
6 m depth	Raw	5.00	18.7	9.48	16.0
	Influent	4.12	16.9	29.2	14.0
	Concentrate	3.94	15.1	36.1	14.4
	Permeate	4.17	14.8	22.4	14.9

G. Absorbance (UV-VIS)

G.1 Instrument settings

Absorbance was measured on a Shimadzu UV-1800 instrument with the settings presented in Table A.3.

Table A.14: Shimadzu UV-1800 instrument settings

Measuring mode	Absorbance
Scan range	800 – 200 nm
Rec. range	0.000 A – 4.000 A
Scan speed	Slow
Scan pitch	1.0 nm
Number of scans	1
Display mode	Sequential
Auto-print	Off

G.2 Absorbance results

Table A.15: UV-VIS values and proxies from the spring samples collected at the outlet, before and after biodegradation.

	OUTLET before biodegradation			**OUTLET after biodegradation**		
	Influent	Concentrate	Permeate	Influent	Concentrate	Permeate
λ 254 nm	0.339	0.349	0.139	0.373	0.352	0.148
λ 400 nm	0.0407	0.041	0.013	0.054	0.0465	0.0173
sUVa	4.69	4.43	3.58	5.16	4.46	3.81
sVISa	0.563	0.520	0.335	0.746	0.590	0.445
SAR	8.336	8.512	10.69	6.907	7.570	8.555

Table A.16: UV-VIS values and proxies from the spring samples collected at the inlet, before and after biodegradation.

	INLET before biodegradation			**INLET after biodegradation**		
	Influent	Concentrate	Permeate	Influent	Concentrate	Permeate
λ 254 nm	0.577	0.608	0.137	0.598	0.606	0.1498
λ 400 nm	0.0747	0.079	0.0137	0.092	0.0825	0.0183
sUVa	4.88	4.98	3.64	5.24	4.97	3.98
sVISa	0.655	0.648	0.364	0.806	0.676	0.486
SAR	7.723	7.696	10.02	6.500	7.348	8.205

Table A.16: UV-VIS values and proxies from the spring samples collected at a depth of 6 meters, before and after biodegradation.

	6 m depth before biodegradation			**6 m depth after biodegradation**		
	Influent	Concentrate	Permeate	Influent	Concentrate	Permeate
λ 254 nm	0.43	0.428	0.198	0.434	0.414	0.198
λ 400 nm	0.0547	0.052	0.019	0.057	0.05325	0.0215
sUVa	4.78	4.43	3.62	4.81	4.28	3.61
sVISa	0.607	0.538	0.347	0.632	0.551	0.393
SAR	7.866	8.237	10.42	7.614	7.775	9.221

H. Biodegradation

H.1 Solutions

Nutrient stock solution with a concentration of 10 mM was prepared by dissolving 1.74312 g K_2HPO_4 and 0.80068 g NH_4NO_3 in type I water and diluting to 1000 mL in a volumetric flask.

Glucose solution was prepared by adding 0.025 g of glucose to a volumetric flask, dissolving and diluting to 1000 mL.

H.2 Parameters

Time interval: 15 seconds

Oxygen unit: $mmol^{-1}$

Incubator temperature: 25 °C

H.3 Respiration rate/DOC of glucose

RR/DOC graphs with glucose values included are presented in Figure A.11, A.12 and A.13. The respiration rate/DOC of glucose varies between the three rounds of analysis. While running the spring samples the highest RR/DOC value is found in the glucose solution. However, when running the late summer samples, the glucose has the lowest RR/DOC, lower than LMW. Biodegradation is a complex process, and many factors contribute to the results. In this experiment, no attempt was made to know how many and what types of bacteria there are in the solution. The different types and relative amounts of bacteria in Langtjern vary over the season, which causes a difference in the

lag phase. After the lag phase, there should be no difference. However, the glucose values differ in this experiment.

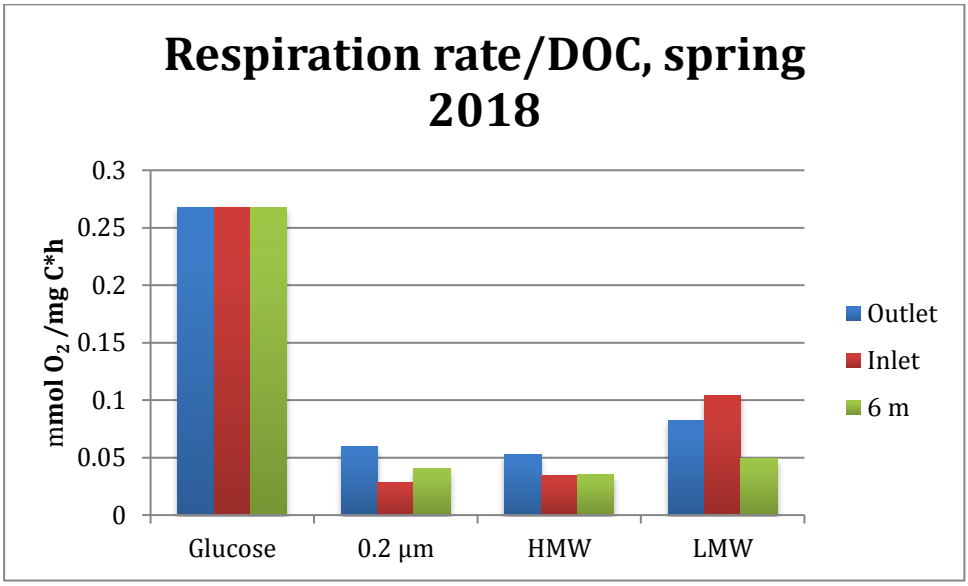

Figure A.12: RR/DOC spring

H.4 Oxygen consumption graphs

Oxygen consumption was measured in the different samples, and the graphs are presented in figure A.10-A.17. Each figure presents three replicates of the same sample, and should ideally look the same. The first concentrate sample at 6 meter depth looks different from the others. This sample should therefore be omitted in the calculations and interpretations.

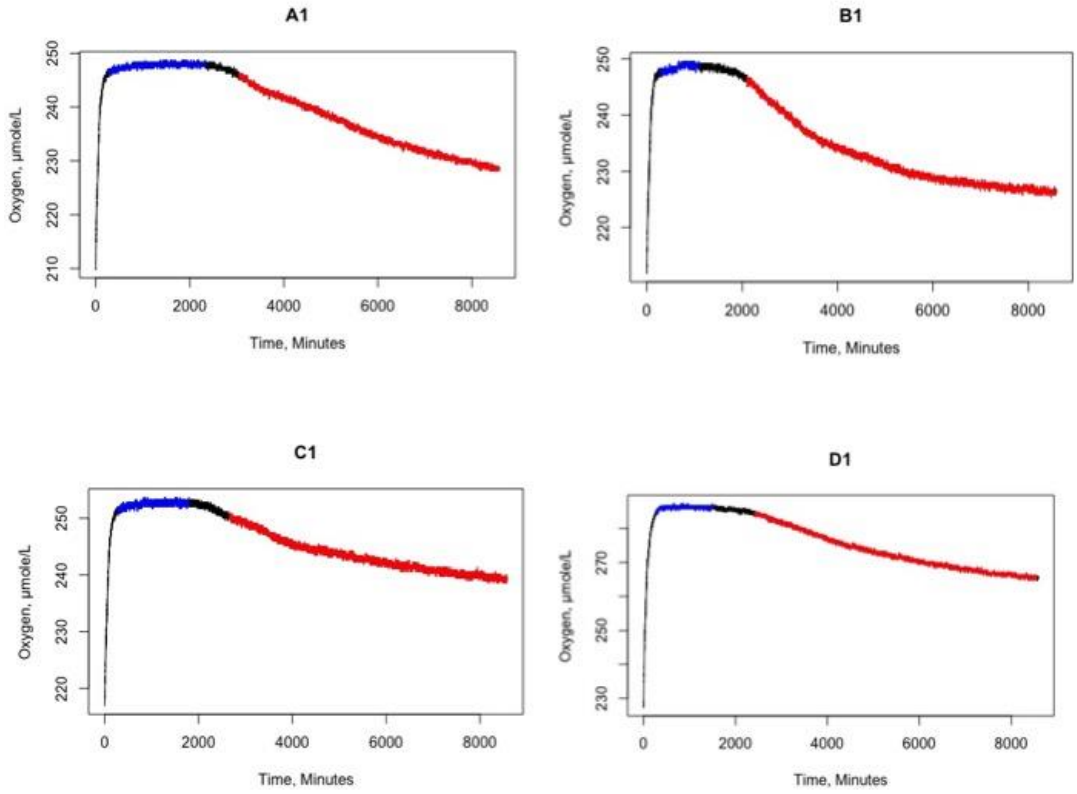

Figure A.13: Blanks

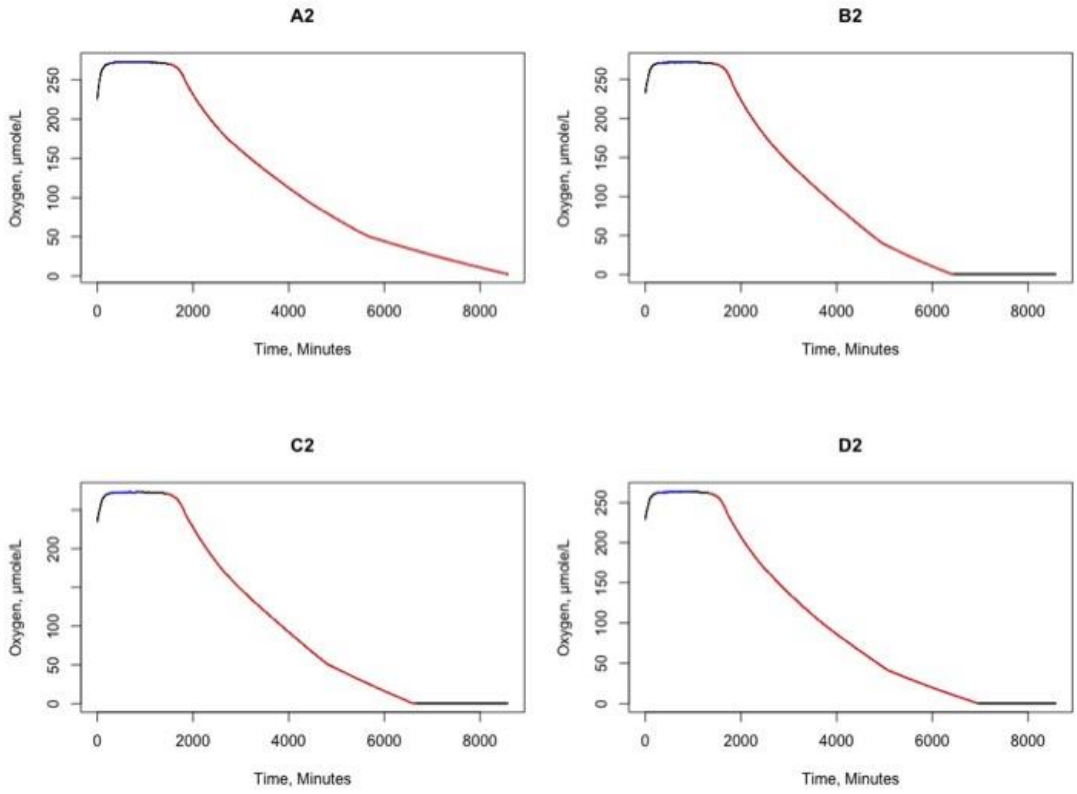

Figure A.14: Glucose used as reference.

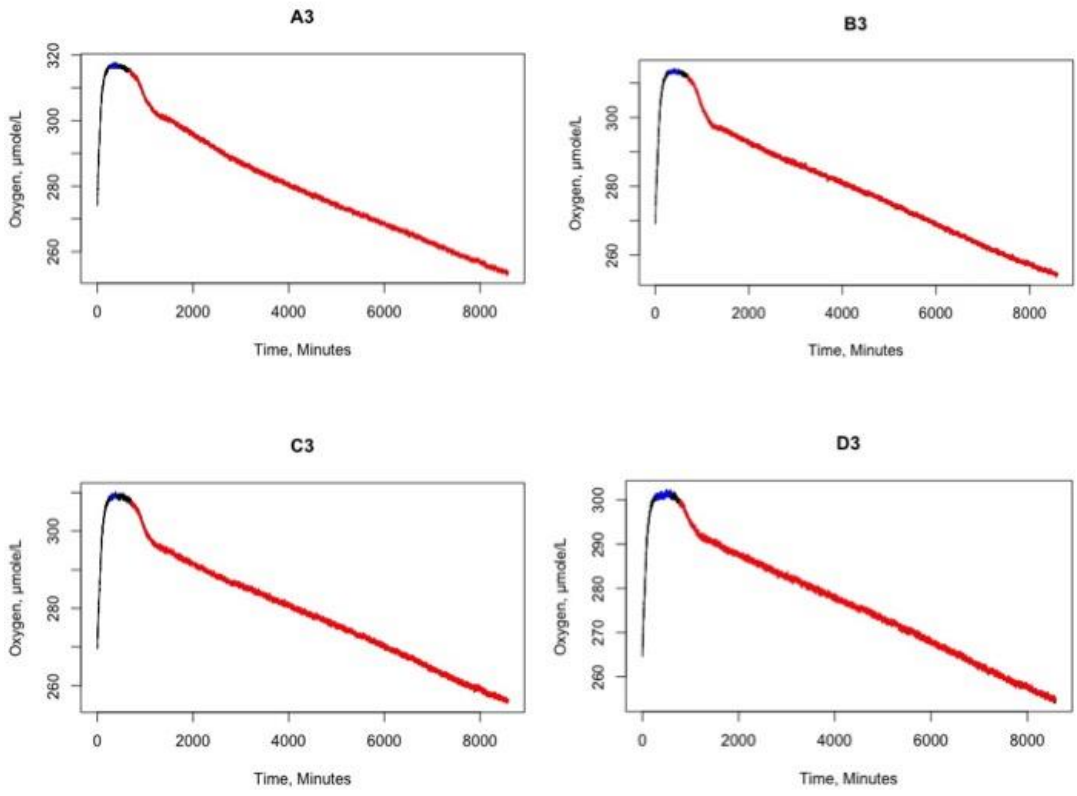

Figure A.15: Outlet concentrate

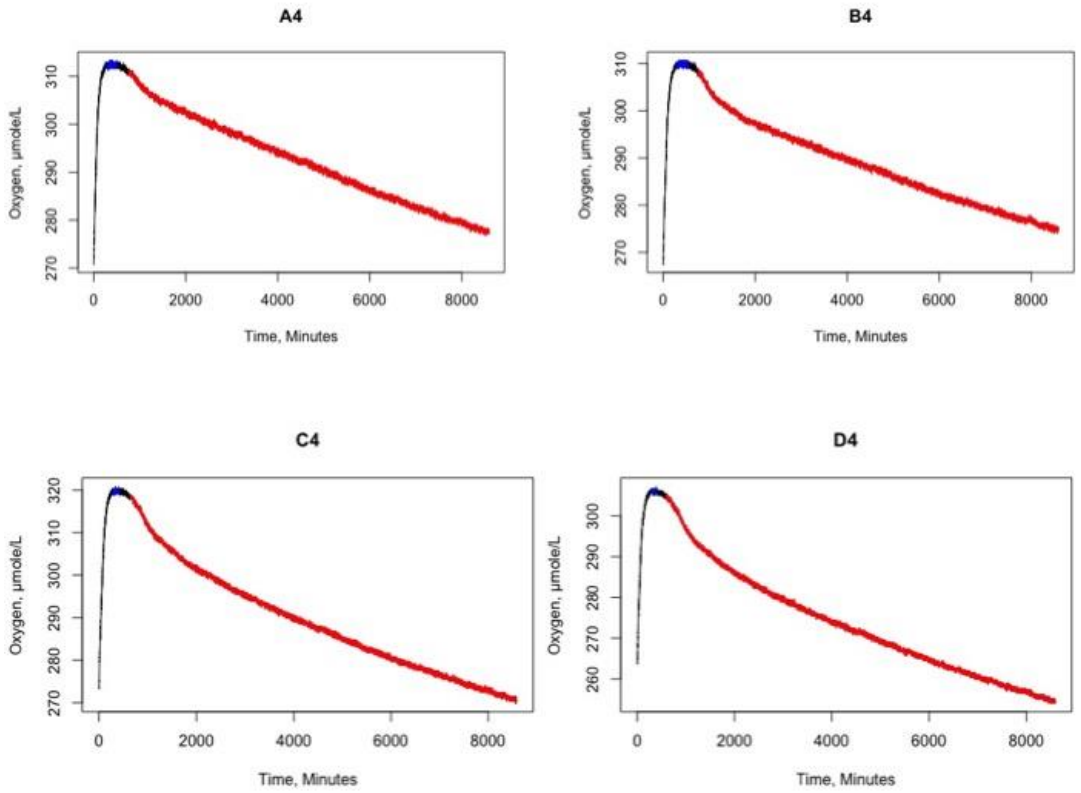

Figure A.16: Outlet permeate

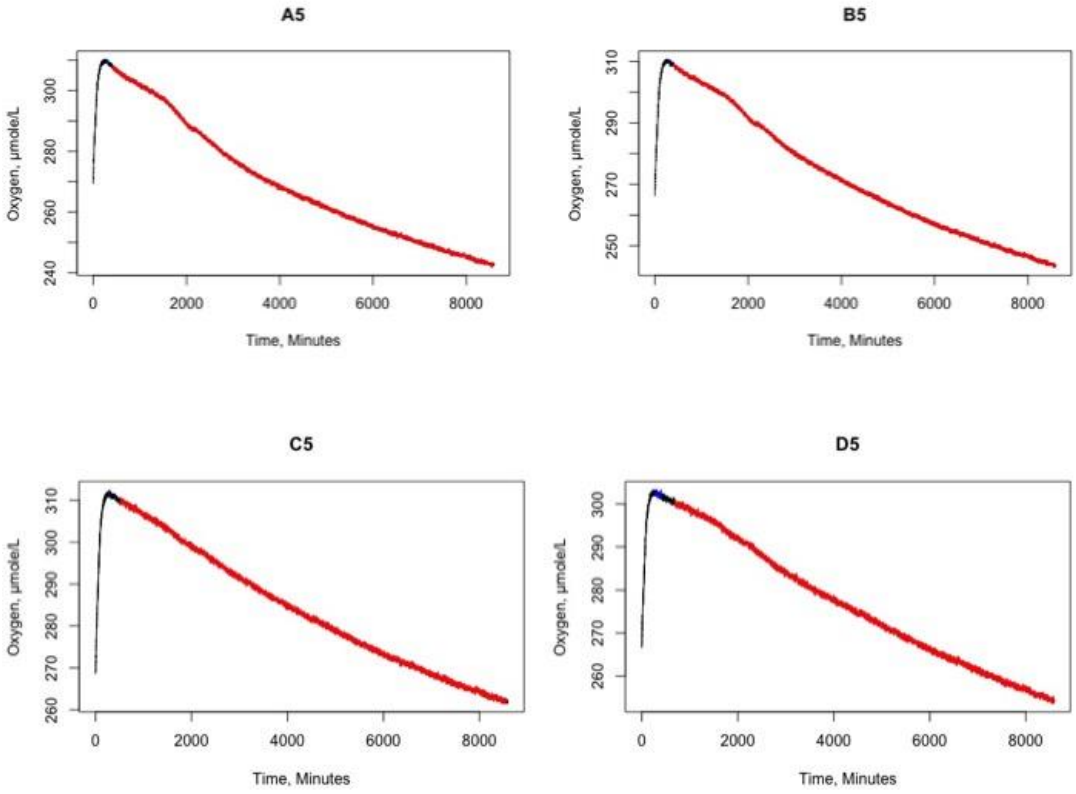

Figure A.17: Inlet concentrate

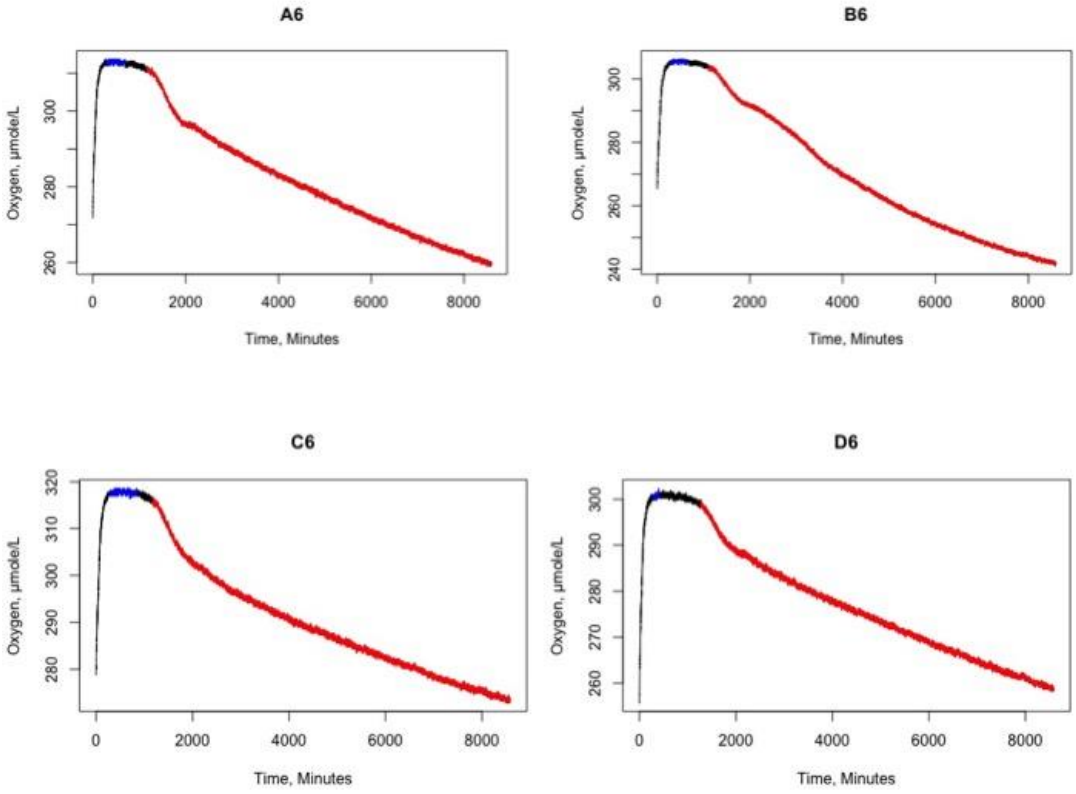

Figure A.18: Inlet permeate

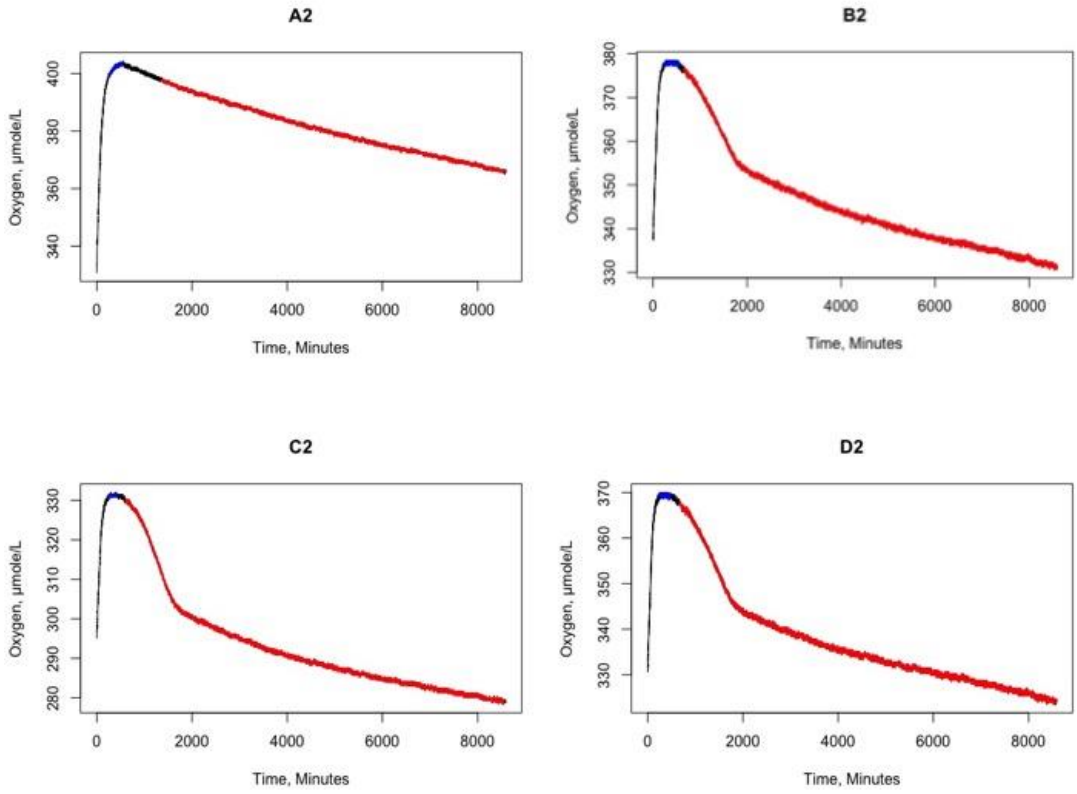

Figure A.19: 6 meter depth concentrate.

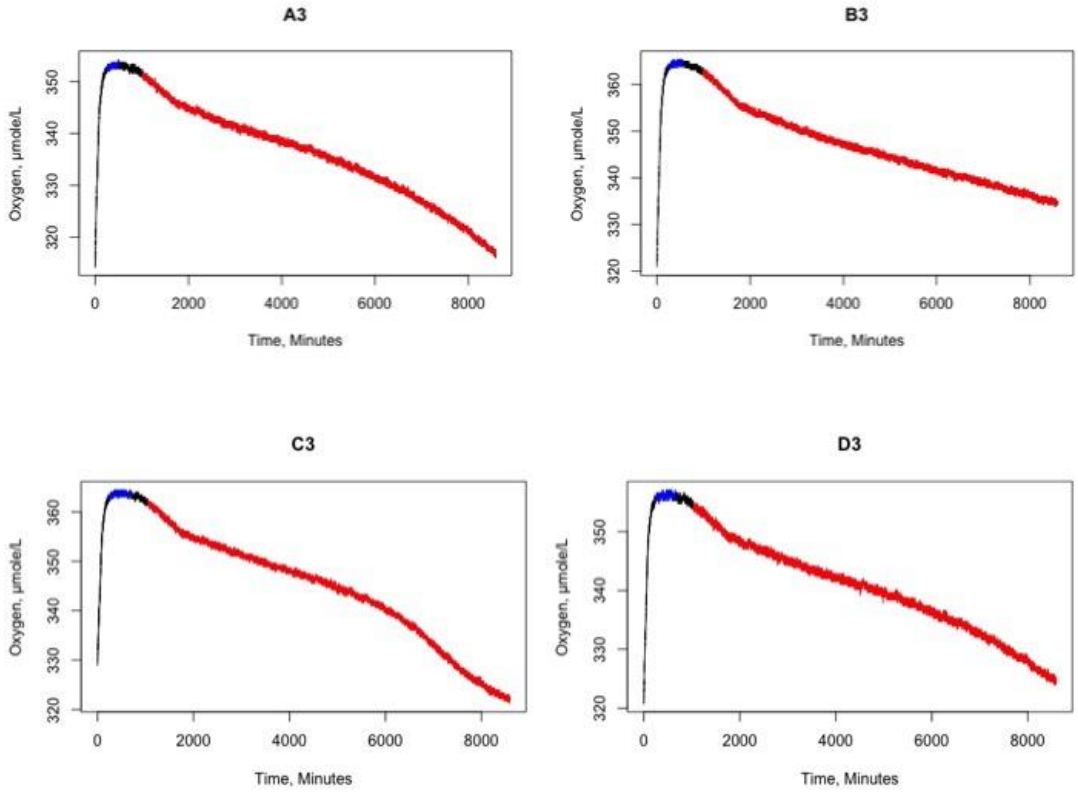

Figure A.20: 6 meter depth permeate